UNIVERSITY OF CALIFORNIA SAN DIEGO

SAN DIEGO STATE UNIVERSITY

Enhancing Myocardial Repair with CardioClusters

A dissertation submitted in partial satisfaction of the requirements for the degree
Doctor of Philosophy

in

Biology

by

Megan Michele Mendes Monsanto

Committee in charge:

University of California San Diego

Professor Asa B. Gustafsson
Professor Nicholas Spitzer

San Diego State University

Professor Mark A. Sussman, Chair
Professor Christopher C. Glembotski
Professor Roland Wolkowicz

2020

The Dissertation of Megan Michele Mendes Monsanto is approved, and it is acceptable in quality and form for publication on microfilm and electronically:

_____

_____

_____

_____

_____

Chair

University of California San Diego

San Diego State University

2020

DEDICATION

I would like to dedicate this work to several influential people in my life, starting with one of the strongest women I know, my mother. Not many women call construction their profession, but my mother works tirelessly beside my father, first drawing the architectural design and then bringing her vision to fruition by helping to build the homes she envisions. Headstrong and passionate she has taught me that with hard work and determination I can accomplish almost anything. My father has been both her rock, as well as mine, with his honest and personable nature it is hard not to smile with him around. Their combined love and nurture shaped me into the passionate women I am today, and without their support I would not be writing this dedication page today.

My older brother Daniel has not only been a sibling, but one of my best friends. Whereas most of my family is talkative, Daniel talks less and listens more. Through observation he has grown wise and is able to give some of the soundest advice. We might have very different personalities, but he has been the yin to my yang. Jacob is the youngest member of our family. Even though I was away at college most of the time Jacob was growing up, he always let me know how proud he was of his ‘big sister’ and his unwavering support gives me a glimpse of what it must feel like to be a parent.

Finally, I would like to dedicate this work to someone who only recently entered my life, my fiancée Will. Even though it is hard for a non-scientist to understand the jargon and details of scientific research, instead of being put off he has instead confessed that listening to me talk about my work and my enthusiasm is actually one of the reasons he was so drawn to me in the first place. His interest and support while I finish my doctoral work has given me the strength to complete this difficult journey.

EPIGRAPH

“When things aren’t going right, go left.”

TABLE OF CONTENTS

LIST OF ABBREVIATIONS

ACTA2	alpha smooth muscle actin
ANGPT2	angiopoietin-2
bMSC	bone marrow derived mesenchymal stem cell
cDNA	complementary DNA
CIC	cardiac interstitial cell
CM	cardiomyocyte
COL1A1	collagen type I alpha 1
COL3A1	collagen type III alpha 1
c-Kit	tyrosine-protein kinase Kit or CD117
CPC	cardiac stem cells
CXCL12	C-X-C motif chemokine 12
ECM	extracellular matrix
EPC	endothelial progenitor cell
FGF2	basic fibroblast growth factor
GATA4	transcription factor GATA-4
HBEGF	heparin-binding EGF-like growth factor
HGF	hepatocyte growth factor
HRP	horseradish peroxidase
HSC	hematopoietic stem cell
HUVEC	human umbilical vein endothelial cell
IGF2	insulin-like growth factor

IL1B	interleukin 1 beta
IL6	interleukin 6
IRF1	interferon regulatory factor 1
LVAD	left ventricular assist device
MACS	magnetic-activated cell sorting
MI	myocardial infarction
MMP1	matrix metalloproteinase-1
MSC	mesenchymal stem cell
NRCM	neonatal rat cardiomyocytes
NRG1	neuregulin 1
PBS	phosphate-buffered saline
PECAM1	platelet endothelial cell adhesion molecule or CD31
qRT-PCR	quantitative reverse-transcriptase polymerase chain reaction
RPM	revolutions per minute
scRNA-seq	single-cell RNA sequencing
SMA	smooth muscle actin
THY1	thymocyte differentiation antigen 1 or CD90
TIMP1	TIMP metallopeptidase inhibitor 1
TNF	tumor necrosis factor
VEGFR2	vascular endothelial growth factor receptor 2

LIST OF FIGURES

LIST OF TABLES

ACKNOWLEDGEMENTS

First, I would like to start by acknowledging my mentor, Dr. Mark A. Sussman, for his wisdom and guidance. The environment he has created in his lab has allowed me grow as both a scientist and a woman. I am very grateful for the opportunity to learn by his example.

I would also like to thank my additional committee members, Dr. Asa Gustafsson, Dr. Nicholas Spitzer, Dr. Christopher C. Glembotski and Dr. Roland Wolkowicz. Their guidance, invaluable input, and expertise are greatly appreciated. I am honored to have them as part of my committee. I would like to acknowledge the Rees-Stealy Research Foundation Phillips Gausewitz, M.D., Scholars of the SDSU Heart Institute and San Diego State University Heart Institute, Achievement Rewards for College Scientists and my sponsor the Hervey Family Fund for supporting my research. I would also like to extend my thanks to the SDSU Flow Cytometry Core and the vivarium staff.

To all the Sussmaniacs I have encountered in the Sussman lab, thank you for allowing me to be part of your group and thank you for the great conversations and many laughs. Without your expertise and unique personalities, I would not have survived the many hours in lab.

And finally, I would like to thank my family and loved ones; my parents who have always showed me what hard work and a good dose of determination can do, my siblings who are some of my biggest supporters and my loved ones who gave me the strength and determination to finish. Thank you all.

Chapter 2, with slight modifications, is a reprint of the material as it appears in Circulation Research, 2017. Concurrent Isolation of Three Distinct Cardiac Stem Cell

Populations from a Single Human Heart Biopsy. Monsanto MM, White KS, Kim T, Wang BJ, Fisher K, Ilves K, Khalafalla FG, Casillas A, Broughton K, Mohsin S, Dembitsky WP, Sussman MA. The dissertation author was the primary author and investigator on this manuscript.

Chapter 3, with slight modifications, has been submitted for publication. Enhancing Myocardial Repair with CardioClusters. Monsanto MM, Wang BJ, Ehrenberg ZR, White KS, Alvarez R, Echeagaray OH, Fisher K, Sengphanith S, Gude N, Sussman MA. The dissertation author was the primary author and investigator on this manuscript.

VITA

EDUCATION

Doctor of Philosophy in Biology
University of California San Diego and San Diego State University
Received 2020

Bachelor of Science in Biology
Clemson University
Received 2009

PUBLICATIONS

Wang BJ, Alvarez R, Muliono A, Sengphanith S, **Monsanto MM**, Weeks J, Sacripanti R, Sussman MA. Adaptation Within Embryonic and Neonatal Heart Environment Reveals Biological Characteristics of Adult c-Kit+ Cardiac Interstitial Cells. (Manuscript in preparation)

Khalafalla FG, Ebeid D, Sacchi V, Hariharan N, Ilves K, Torre ADL, Cottage C, **Monsanto MM**, Esquer C, Gude N, Goumans MJ, Sussman MA. Pim1 maintains Telomere length in Mouse Cardiomyocytes by inhibiting TGFβ signaling. (Manuscript in preparation)

Monsanto MM, Wang BJ, Ehrenberg ZR, White KS, Alvarez R, Echeagaray OH, Fisher K, Sengphanith S, Gude N, Sussman MA. Enhancing Myocardial Repair with CardioClusters. (Manuscript in preparation)

Broughton K, Khieu T**,** Nguyen N, Rosa M, Mohsin S, Quijada P, Wang BJ, Echeagaray OH, Kubli DA, Kim T, Firouzi F, **Monsanto MM**, Gude NA, Adamson RM, Dembitsky WP, Davis ME, Sussman MA. Cardiac interstitial tetraploid cells can escape replicative senescence in rodents but not large mammals. (2019) Communications Biology. DOI: 10.1038/s42003-019-0453-z

Alvarez R, Wang BJ, Quijada PJ, Avitabile D, Ho T, Shaitrit M, Chavarria M, Firouzi F, Ebeid D, **Monsanto MM**, Sussman MA. Cardiomyocyte Cell Cycle Dynamics and Proliferation Revealed Through Cardiac-Specific Transgenesis of Fluorescent Ubiquitinated Cell Cycle Indicator (FUCCI). (2019) Journal of Molecular and Cellular Cardiology. DOI: 10.1016/j.yjmcc.2018.12.007

Ilves K, Kubli D, Khalafalla FG, **Monsanto MM**, Firouzi F, Echeagaray O, Kim T, Adamson R, Dembitsky WP, Gustafsson A, Sussman MA. Hypoxia Prevents Mitochondrial Dysfunction and Senescence in Human c-Kit+ Cardiac Progenitor Cells. (2019) Stem Cells. DOI: 10.1002/stem.2970

Gude NA, Firouzi F, Broughton KM, Ilves K, Nguyen KP, Panye CR, Sacchi V, **Monsanto MM**, Casillas AR, Khalafalla FG, Wang BJ, Edeid D, Alvarez R, Dembitsky WP, Bailey BA, Berlo JH, Sussman MA. Cardiac c-Kit Biology Revealed by Inducible Transgenesis. (2018) Circulation Research. DOI: 10.1161/CIRCRESAHA.117.311828

Khalafalla FG, Kayani W, Kassab A, Ilves K, **Monsanto MM**, Alvarez R Jr, Chavarria M, Norman B, Dembitsky WP, Sussman MA. Empowering human cardiac progenitor cells by $P2Y_{14}$ nucleotide receptor overexpression. (2017) The Journal of Physiology. DOI: 10.1113/JP274980

Khalafalla FG, Greene S, Khan H, Ilves K, **Monsanto MM**, Alvarez R Jr, Chavarria M, Nguyen J, Norman B, Dembitsky WP, Sussman MA. $P2Y_2$ Nucleotide Receptor Prompts Human Cardiac Progenitor Cell Activation by Modulating Hippo Signaling. (2017) Circulation Research. DOI: 10.1161/CIRCRESAHA.117.310812

Monsanto MM, White KS, Kim T, Wang BJ, Fisher K, Ilves K, Khalafalla FG, Casillas A, Broughton K, Mohsin S, Dembitsky WP, Sussman MA. Concurrent Isolation of Three Distinct Cardiac Stem Cell Populations from a Single Human Heart Biopsy. (2017) Circulation Research. DOI: 10.1161/CIRCRESAHA.116.310494

Monsanto MM, Wang BJ, Sussman MA. Synthetic MSC? Nothing Beats the Real Thing. (2017) Circulation Research. DOI: 10.1161/CIRCRESAHA.117.310986

Samse K, Emathinger J, Hariharan N, Quijada P, Ilves K, Völkers M, Ormachea L, Torre ADL, Orogo A, Alvarez R, Din S, Mohsin S, **Monsanto M**, Fischer K, Dembitsky W, Gustafsson A, Sussman M. Functional Effect of Pim1 Depends upon Intracellular Localization in Human Cardiac Progenitor Cells. (2015) Journal of Biological Chemistry. May 29;290(22):13935-47.

Monsanto M, Sussman MA. Myocardial Infarct Scar: Hunting Down the Responsible Cells, But Then What? (2015) Journal of the American College of Cardiology. DOI: 10.1016/j.jacc.2015.03.519

Hariharan N, Quijada P, Mohsin S, Joyo AY, Samse KM, **Monsanto M**, De La Torre A, Avitabile D, Ormachea L, McGregor MJ, Tsai E, Sussman MA. Nucleostemin rejuvenates cardiac progenitor cells and antagonizes myocardial aging. (2015) Journal of the American College of Cardiology. DOI: 10.1016/j.jacc.2014.09.086

Mohsin S, Khan M, Nguyen J, Alkatib M, Siddiqi S, Hariharan N, Wallach K, **Monsanto M**, Gude NA, Dembitsky WP, Sussman MA. Rejuvenation of Human Cardiac Progenitor Cells with Pim-1 Kinase. (2013) Circulation Research. DOI: 10.1161/CIRCRESAHA.113.302302

Fang GC, Blackmon B, Staton M, Dana C, Kubisiak T, Olukolu B, Henry D, Zhebentyayeva T, Saski C, Cheng CH, **Monsanto M**, Ficklin S, Atkins M, Georgi L,

Barakat A, Wheeler N, Carlson J, Sederoff R, and Albert B. A physical map of the Chinese chestnut (Castanea mollissima) genome and its integration with the genetic map. (2013) Tree Genetics & Genomes. DOI: 10.1007/s11295-012-0576-6

HONORS AND AWARDS

2018-2019	Inamori Fellowship, San Diego State University
2015-2019	ARCS Scholarship, San Diego State University
2016-2017	Elliott Family Fund Scholarship, San Diego State University
2016	ISHR-NAS Travel Award recipient, Buenos Aires, Argentina
2014-2018	NIH, NHLBI, R01 Co-investigator "Enhanced Myocardial Repair with CardioClusters and CardioChimeras," San Diego State University
2014-Present	Rees-Stealy Research Foundation Fellowship, San Diego State University
2014	American Heart Association Cardiovascular Disease Student Scholarship, San Diego State University
2014	Gordon Research Seminar Best Graduate Student Poster Award, Colby-Sawyer College
2013-14	Harold & June Grant Memorial Scholarship, San Diego State University
2013	CSUPERB Travel Award, San Diego State University
2013	Student Research Symposium Provost's Award, San Diego State University
2013	Department of Biology's Outstanding Graduate Teaching Assistant, San Diego State University
2012-13	Mabel Myers Memorial Scholarship, San Diego State University
2006-09	Philip Prince Alumni Presidential Scholarship, Clemson University
2005-09	Palmetto Fellows Scholarship, Clemson University
2005-09	Trustee Scholarship, Clemson University
2005-09	Selected to the Dean's List & President's List, Clemson University

SCIENTIFIC PRESENTATIONS

Oral Presentations

Megan Monsanto, Jessica Wang, Zach Ehrenberg, Roberto Alvarez, Mark A. Sussman. "CardioClusters: Enhancing Stem Cell Engraftment and Myocardial Repair"
International Society for Heart Research- North American Section 37th Meeting, 2018. Lord Nelson Hotel, Halifax, Nova Scotia, Canada.

Monsanto M. "Enhancing Myocardial Repair with CardioClusters"
Graduate Student Seminar, 2018. San Diego State University, San Diego, CA.

Monsanto M. "Enhancing Myocardial Repair with CardioClusters"
Graduate Student Seminar, 2017. San Diego State University, San Diego, CA.

Megan Monsanto, Kevin White, Jessica Wang, Kristina Fisher, Natalie Gude, Mark A. Sussman. "CardioClusters: Harnessing the power of multi-lineage cardiac stem cells"
International Society for Heart Research XXII, 2016. Universidad Catolica Argentina, Buenos Aires, Argentina.

Monsanto M. "Generation of CardioClusters from Human Cardiac Stem Cells"
Graduate Student Seminar, 2016. San Diego State University, San Diego, CA.

Monsanto M. "Generation of CardioClusters from Human Cardiac Stem Cells"
Graduate Student Seminar, 2015. San Diego State University, San Diego, CA.

Monsanto M, Mohsin S, Fisher K, Emathinger J, Gude N, and Sussman MA. "Enhancing Myocardial Repair with CardioClusters"
Student Research Symposium (SRS), 2014. San Diego State University, San Diego, CA.

Monsanto M, Mohsin S, Fisher K, White K, Gude N, and Sussman MA. "Generation of CardioClusters from Human Cardiac Stem Cells"
Graduate Student Seminar, 2014. San Diego State University, San Diego, CA.

Monsanto M, Park SH, and Cao W. "Mutational Study of a DNA Repair Enzyme (Rv3297) from DNA Glycoslyase Fpg/EndoVIII Superfamily in *Mycobacterium tuberculosis"*
SC Life Colloquium of Undergraduate Research, 2009. Morris College, SC.

Poster Presentations

Megan Monsanto, Jessica Wang, Zach Ehrenberg, Roberto Alvarez, Mark A. Sussman. "CardioClusters: Enhancing Stem Cell Engraftment and Myocardial Repair"
Alternative Muscle Conference, 2018. University of California San Diego, San Diego, CA.

Megan Monsanto, Jessica Wang, Zach Ehrenberg, Roberto Alvarez, Mark A. Sussman. "CardioClusters: Enhancing Stem Cell Engraftment and Myocardial Repair"
International Society for Heart Research- North American Section 37th Meeting, 2018. Lord Nelson Hotel, Halifax, Nova Scotia, Canada.

Megan Monsanto, Kevin White, Jessica Wang, Kristina Fisher, Mark A. Sussman. "CardioClusters: Harnessing the power of multi-lineage cardiac stem cells"
Basic Cardiovascular Sciences, Scientific Sessions: Pathways to Cardiovascular Therapeutics, 2017. Hilton Portland & Executive Tower in Portland, OR.

Megan Monsanto, Kevin White, Jessica Wang, Kristina Fisher, Mark A. Sussman. "CardioClusters: Harnessing the power of multi-lineage cardiac stem cells"

AHA Scientific Sessions Conference, 2016. Ernest N. Morial Convention Center, New Orleans, LA.

Megan Monsanto, Kevin White, Jessica Wang, Kristina Fisher, Natalie Gude, Mark A. Sussman. “CardioClusters: Harnessing the power of multi-lineage cardiac stem cells”
Gordon Research Seminar and Conference, 2016. Colby-Sawyer College, New London, NH.

Monsanto M, Mohsin S, Fisher K, White K, Gude N, and Sussman MA. “Generation of CardioClusters from Human Cardiac Stem Cells”
International Society for Heart Research, 2015. Grand Hyatt Seattle, Seattle, WA.

Monsanto M, Mohsin S, Fisher K, Emathinger J, Gude N, and Sussman MA. “Enhancing Myocardial Repair with CardioClusters”
Gordon Research Seminar and Conference, 2014. Colby-Sawyer College, New London, NH.

Monsanto M, Mohsin S, Fisher K, Gude N, and Sussman MA. “Enhancing Myocardial Repair with CardioClusters”
AHA Scientific Sessions Conference, 2013. Dallas Convention Center, Dallas, TX.

Monsanto M, Mohsin S, and Sussman MA. “Recreating the Cardiac Stem Cell Niche to Improve Regeneration”
Student Research Symposium (SRS), 2013. San Diego State University, San Diego, CA.

Monsanto M, Zhebentyayeva T, Kubisiak TL, Hebard F, Fang GC, Olukolu BA, Fan S, and Abbott AG. “Comparative Genomic Study of Dormancy Associated MADS-box Genes in Woody Perennials”
Plant & Animal Genome XVX Conference, 2011. San Diego, CA.

PROFESSIONAL EXPERIENCE

Doctoral Candidate, San Diego State University	2014-2020
Graduate Teaching Assistant, Microbiology, SDSU	2012-2013
Masters Candidate, San Diego State University	2012-2014
Research Associate, Clemson University	2009-2011
SC LIFE Undergraduate Research Program, Clemson University	2008-2009

ABSTRACT OF THE DISSERTATION

Enhancing Myocardial Repair with CardioClusters

by

Megan Michele Mendes Monsanto

University of California San Diego, 2020

San Diego State University, 2020

Professor Mark A. Sussman, Chair

Heart disease leading to cardiovascular failure is a major public health issue in the United States with a considerable burden for the health care system. Despite recent progress to advance stem cell-based therapy for patients, heart failure carries a five-year mortality that rivals most cancers. This proposal describes an approach to control and pattern three distinct stem cell populations derived from the human heart to promote superior repair and regeneration after myocardial infarction.

Regenerative capacity of the heart is mediated through multiple distinct populations of stem cell types that are the subject of ongoing intense study. In the past decade, isolation and characterization of c-kit^{+} cardiac progenitor cells (CPCs), mesenchymal stem cells (MSCs) and endothelial progenitor cells (EPCs) have provided substantial insight to the capabilities of stem cells to rebuild the damaged heart and advance clinical therapy. Clinical trials have proven the efficacy and safety of autologous and allogeneic cell delivery to human patients, yet improvements in cardiac function and reduction in scar tissue remain modest and far below that needed for restoration of normal functional output.

The work presented in this dissertation project overcomes these current cell-based limitations by using a novel method for improving myocardial repair: CardioClusters, a three-dimensional microenvironment consisting of CPCs, MSCs and EPCs. The innovation of this project is the creation of CardioClusters with the ability to capitalize upon beneficial attributes of multiple human stem cells from a single human heart providing a clinically relevant translational strategy. Collectively, studies in this dissertation will pave the way for interventional approaches to selectively adapt stem cell behavior and merge beneficial attributes of stem cell populations found within the human heart for prevention of heart failure after cardiomyopathic injury.

CHAPTER 1

Introduction of the Dissertation

Cell therapy for cardiovascular disease

Cellular therapy using stem cells derived from bone marrow and cardiac origin are validated to treat damage after myocardial infarction (MI) in both small animal models and human clinical trials[1-6]. Efforts to publicize widespread application of cellular therapy are hindered by results of little to no improvement in cardiac function after long-term follow up studies. The inherent limitation of autologous stem cell therapy is that cells derived from aged organs have increased expression of senescent markers and acquisition of chromosomal abnormalities leading to undesirable cellular characteristics such as slowed proliferation and increased susceptibility to cellular death[7]. Furthermore, based on animal models, cellular survival and engraftment are hindered by adverse inflammation, inhibiting the ability of transplanted stem cells to efficiently differentiate into cardiac cells. Improvement of stem cell engraftment and survival has been attempted by injection of stem cells in biomaterials[8, 9], with cytokines and growth factors[10], or genetic enhancement with pro-survival and anti-apoptotic genes[11, 12]. Our laboratory has established protocols to derive human stem cells from fetal hearts that are in the midst of cardiogenesis as well as stem cells from adult hearts[13]. Routine sorting protocols allow for successful isolation of CPCs, MSCs, and EPCs from patients of varying age and gender. Firsthand experience has led our group to understand that each stem cell type exhibits characteristics that render them desirable to promote regenerative repair[13]. MSCs are multipotent stem cells that give rise to bone, cartilage and adipose tissue[13, 14]. MSC adoptive transfer to the heart supports endogenous regeneration by secretion of paracrine factors that activate endogenous stem cells, promote angiogenesis, protect cardiomyocytes and reduce scar formation[14, 15].

Furthermore, MSC transplantation suppresses immune rejection, decreasing inflammation after acute MI, due to enhanced secretion of anti-inflammatory factors[14, 16]. In animal models, as well as in studies completed by our laboratory, transplanted CPCs give rise to cardiomyocytes, smooth muscle and endothelial cells, but lack the power of MSCs to activate and recruit endogenous stem cells[11, 12]. EPCs mobilized from bone marrow promote paracrine dependent vasodilation, vasculogenesis and angiogenesis, and differentiate into mature endothelial cells[17, 18]. Combinatorial cell therapies have been suggested in hopes of initiating additive or synergistic effects in myocardial repair such as with the delivery of MSCs and c-Kit$^+$ CPCs into an infarcted swine model[19]. However, the retention of adoptively transferred stem cells remains quite poor regardless of whether it involves single or combinatorial stem cell delivery due to adverse inflammation. More importantly, arbitrary transfer of two or more stem cell populations together does not ensure stem cell interaction and cross talk that are essential for repair of advanced organ damage. Therefore, it is imperative to design new strategies of *ex vivo* cellular manipulation, which will retain naïve phenotypic characteristics for enhanced proliferation and survival as well as drive cardiogenic commitment after engraftment in the myocardium.

Microenvironments for enhanced stem cell proliferation and regenerative potential

Stem cell self-renewal and differentiation are tightly controlled in defined locations of all regenerative tissues, including the heart[20, 21]. Key functions of microenvironments include the maintenance of a quiescent stem cell population sensitive to stimuli such as

molecular signaling and extracellular matrix remodeling[22]. Recapitulation of cardiac microenvironments *ex vivo*, such as with cardiospheres[23, 24], allows for enhanced cellular communication through gap junction protein connexin 43, improving cell propagation and differentiation *in vitro*[20, 25, 26]. However, cardiosphere capacity for *in vivo* differentiation is minimal with most improvements arising from paracrine affects[27]. Cardiospheres are composed of a heterogeneous cell population that lack ability to directly restore vasculature, as cardiospheres do not retain an endothelial precursor cell[23, 28]. Cardiospheres are formed by random aggregation leading to inconsistent cell characterization markers[23, 24] variable sphere size and muddled communication within the microenvironment[23, 24, 28]. Based on these observations, the rationally designed CardioCluster presents itself as a superior application of microfabrication that will enhance stem cell responses to internal and external cues, which are imperative properties for stem cell survival and differentiation potential.

CardioClusters the next generation approach to cellular therapy

Blind application of stem cell populations to treat cardiovascular disease is not a sustainable approach, what is needed is a better understanding of stem cell attributes for more efficient cardiac regeneration. The heart is composed of diverse cell populations where no single cell type can compensate for the great cellular loss following MI. To adequately amend acute cell death and replace scare tissue the various cardiac cells found within the myocardium have to be restored. MSCs from the bone marrow are of interest because of their ability to secrete a diverse assortment of paracrine factors, but unfortunately present uncontrolled differentiation into non-cardiac tissue such as

skeletal muscle and adipose[29-31]. EPCs transplanted *in vivo* are capable of forming microvessels but are shown to regress without MSCs to support vessel maturity[29]. The regenerative potential of EPCs and MSCs warrants investigation, as achieving long-lasting myocardial benefits requires the interaction of multiple cell types. Studies have investigated the added benefit of transferring two stem cell populations[19], but no one to date has attempted to inject multiple stem cells explanted solely from a single human heart. Resident CPCs are pre-committed to the cardiovascular fate and can produce new cardiogenic cells without inducing arrythmyogenesis, a distinct advantage over other cell types for cardiac cell therapy[32]. Cardiovascular research is at a threshold and the CardioCluster proposed in this dissertation will push the field forward by integrating unique characteristics from each cell type. CPCs and MSCs prefer hypoxic conditions[33, 34] and will form the central core of the CardioCluster as seen in Figure 1.1. EPCs will surround the CardioCluster and provide for endothelial specific differentiation and production of tubular networks to reconnect with native blood vasculature, restore blood flow and aid in nutrient absorption in the heart[29, 35]. MSCs will be mixed in the interior with CPCs, as MSCs secrete cell adhesion molecules such as integrins and cadherins, which are integral to cellular aggregation[36]. Furthermore, MSCs will be an imperative supporting cell type to EPC maturation by secretion of paracrine factors to promote long-term EPC-dependent vasculogenesis[37]. CardioClusters form a microcosm that will support cell survival and proliferation, making this approach an ideal route for cardiac restoration.

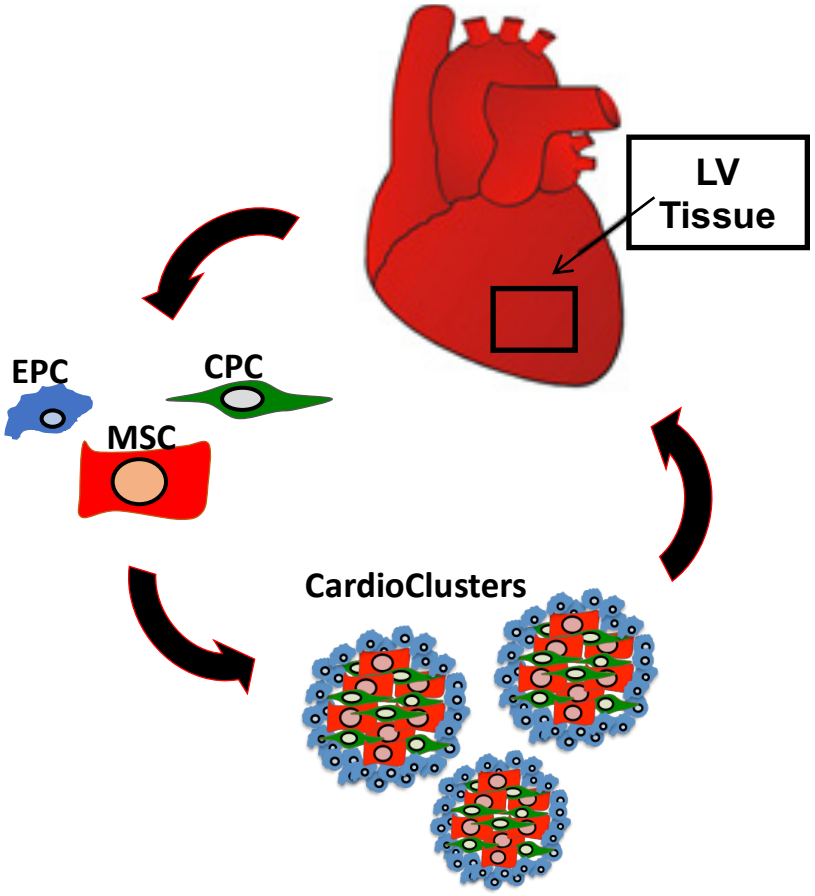

Figure 1.1. Schematic of study overview. CPCs, EPCs and MSCs can be isolated from the human heart, combined in a CardioCluster and re-introduced into the left ventricle (LV) for autologous cellular therapy.

GOALS OF THE DISSERTATION

Overarching Theme: In the past decade, identification and testing of stem cells to treat myocardial infarction (MI) has proceeded with ferocious intensity. Meta-analysis reveals that specific stem cell types promote myocardial repair through distinct mechanisms. Even so, despite "priming" of stem cells with growth factors or engineering of three-dimensional (3D) cardiac tissues, current approaches fall short of mediating myocardial repair that requires harnessing an optimal mix of both paracrine dependent secretion and direct commitment of injected cells. Although this deficiency has been attacked through combinatorial stem cell delivery, there is no evidence that dual stem cell injection provides for direct cellular cross talk to promote stem cell survival and proliferation. The field of myocardial regeneration desperately needs innovative, novel, and creative solutions building upon our existing knowledge that will raise efficacy of repair to a new level, rather than simply reiterating existing approaches providing modest improvements. Here I propose a novel manipulation of cardiac interstitial cells to enhance myocardial repair. The approach creates CardioClusters, defined as a three-dimensional microenvironment consisting of three defined cell populations from the human heart: cardiac progenitor cells (CPCs), mesenchymal stem cells (MSCs) and endothelial progenitor cells (EPCs). CardioClusters will be created with MSCs as a support cell, increasing CPC and EPC commitment into cardiac and endothelial lineages. CardioClusters will enhance cellular communication and regenerative capacity by increasing the ability of adoptively transferred cells to adapt during hypoxia and

inflammation, as well as commit and secrete factors to support myocardial structure and contractility after myocardial injection.

Hypothesis: **CardioClusters improve regeneration of damaged myocardium by enhancing direct and indirect mechanisms of repair compared to current approaches using single cell suspension delivery.** This dissertation project will validate the use of CardioClusters to combine beneficial cellular characteristics for cardiac repair. The **SPECIFIC AIMS**, experimental approaches and hypotheses of the proposal are:

Specific Aim 1: CardioClusters exhibit enhanced proliferation, survival and cardiac commitment relative to single cell populations.

Experimental approach: Genotypic and phenotypic markers will be analyzed in CardioClusters, CPCs, MSCs, EPCs, and the three populations combined (C+E+M).

A. Isolate stem cell populations from the human heart and characterize marker expression, proliferation rates, and resistance to apoptotic challenge.
B. Determine cardiac lineage commitment and paracrine secretion of each distinct stem cell population at baseline and following differentiation stimuli.
C. Apoptosis and cell death are reduced by incorporation of cells into CardioClusters.
D. Paracrine secretion is increased after differentiation stimuli such as co-culture of CardioClusters with cardiomyocytes.

Specific Aim 2: CardioClusters restore myocardial structure and function after intramyocardial injection better than single cell populations or a mixture of the three populations (C+E+M) injected combinatorially.

Experimental Approach: Stem cells delivered following acute myocardial infarction will be monitored for reparative potential and stimulation of endogenous regeneration.

A. Survival, engraftment, and persistence of injected cells is improved by incorporation of stem cells into CardioClusters.
B. Cardiac structure and function are enhanced by injection of CardioClusters.
C. CardioClusters restore cardiomyocyte size and vasculature following myocardial infarction injury.

CHAPTER 2

Concurrent Isolation of Three Distinct Cardiac Stem Cell Populations from a Single Human Heart Biopsy

INTRODUCTION

Identification and selection for optimal stem cell type(s) remains a critical issue for successful therapeutic implementation of myocardial regeneration in patients suffering from heart failure. Cell populations from a variety of tissue sources, including bone marrow mononuclear cells, skeletal myoblasts, hematopoietic and endothelial progenitors, and induced pluripotent or embryonic stem cells have been extensively tested for their ability to regenerate lost myocardium[38, 39]. However, clinical trial outcomes repeatedly fall short of expectations raised by preclinical animal studies[40-45] prompting concern regarding the translational impact of experimental models. Nevertheless, there is growing acceptance of the new dogma that the adult mammalian heart is capable of cellular replacement throughout life and in response to pathologic injury, including the cardiomyocyte population (CM)[46]. Myocardial regeneration is facilitated by resident stem cells that activate endogenous tissue repair by both direct and indirect contribution to cellular replacement of CMs, smooth muscle cells, and endothelial cells. Considering the heart as a self-renewing organ opens up exciting possibilities for therapeutic intervention by cellular activation to promote regenerative processes.

Effective tissue regeneration necessitates not only replacement of CMs, but also vasculature comprised of smooth muscle and endothelial cells. Relative contributions of divergent resident cardiac stem cell types must be appreciated and delineated to maximize therapeutic potential of cell-mediated repair. Coordinated action of multiple cardiac stem cell types forms the basis for normal myocardial biology and therefore will likely be essential to achieve clinically meaningful restoration of tissue structure and

function in the wake of pathologic damage. Regardless of whether the ultimate effectors of repair are derived from an adoptively donated cell population or recruited from the endogenous pool(s) of resident cells, it is imperative to establish a working understanding of interactions and contributions of the distinct stem cell types participating in mediation of myocardial homeostasis and repair. Toward that goal, a simple and cost-effective protocol to separate and enrich multiple cardiac stem cells into distinct subsets is essential. Based upon established precedents, three such resident adult cardiac stem cells include cardiac progenitor cells (CPCs) as well as supportive cell types comprised of mesenchymal stem cells (MSCs) and endothelial progenitor cells (EPCs) that can be differentially separated based upon surface marker expression profiling.

Cardiac stem cells were originally isolated in the adult rat heart on the basis of tyrosine-protein kinase Kit (c-Kit) or CD117 expression and were found to lack hematopoietic lineage markers[47]. A similar population of c-Kit$^+$ CPCs was identified in the adult human heart[48, 49], prompting clinical testing to assess their potential efficacy for enhancing myocardial regeneration[50, 51]. Early patient results have been encouraging showing improved heart function, however advanced age, comorbidities, and genetic factors in patients with heart failure constrain the regenerative capacity of CPCs. Rejuvenation of senescent CPCs, such as with genetic modification[52, 53], repeated cell administrations[54], or in conjunction with additional supportive cell types[55] may improve outcomes for a substantial patient population possessing functionally impaired stem cells.

Stromal MSCs are a supportive cell that contributes to regeneration by secretion of paracrine factors that activate endogenous stem cells, promote angiogenesis, protect CMs and reduce scar formation[56, 15, 57]. MSCs are multipotent stem cells that give rise to skeletal myoblasts, chondrocytes, and adipose tissue [56, 58]. Adherent MSCs express cell surface markers CD73, CD105, CD29, CD44, and CD90 while lacking CD45 that is expressed by hematopoietic stem cells (HSCs)[59]. Lack of major histocompatibility complex II expression allows MSCs to evade host immune responses and overcome host rejection[16, 56] leading to their suggested use for allogeneic transplantation into patients[60, 61].

EPCs were formerly defined as progenitor cells positive for both the HSC marker CD34 and the endothelial receptor known as vascular endothelial growth factor receptor 2 (VEGFR2)[62]. Because CD34 is not exclusively expressed on progenitor cells, but also on mature endothelial cells, enrichment with an additional early lineage stem cell marker CD133[63] demonstrated that purified $CD133^{+}$ EPCs differentiate into endothelial cells *in vitro*[64]. CD133, also known as prominin or AC133, is a highly conserved antigen with unknown biological activity expressed on EPCs but absent on mature endothelial cells[65]. EPCs promote paracrine-dependent vasculogenesis and angiogenesis, and form microvessels upon transplantation *in vivo*[17]. However, these microvessels regress without support from MSCs to allow vessel maturity[66]. For this reason, combinatorial cell therapies have been suggested for the treatment of heart failure in hopes of synergistic effects, [55] but isolation and examination of multiple enriched stem cell subpopulations from a single human heart has not been previously performed.

Knowledge and understanding of myocardial regenerative mechanisms will be facilitated by adoption of the protocol to derive three resident cardiac stem cell populations from adult heart biopsies procured during left ventricular assist device (LVAD) implantation described herein. Our sorting protocol allows for isolation of c-Kit$^+$ CPCs, c-Kit$^+$CD133$^+$ EPCs, and c-Kit$^-$CD90$^+$CD105$^+$ MSCs from patients of varying age and gender. Here we show these three cell populations maintain their unique phenotypic properties during *ex vivo* cell culture. Phenotypically, these cells show distinct morphology, growth kinetics, cell surface marker and gene expression profiles, and cardiac lineage potential. Isolation of multiple cells types from a single tissue source will allow for concurrent study of cell interactions, empower studies using cells derived from the target human heart failure population that will be involved in regenerative therapy, and expand the repertoire of possibilities for manipulation and modification of stem cells to treat cardiovascular disease. Therefore, the protocol and initial characterizations in this report represent an important and valuable technical advance in the development of novel techniques to facilitate understanding and implementation of regenerative medicine.

METHODS

Human Cardiac Stem Cell Isolation

Cardiac biopsies were obtained from patients undergoing LVAD implantation. NIH guidelines for human subject research are consistent with Institutional Review Board (IRB) exemption based upon the use of tissues that are waste discards from normal and routine clinical procedures of LVAD surgery (45 CFR 46.101). After excision, cardiac tissue remained on ice in cardioplegic solution until processed. Fatty tissue was excised and remaining cardiac tissue was suspended in Basic Buffer (15 mL) and minced into 1 mm^3 pieces. After mincing, tissue and Basic Buffer were collected in 50 mL Falcon tube. Digestive solution containing collagenase, type II 225 U/mg dry weight (Worthington, catalog #LS004174, Bio Corp, Lakewood, NJ) was dissolved in Basic Buffer (2-2.5 mg/mL) and incubated with tissue pieces for 1.5-2 hours at 37°C with continuous shaking. Digestion solution was refreshed at the one-hour time point and resulting suspensions were centrifuged at 350 *g* and resuspended in CPC media (see Table 1). Final suspension was filtered through a 100-μm filter (Corning, Inc., catalog #352360) followed by a 40-μm filter (Corning, Inc., catalog #352340) and centrifuged at 150 *g* for 2 minutes to collect CMs. The supernatant was collected and centrifuged at 350 *g* and resuspended in CPC media and incubated overnight at 37°C in CO_2 incubator.

The following day, cells in suspension were collected in 50 mL Falcon tube. Any cells attached were dissociated using a 1:1 mixture of Cellstripper (Corning, catalog #25-056-CI) and TrypLE Express (1X) (Thermo Fisher Scientific, catalog #12604-013). Resulting suspension was filtered through a 40-μm filter, centrifuged at 350 *g*, and

resuspended in wash buffer (PBS plus 0.5% bovine serum albumin). To isolate c-Kit$^+$ cells, suspension was incubated with c-Kit–labeled beads (Miltenyi Biotec, catalog #130-091-332) and sorted according to the manufacturer's protocol. The c-Kit$^+$ fraction was divided as such: half the population was suspended in CPC media (see Table 1) and the other half was suspended in EPC media (see Table 1). The c-Kit$^-$ population was further incubated with CD90/CD105–labeled beads and sorted according to the manufacturer's protocol (Miltenyi Biotec, catalog #130-096-253/130-051-201). Cells positive for CD90/CD105 were suspended in MSC media (see Table 1). To isolate an EPC population, at 1 week the c-Kit$^+$ population plated in EPC media was further sorted using CD133–labeled beads and sorted according to the manufacturer's protocol (Miltenyi Biotec, catalog #130-097-049). All cells were cultured at 37°C in CO_2 incubator in their respective growth media. CPC and EPC were split 1:2 when they reached 60-70% confluency. MSC were split 1:2 when they reached 90% confluency. Patient information for the five cardiac samples used in this study can be found in Table 4. All cells used in this study were mid-passage (passages 5–9).

Quantitative Reverse-Transcriptase Polymerase Chain Reaction (qRT-PCR) and Bioinformatics

Total RNA was isolated from cardiac stem cell populations using Quick-RNA MiniPrep kit (Zymo Research, catalog #R1055) according to manufacturer's protocol. 500 nanograms of RNA were used to generate complementary DNA (cDNA) using an iScript cDNA Synthesis kit (Bio-Rad Laboratories, Inc, catalog #170-8891). The amplified cDNA was diluted at a ratio of 1:10 in DNase- and RNase- free water. qRT-

PCR were completed using iQ SYBER Green (Bio-Rad Laboratories, Inc, catalog #170-8882) on a CFX Real-Time PCR Detection System (Bio-Rad). cDNA was amplified using primers specific to genes of interest (listed in Table 3). The comparative or ΔΔCt method of qRT-PCR data analysis was used to analyze samples; variability in cDNA concentration was normalized using 18S. Hierarchical clustering and supervised clustering for gene expression profiling were performed using Expander 7.1 software[67].

Immunocytochemistry

Cardiac stem cell populations were plated on 2-well chamber glass slides (10,000 cells/well) in their respective growth media (see Table 1) for a minimum of 24 hours. After incubation, slides were washed with phosphate-buffered saline (PBS) (Corning, catalog #21-040-CV) and fixed in 4% paraformaldehyde for 5 minutes at 4°C. Following fixation, the slides were washed twice with PBS and permeabolized in PBS plus 0.1% Triton X-100, 0.1 M Glycine for 3 minutes, then washed once with PBS and blocked with TNB (1X TN (Tris-HCl, NaCl) Buffer, 5 µg/mL blocking reagent (PerkinElmer, catalog #FP1012)) for 30 minutes. Primary antibodies were diluted in TNB (see Table 2) and incubated overnight at 4°C. The following day slides were washed twice with PBS. Fluorescently conjugated secondary antibodies were diluted in TNB (1:200) and incubated 1.5 hours at room temperature. For c-Kit staining a horseradish peroxidase (HRP)-linked secondary antibody (1:500) was used, followed by tyramide signal amplification (1:50) (PerkinElmer, catalog #NEL753001KT). After washing twice with PBS, DAPI was included in a final wash to fluorescently label the nuclei, and slides were coverslipped with Vectashield® mounting reagent (Vector Laboratories, catalog #H-

1000). All slides were imaged using a Leica TCS SP8 confocal microscope. A table of antibodies and dilution ratios is available in Table 2.

Cell Morphology Measurement

Cardiac stem cell populations were imaged using a Leica DMIL inverted tissue culture phase contrast microscope. Cell morphology was measured by tracing the outline of the cells using Image J software. The three measurements analyzed were Area, Roundness, and Length-to-Width (L/W) ratios. L/W ratios were calculated by dividing Feret/Min Feret measurements. A minimum of 30 cells was measured per cell line.

Cell Proliferation Assay

Cell populations were plated in quadruplicate (1,000 cells/well) in a 96-well black flat bottom plate with 100 µL/well of their respective growth media. Cell proliferation rate was determined using a CyQUANT Direct Cell Proliferation Assay (Thermo Fisher Scientific, catalog #C35011) on days 0, 1, 3 and 5. Doubling times were calculated based on periods of exponential growth using a population doubling time online calculator (http://www.doubling-time.com/compute_more.php).

Flow Cytometry

For live cell analysis, single cells were suspended in 100 µL wash buffer and incubated with primary antibody (see Table 2 for dilutions) on ice for 30 minutes. Following, cells were washed with wash buffer and incubated with secondary antibody (1:100) for 20 minutes on ice. For fixed cell analysis, cells were suspended in 4%

paraformaldehyde for 5 minutes at room temperature and then washed twice with wash buffer. For c-Kit analysis requiring permeabilization, cells were washed twice and resuspended in PBS plus 0.1% Triton X-100, 0.1 M Glycine for 3 minutes, then washed once. Fixed cells were suspended in 100 µL wash buffer and incubated with primary antibody on ice for 1 hour. Following, cells were washed twice and incubated with secondary antibody (1:100) for 30 minutes on ice. For both fixed and live cells a total of 300 µl wash buffer was added post secondary incubation and the cells were analyzed by flow cytometry with a BD FACS Canto instrument. Unstained and isotype controls were used to establish baseline fluorescence levels. Data was analyzed by Flow Jo software (BD Biosciences). A minimum of 10,000 cell counts was analyzed. Due to low cell count for H13-066 MSC, the c-Kit count was 5,000.

Matrigel Tube Formation

Growth factor reduced matrigel (Corning, catalog #356231) was used to coat a 96-well flat bottom plate (50 µl/well) and incubated for 30 minutes at 37°C. Cardiac stem cell populations were plated in duplicate (5,000 cells/well) suspended in 100 µL/ well of EPC basal medium (see Table 1) and incubated at 37°C in CO_2 incubator. Cell tube formation was imaged using a Leica DMIL inverted tissue culture phase contrast microscope after 12-16 hours.

MSC- Colony-forming unit-fibroblast (CFU-F) Assay

Cells were suspended in CFU-F assay medium: DMEM-low glucose (Thermo Fisher Scientific, catalog # 11054-020) with 10% FBS, 2 mM L-Glutamine and

Gentamicin (10 mg/mL) and plated at 200 cells per 100 mm. Medium changed every 3 days and after 14 days of growth, dishes were washed with PBS and incubated in crystal violet at room temperature for 30 minutes. Solution removed by 4 washes of PBS. A minimum of 3 dishes plated per cell line.

Multilineage Mesenchymal Differentiation Potential

The potential for osteogenesis, adipogenesis, and chondrogenesis differentiation was assessed for the three cardiac stem cell populations using StemPro Differentiation Kits following manufacturer's protocol (Thermo Fisher Scientific, catalog #A1007201, #A1007001, and #A1007101). For osteocyte differentiation cells were stained with Alizarian-Red Staining Solution (Millipore, catalog #TMS-008-C), for adipocyte differentiation cells were stained with Oil Red O (Sigma-Aldrich, catalog #O0625), and for chondrocyte differentiation cells were embedded in optimal cutting temperature (OCT) compound, cryosectioned, and stained with Alcian-Blue Staining Solution (Millipore, catalog #TMS-010-C).

Statistical Analysis

Data expressed as mean±SEM. Statistical analyses of multiple groups were assessed by 1-way ANOVA with Bonferroni post hoc test. Multiple groups over time were analyzed by 2-way ANOVA. Statistical analysis was performed using GraphPad Prism version 5.0 software. The Pearson product-moment correlation coefficient was calculated using Microsoft Excel 2010. Experiments were performed in triplicate unless stated otherwise. A p-value of less than 0.05 was considered statistically significant.

RESULTS

Isolation of Three Distinct Cardiac Stem Cell Populations

The three different cardiac stem cell populations were isolated and expanded as described in the Methods section: *Human Cardiac Stem Cell Isolation* (Figure 2.1). At the time of extraction, the c-Kit$^-$ MSC population is relatively abundant in comparison to the c-Kit$^+$ cells which are a rare population comprising only 3-5% of the isolated stem cells. Of the c-Kit$^+$ cells, roughly half are also CD133$^+$.

Distinctive Cell Morphology among Cardiac Stem Cell Populations

After expansion *ex vivo*, mid-passage cells were assessed for morphometrics. Phase contrast imaging (Figure 2.2A) measured parameters of Area, Roundness, and L/W Ratio. MSC area is significantly larger (23,301±1,018) relative to both CPC (7,435±358) and EPC (4,738±202) (Figure 2.2B). EPCs are significantly more round (EPC, 0.57±0.016; CPC, 0.26±0.012; MSC, 0.38±0.016) (Figure 2.2C), while CPCs show increased L/W ratio (CPC, 4.2±0.16; EPC, 2.0±0.081; MSC, 3.0±0.12). Representative examples of cultures of the three cell types show close clustering of morphometric parameters with minor variation between individual patients (data not shown).

Cell Population Kinetics Vary by Cell Type

Population growth kinetics was determined by CyQuant proliferation assay (Figure 2.3A-2.3C). The MSC population exhibited slowest proliferation rate (doubling time: 119±35 hours) in agreement with prior studies using mid-passage MSC

populations[68-70]. CPCs and EPCs show markedly faster proliferation rates (doubling times: CPC, 33±2 hours; EPC, 35±7 hours) (Figure 2.3D and 2.3E). Cell type growth kinetics varies by patient indicative of heterogeneity in cell biology between patient isolates.

Flow Cytometry Analysis of Markers Expressed upon In vitro Culture

Persistence of markers used to isolate the cardiac subpopulations was analyzed by flow cytometric analysis of single cell suspensions with fluorescence signal comparison between the differentially enriched cell types (Figure 2.4 and Figure 2.5) and variance among patients (Figure 2.6). All cells were negative for HSC marker CD45 (CPC, <1%; EPC, ~3%; MSC, <1%) (Figure 2.6) as expected for cardiac-derived cell populations. CPCs and EPCs were initially isolated for c-Kit surface expression, however the extent of c-Kit expression and internalization varied among the three populations: CPC were ~97% positive for c-Kit, while EPC were ~43% and MSC were ~27% (Figure 2.4A). CPCs internalized c-Kit, while c-Kit expression did not change upon permeabilization for EPCs and MSCs (Figure 2.7). These observations are consistent with prior studies showing surface c-Kit expression is variable[71-73], a characteristic of rapidly cycling receptors.

MSC populations were ~100% positive for both mesenchymal markers CD90 and CD105, with insignificant change between live (Figure 2.4B and 2.4C) and fixed cells (Figure 2.6). While ~99% of CPCs expressed CD105, only a little over half (~64%) expressed CD90 (Figure 2.4B and 2.4C). Of the three cell populations, EPCs had the lowest parentage of cells positive for mesenchymal markers (CD105: ~56%; CD90:

<1%) (Figure 2.4B and 2.4C). Whereas fixation did not alter the percent of MSCs positive for CD90 and CD105, fixation did decrease the percent of CPCs and EPCs positive for these two mesenchymal markers (CD90: fixed CPC, ~40%; fixed EPC, <1% and CD105: fixed CPC, ~28%; fixed EPC ~11%) (Figure 2.6). CD133 could not be detected on live cells; with fixation CD133 could be identified on all cell populations (EPC, ~67%; CPC, ~63%; MSC, ~92%) (Figure 2.4D and Figure 2.6).

Immunocytochemistry Corroboration of Flow Cytometry Data

Immunofluorescence microscopy was utilized to assess endogenous expression levels of the panel of markers used for stem cell isolation. Expression of c-Kit in CPCs was uniformly high, whereas c-Kit expression was comparatively low in MSCs. While a subset of the EPC population (marked by asterisks) expressed high levels of c-Kit, the majority expressed low to undetectable levels (Figure 2.8A). CD133 was prominently expressed by all three cells types (Figure 2.8B), consistent with flow cytometry data. Antibody labeling confirmed clear expression of mesenchymal markers CD90 and CD105 by the MSC population. Both mesenchymal markers were barely detectable above background in the EPC population with very low immonolabeling for CD105. While CPCs expressed CD105, CD90 level in CPCs was relatively low in comparison to the MSC population (Figure 2.8C).

Gene Expression Profiles Show EPCs Diverge from CPCs and MSCs

Transcriptional signatures for each cell type from various patients was performed using quantitative qRT-PCR focused upon three groups of genes: 1) growth factors and

cytokines 2) extracellular matrix (ECM) proteins and 3) inflammatory factors (Table 3). Results of qRT-PCR were subjected to bioinformatic analyses by hierarchical clustering for 45 samples (5 patients x 3 cell types x 3 replicates). Supervised clustering analysis revealed that CPCs and MSCs have closely related transcriptional profile, whereas EPCs are divergent. Two groups of genes differentiate EPCs from CPCs and MSCs: one group showed elevated gene expression (ANGPT2, PECAM1, COL3A1, HGF, IGF2, IRF1, TIMP1 and TNF) whereas another showed diminished gene expression only in EPCs (COL1A1, FGF2, HBEGF, IL1B, IL6, MMP1, NRG1 and CXCL12) (Figure 2.9A and 2.9B). Pearson product-moment correlation coefficient heat map matrix of individual patients revealed that four out of five patients showed high gene expression correlation (>0.82), meaning although there is inherent heterogeneity among patient samples, individual cell types display characteristic profiles (data not shown).

In Vitro Lineage Assessment and Comparison to Non-Cardiac Controls

Tube formation assay using growth factor-reduced Matrigel demonstrates angiogenic potential of the three cardiac stem cells *in vitro*. Ability to form tubular networks varied among patients as well as cell types, with only a few CPC lines being able to form rudimentary tubules (Figure 2.10A), EPCs were able to form robust tubular networks within 15 hours (Figure 2.10B) similar to HUVEC control (data not shown), whereas MSCs could not form tubular structures, instead producing “star-burst” structures (Figure 2.10C).

Multilineage mesenchymal differentiation assays were performed to determine adipocyte, chondrocyte, and osteocyte potential (Figure 2.11). Similar to bMSC, the

cardiac derived MSC were able to differentiate into these three lineages, whereas EPCs and CPCs were unable to fully commit, demonstrating distinctly different cell lineages. Cardiac derived MSCs also showed comparably low levels of major histocompatibility complex (MHC) molecules, both MHC Class I, Class II, as well as co-stimulatory molecules as bMSC (Figure 2.12) and were successfully able to give rise to colony forming units (data not shown).

HUVECs and bMSCs were used to assess the potential of cardiac stem cell commitment toward angiogenic or smooth muscle fate. HUVECs and EPCs expressed the highest levels of PECAM-1 (HUVEC, 1,967±106; EPC 181±47) with respect to either CPCs (1.9±0.69) or MSCs (0.85±0.25) (Figure 2.10D). SMA is expressed by both bMSCs (1.0±0.12) and cardiac MSCs (52.67±10.06), and to a lesser extent CPCs (18.60±7.27). Both the EPCs and HUVECs expressed near undetectable levels of SMA (EPC, 0.04±0.01; HUVEC, 0.01±0.01) (Figure 2.10E). GATA4 is expressed by the adult CMs (22.19±0.06) and to a lesser degree by the CPCs (3.6±0.91). The other cell types showed decreasing expression of GATA4 (EPC, 3.09±0.31; MSC, 1.57±0.34) (Figure 2.10F).

DISCUSSION

Unbiased sampling of tissue biopsies from heart failure patients undergoing LVAD implantation represents an ideal source for tissue to isolate and study characteristics of CPCs, EPCs, and MSCs in the context of decompensated heart failure. LVAD recipients on “destination therapy” are desperately in need of regenerative therapy as the only other available option for treatment is cardiac transplantation. In an effort to improve the rather modest outcomes of current cell-based regenerative medicine intervention, the use of multiple cell types in combination or sequentially could enhance efficacy. Indeed, experimental animal studies support the premise of combining CPC and MSC to enhance beneficial effect[55] and ongoing clinical trials are moving this concept into patients. However, these studies are focused upon allogeneic approaches that limit survival, engraftment, and persistence of the donated cell population. The protocol described in this report allows for simultaneous isolation of three distinct cell populations from a single tissue sample: CPC, MSC, and EPC. Each cell type exhibits characteristics that render them desirable to promote regenerative repair. EPCs promote vasculogenesis and angiogenesis and differentiate into mature endothelial cells. *In vivo*, MSCs have been shown to contribute to endogenous regeneration by secretion of paracrine factors that activate endogenous stem cells, promote angiogenesis, protect CMs and reduce scar formation[56, 15, 57]. In animal models, transplanted CPCs give rise to CMs, smooth muscle cells, and endothelial cells[11, 74], but lack the power of MSCs to activate and recruit endogenous stem cells. For this reason, combinatorial cell therapies have been advanced in hopes of initiating synergistic effects in myocardial repair, but no one to date has attempted to inject multiple stem cells

expanded solely from the human heart. With this protocol, combinatorial studies can be performed using three cardiac cell populations isolated from a single heart. These cells can be studied combinatorial or individually to better elucidate how these distinct cell populations regulate and/or contribute to cardiac regeneration following ischemic injury.

Cardiac stem cell populations play intrinsically distinct roles in cardiac regeneration. Insight into what makes each cell type unique will translate to superior clinical application depending upon disease state of the patient. For example, for chronic ischemia the primary intent may be to salvage the CMs and improve blood supply. Consequently, using a cell type that induces vascular regeneration such as EPCs would be important. On the other hand, if the goal were to replace lost CMs, perhaps CPCs supported by MSCs would favor activation of endogenous cardiomyocytes as well as exhibiting inherent cardiomyogenic potential. Alternatively, co-injection of all three cardiac stem cell types may provide the most robust reparative and regenerative outcome. Achieving long-lasting myocardial benefits likely requires the interaction of multiple cardiac cell types and testing this hypothesis is the focus of ongoing experimental studies.

The CPC, MSC, and EPC populations can be reproducibly isolated using samples obtained from multiple patients with varying age and disease etiologies up to 84 years of age. Patients presented with a range in cardiomyopathies and comorbidities including diabetes and coronary artery disease, and/or heavy smokers and drinkers. Success rate of isolating the three cell populations was 80-90 percent. For a minority of patient samples received the *ex vivo* culture resulted in outgrowth from only two populations, which we attribute to a number of possible factors including tissue size,

culture error, or absence of a particular cell type in the biopsy sample received. Not to be overlooked, another potential explanation for inability to expand a particular cell type could be correlated patient etiology and will be interesting to examine in future studies. We were unable to establish such relationships owing to the relatively small number of patients assessed in our isolation sampling. While showing some variation, consistent trends are evident with regard to cell morphology (Figure 2.2), growth kinetics (Figure 2.3), and gene profiles (Figure 2.9). Specifically, gene expression levels for cytokines, extracellular matrix proteins, paracrine and inflammatory factors clustered based on the three cardiac stem cell lineages. EPCs were transcriptionally distinct from CPCs and MSCs that possessed more similar profiles (Figure 2.9). Transcript profiles of EPCs isolated from the heart were comparable to observed profiles in HUVECs (an established endothelial cell line) and cardiac EPCs also retain the capacity to form tubular networks on Matrigel, consistent with endothelial cell phenotypic properties (Figure 2.10).

This protocol provides detailed culture procedures that will allow for stem cell maintenance evidenced by preservation of stem cell markers (Figure 2.4 and Figure 2.8). Key factors for successful propagation and expansion *ex vivo* are culture conditions and growth medium. Each cell type has its own preferential plating density and depending on cell type, differentiation and/or senescence can occur with prolonged culture[52, 68] or due to cell-cell contact if cultured to confluency[75, 76]. CPCs and EPCs are successfully cultured at 50-70% confluency. On the other hand, MSCs prefer close contact with neighboring cells (70-90% confluency), appear cytopathic, and grow extremely slow when cultured below 60% confluency.

Observations when working with these cells have shown that while initially the relative abundance of MSCs is higher compared to either CPCs or EPCs, the latter two populations proliferate quickly (Figure 2.3) and senesce at a later passage than MSCs. For a majority of patients, the MSC population begins to show decreased proliferation around passages 8-10 and will completely senesce a few passages later. From a cell manufacturing point of view, we are able to obtain roughly 100 million cells by passage 10. The majority of CPC and EPC lines will continue to proliferate until passages 15-20, and thus hundreds of millions of cells can be obtained.

The protocol described herein is a highly reproducible and straightforward method independently conducted by multiple individuals at varied training levels ranging from graduate to post-doctoral level. Additionally, the procedure is amenable to being performed under a wide variety of experimental conditions. An example already initiated in our laboratory includes: splitting a single cardiac biopsy in half and conducting initial isolation under normoxic versus hypoxic conditions to study altered oxygen concentration and resulting phenotypic changes that occur in the isolated cardiac stem cell populations. Other applications could include variation in media formulation, such as glucose or growth factor supplementation, or examining differences caused by extracellular matrices and biologically coated surfaces.

Desperate unmet need to alleviate the suffering and burden of heart failure has understandably prompted a rapid progression into clinical trials while necessarily foregoing a deeper fundamental understanding of cardiac stem cell biology or identification of which cell or combination of cells yields the most efficacious outcome to mediate repair and regeneration *in vivo*. Initial clinical trials performed using bone

marrow-derived stem cells were quickly pursued, in part owing to relative ease of isolation and established protocols, but yielded generally disappointingly modest myocardial recovery.[77] The challenging frontier for myocardial regenerative medicine with the ever-expanding tapestry of potential interventional strategies requires careful analysis of critical factors in cell biology such as self-renewal potential, survival, and mechanisms that allow particular cell population(s) to repopulate the damaged myocardium more effectively than others. Each individual cell type may be specialized to perform in a specific context, and combinations of cell types likely will exert actions through concerted cooperative networking that any one single cell type cannot provide. Equipped with this basic understanding, secondary considerations of cell dosage, timing and delivery approach will need to be optimized. These concepts represent a small sampling of the nearly limitless conceptual possibilities that lie ahead for myocardial regenerative research. All journeys begin with a single step, and this protocol paves the way by isolating multiple cardiac cell populations that can be studied individually or combinatorial so that the field of cardiac stem cell therapy can come to a better understanding on which stem cell population(s) hold the most promise for cardiac regeneration.

TABLES

Table 2.1. List of Media

	Component	Catalog Number
Cardiac Stem Cell Medium	F12 HAM's (1x)	SH30026.01, HyClone
	10% ES FBS	16141079, Gibco
	1% Penicillin-Streptomycin-Glutamine (100X)	10378016, Gibco
	5 mU/mL human erythropoietin	E5627, Sigma-Aldrich
	10 ng/mL human recombinant basic FGF	HRP-0011, Biopioneer
	0.2 mM L-Glutathione	66013-256, Sigma-Aldrich
Endothelial Progenitor Cell Medium	EBM-2 Basal Medium	CC-3156, Lonza
	EGM-2 Kit Supplements and Growth Factors: • 0.5 mL Human Epidermal Growth Factor • 0.5 mL Insulin-Like Growth Factor-1 • 0.5 mL Vascular Endothelial Growth Factor • 0.5 mL HEPARIN • 0.5 mL Gentamicin Sulfate Amphotericin-B • 0.5 mL Ascorbic Acid • 2.0 mL Human Fibroblast Growth Factor-B • 2.0 Hydrocortisone • 10 mL FBS	CC-4176, Lonza
Mesenchymal Stem Cell Medium	10.1 g/L MEM Eagle, Alpha Modification	M0644, Sigma-Aldrich
	20% FBS	FB-01, Omega Scientific, inc.
	1% Penicillin-Streptomycin-Glutamine (100X)	10378-016, Gibco
	Cell Culture Grade Water	
Basic Buffer	11 g/L MEM Eagle, Joklik Modification	M0518, Sigma-Aldrich
	3 mM HEPES	H3375, Sigma-Aldrich
	1% Penicillin-Streptomycin-Glutamine (100X)	10378-016, Gibco
	10 mM Taurine	T0625, Sigma-Aldrich
	Insulin, solvate in 3% Acetic Acid/PBS	I-5500, Sigma-Aldrich
	1% Amphotericin B	15290-018, Invitrogen
	50 mg Gentamicin	G1397, Sigma-Aldrich
	Cell Culture Grade Water	

Table 2.2. List of Antibodies

Antibody	Vendor	Catalog Number	Dilution Flow	Dilution Slides
C-Kit (CD117)	R&D systems	AF1356	1:33	1:200
Thy-1 (CD90)	Biolegend	328109	1:33	1:200
Endoglin (CD105)	Biolegend	323203	1:33	1:200
Prominin-1 (CD133)	Thermo Fisher Scientific	PA5-38014	1:50	1:600
CD34	Santa Cruz Biotechnology	Sc-9095	1:33	-
PTPRC (CD45)	Biolegend	368507	1:33	-
DAPI	Sigma-Aldrich	D9542	-	1:10,000
Phalloidin	Thermo Fisher Scientific	A12379	-	1:1,000

Table 2.3. List of Primers

	Target	Fwd Primer Sequence	Rev Primer Sequence
Growth Factors and Cytokines	ANGPT2	TCCAAGCAAAATTCCATCATTG	GCCTCCTCCAGCTTCCATGT
	NRG1	GCCAATATCACCATCGTGGAA	CCTTCAGTTGAGGCTGGCATA
	PECAM1	CCAAGCCCGAACTGGAATCT	CACTGTCCGACTTTGAGGCT
	FGF2	CTGGCTATGAAGGAAGATGGA	TGCCCAGTTCGTTTCAGTG
	GATA4	CTCAGAAGGCAGAGAGTGTGTCAA	CACAGATAGTGACCCGTCCCAT
	HBEGF	ACAAGGAGGAGCACGGGAAAAG	CGATGACCAGCAGACAGACAGATG
	HGF	GGCTGGGGCTACACTGGATTG	CCACCATAATCCCCCTCACAT
	IGF2	GACCGCGGCTTCTACTTCAG	AAGAACTTGCCCACGGGGTAT
	SMA	CCCAGCCAAGCACTGTCAGGAATCCT	TCACACACCAAGGCAGTGCTGTCC
	CXCL12	CAGTCAACCTGGGCAAAGCC	AGCTTTGGTCCTGAGAGTCC
	TGFβ1	AAGGACCTCGGCTGGAAGTGC	CCGGGTTATGCTGGTTGTA
ECM Proteins	FN1	GAAGGCTTGAACCAACCTACG	TGATTCAGACATTCGTTCCCAC
	MMP1	CTCAATTTCACTTCTGTTTTCTG	CATCTCTGTCGGCAAATTCGT
	COL1A1	GTCGAGGGCCAAGACGAAG	CAGATCACGTCATCGCACAAC
	COL3A1	GGTGCTCGGGGTAATGACG	TCCAGGGAATCCGGCAGTT
	TIMP1	TGCCGCATCGCCGAGAT	ATGGTGGGTTCTTGGTG
Inflammatory Factors	IL1B	CCCTAAACAGATGAAGTGCTCCTT	GTAGTCGGATGCCGCCAT
	IL6	TCGAGCCCACCGGGAACGAA	GCAGGGAAGGCAGCAGGCAA
	TNF	GCCGCATCGCCGTCTCCTAC	AGCGCTGAGTCGGTCACCCT
	IRF1	TTTGTATCGGCCTGTGTGAATG	AAGCATGGCTGGGACATCA
	MHC Iα	GCCCACTCACAGACTGACC	CTGGATGGTGTGAGAACCGTC
	MHC Iβ	CCTGAGATGGGAGCCGTCTT	CTCCGATGACCACAACTGCT
	MHC II DQα	TGTCTGGCAGTTGCCTATGT	TCAGGAACCTCATTGGTGGC
	MHC II DQβ	CCTCCACCAGCAGGACTC	GCAGCTAGGAATTCTGGGCA
	MHC II Trans	AGAGCACATAGGACCAGATGA	GCTTCCAGTGCTTCAGGTCT
	CD40	ACCCTTGGACAAGCTGTGAG	TAAAGACCAGCACCAAGAGG
	CD80	GCAGGGAACATCACCATCCA	TCACGTGGATAACACCTGAACA
	CD86	GGGACTAGCACAGACACACG	CTGAAGTTAGCAGAGAGCAGGAA
	18S	CGAGCCGCCTGGATACC	CATGGCCTCAGTTCCGAAAA

Table 2.4. Clinical Profile of Patients Used for Stem Cell Isolation

Patient ID	Age, y	Sex	EF%	Cardiac Index	Diabetes	Hyper-lipidemia	Smoker	Infarct	Ischemia	Ace Inhibitor	β-blocker	Anticoagulant	NYHA
H13-064	38	M	15-25%	-	X	X	X	✓	✓	X	✓	✓	IV
H13-065	54	M	-	-	-	-	-	-	-	-	-	-	-
H13-066	55	M	15%	1.62	X	-	✓	✓	✓	✓	✓	✓	IV
H13-068	62	M	20%	-	✓	✓	✓	✓	✓	✓	✓	✓	III
H13-070	42	M	20%	1.54	X	-	-	✓	-	✓	✓	-	IV

EF indicates ejection fraction; NYHA, New York Heart Association; patient information is (✓) positive; (X) negative; (-) unavailable

FIGURES

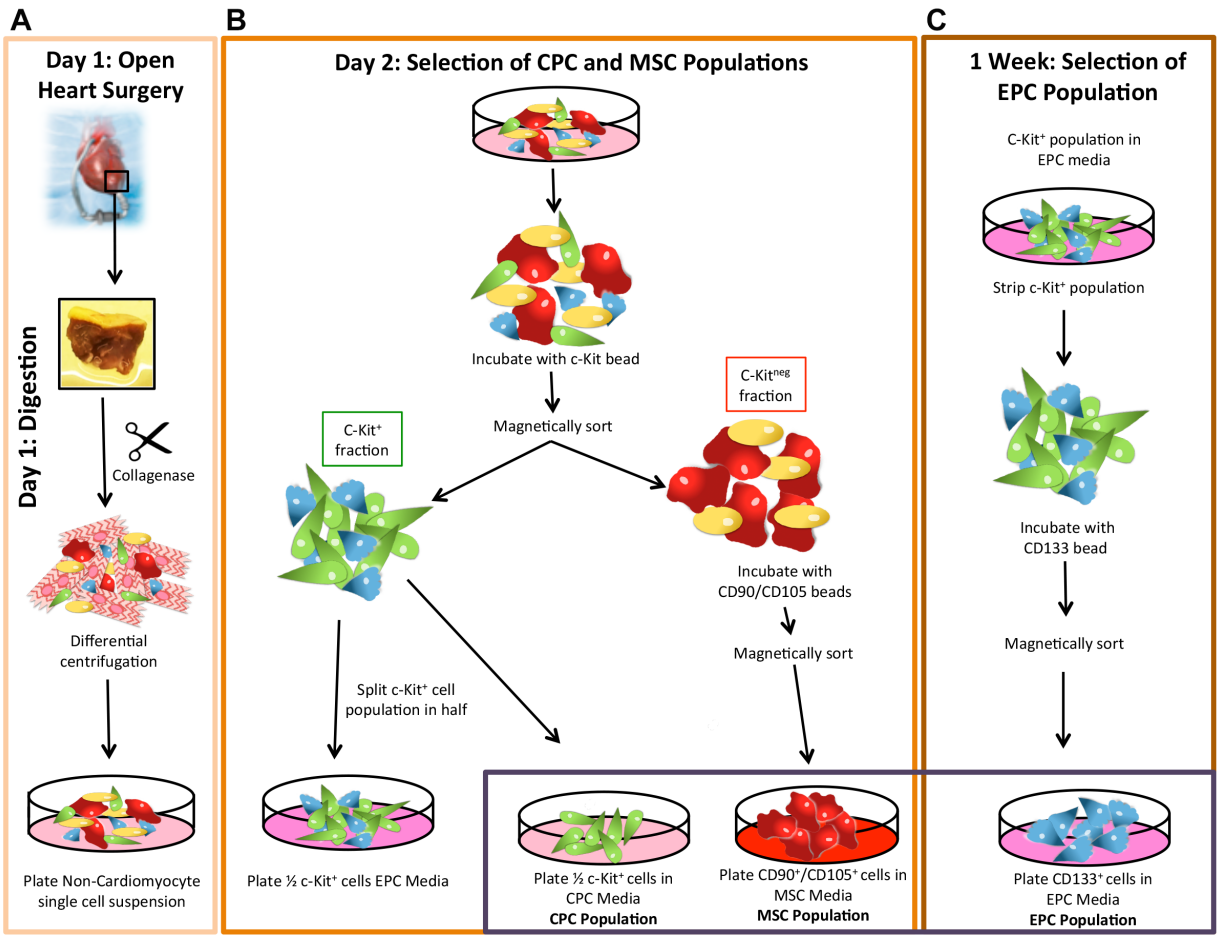

Figure 2.1. Cardiac stem cell isolation protocol
Schematic representation of the process used to isolate cardiac cells from LVAD tissue. Following open-heart surgery, the tissue plug is digested to the single cell level and, following centrifugation to remove the CMs, plated overnight at 37°C in CO2 incubator. Day 2, the single cell suspension is incubated with microbeads conjugated to c-Kit and magnetically sorted. C-Kit+ cells are split in half with a portion being plated in CPC media and the other half being plated in EPC media. The c-Kit- fraction is further sorted for CD90 and CD105 with positive cells being plated in MSC media. 1 week later, the c-Kit+ cells plated in EPC media are further enriched for CD133. Red cells indicate mesenchymal stem cell (MSC) population; green cells indicate cardiac progenitor cell (CPC) population; blue cells indicate endothelial progenitor cell (EPC) population; yellow cells indicate non-specific cell population.

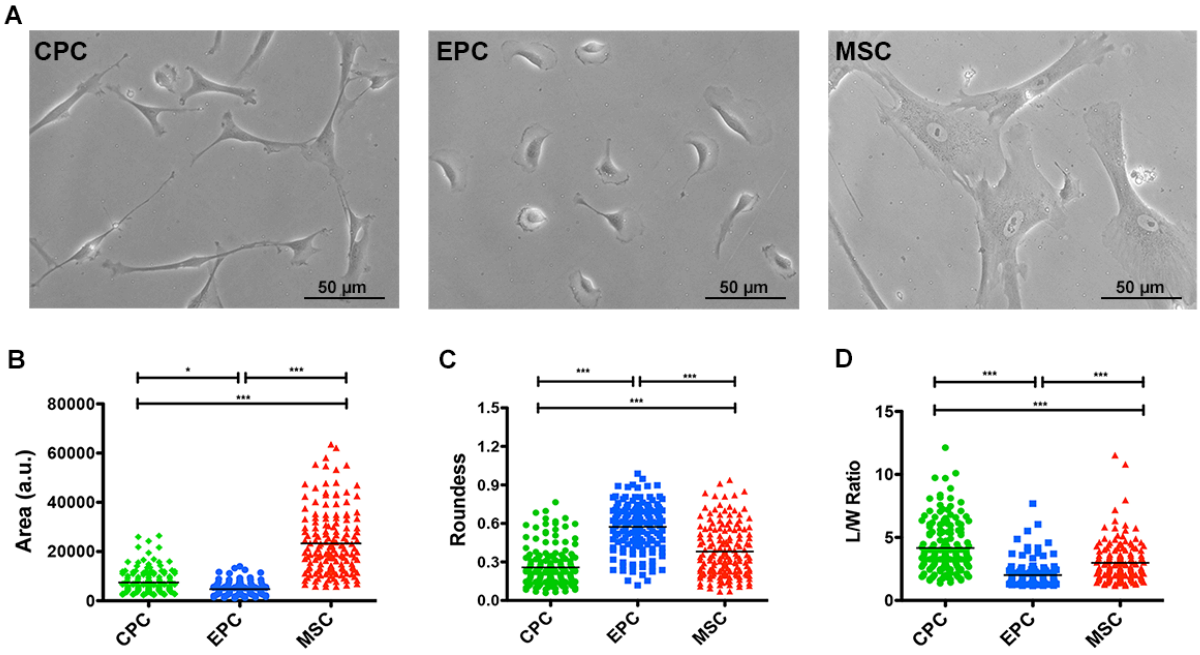

Figure 2.2. Isolation of three distinct cardiac stem cell populations from LVAD patients
A, Representative phase contrast images for the three isolated cardiac cell populations. B-D, Cell morphometric parameters measuring Area (B), Roundness (C), and Length-to-Width (L/W) ratio (D) (n=4-5 patients, minimum of 30 cells traced per cell type per patient). Data are presented as 1-way ANOVA, *p<0.01, **p<0.001, ***p<0.0001. Scale bar, 50 uM.

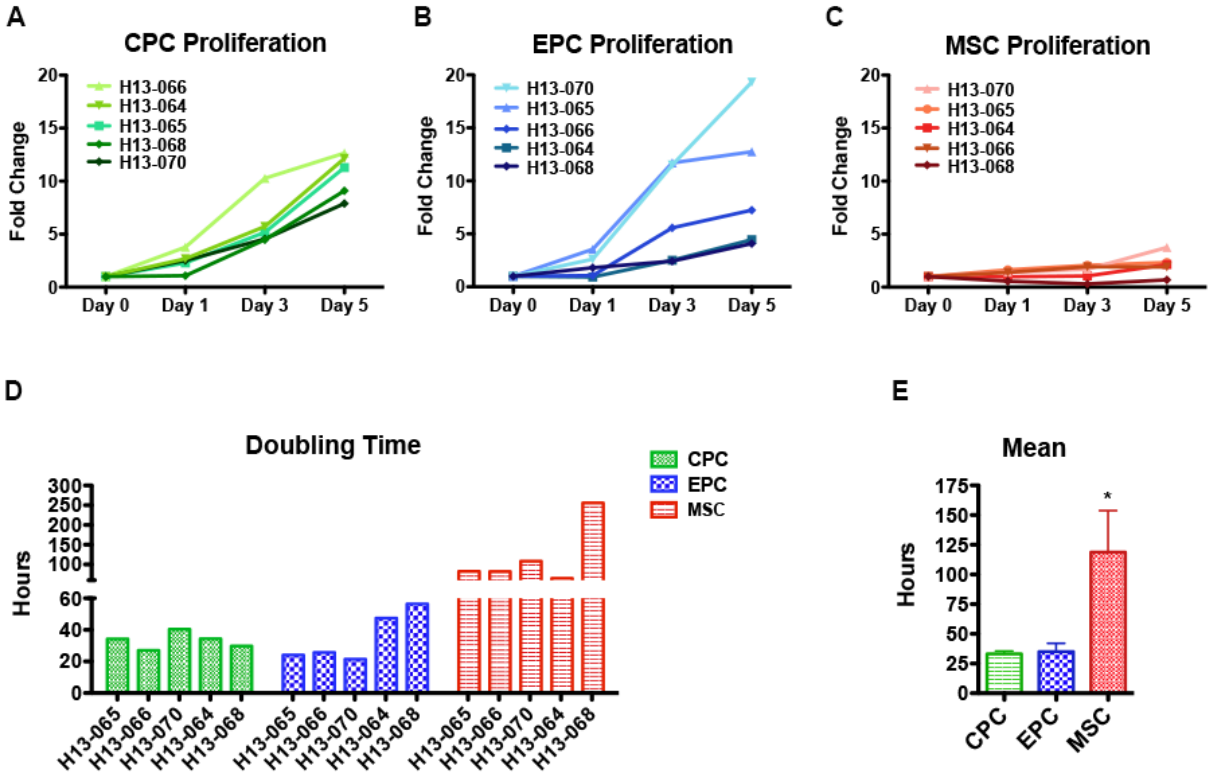

Figure 2.3. Cardiac stem cell populations exhibit distinct growth kinetics
A-C, Cardiac cell proliferation measured using CyQuant assays at Day 0, Day 1, Day 3, and Day 5 for CPC (A), EPC (B), and MSC (C). D, Bar graph of doubling times calculated using periods of exponential cell growth for each cell line. E, Bar graph of mean doubling time for each cell type (n=5 patients). Data are presented as 1-way ANOVA, •p<0.05.

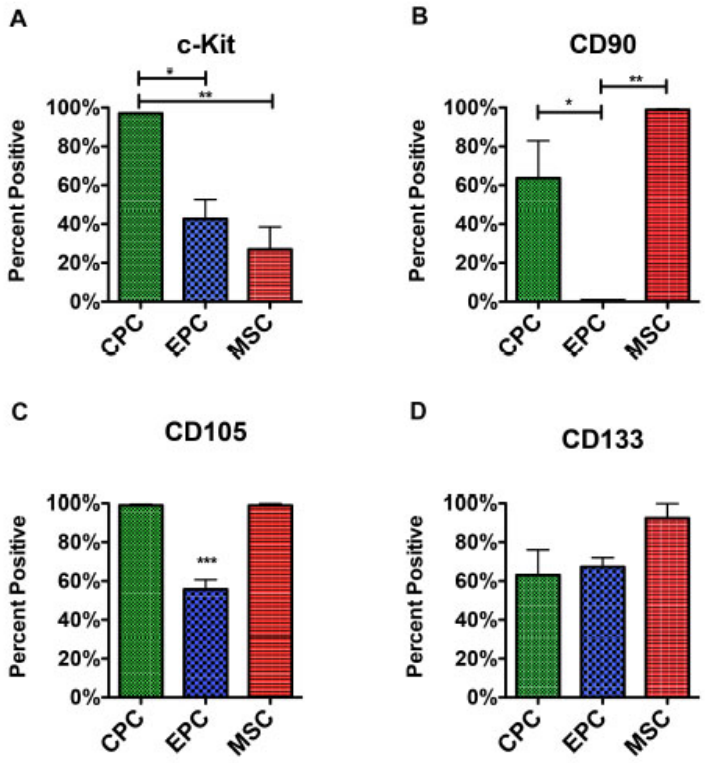

Figure 2.4. Flow cytometry analysis of markers expressed upon in vitro culture
A-D, Single cell suspensions stained with antibodies for the markers used in cell isolation. Flow cytometry analysis of cardiac cell populations sorted for the presence of c-Kit (A), CD90 (B), CD105 (C), and CD133 (D) (n=3 patients per marker). Data are presented as 1-way ANOVA, *p<0.05, **p<0.01, ***p<0.001.

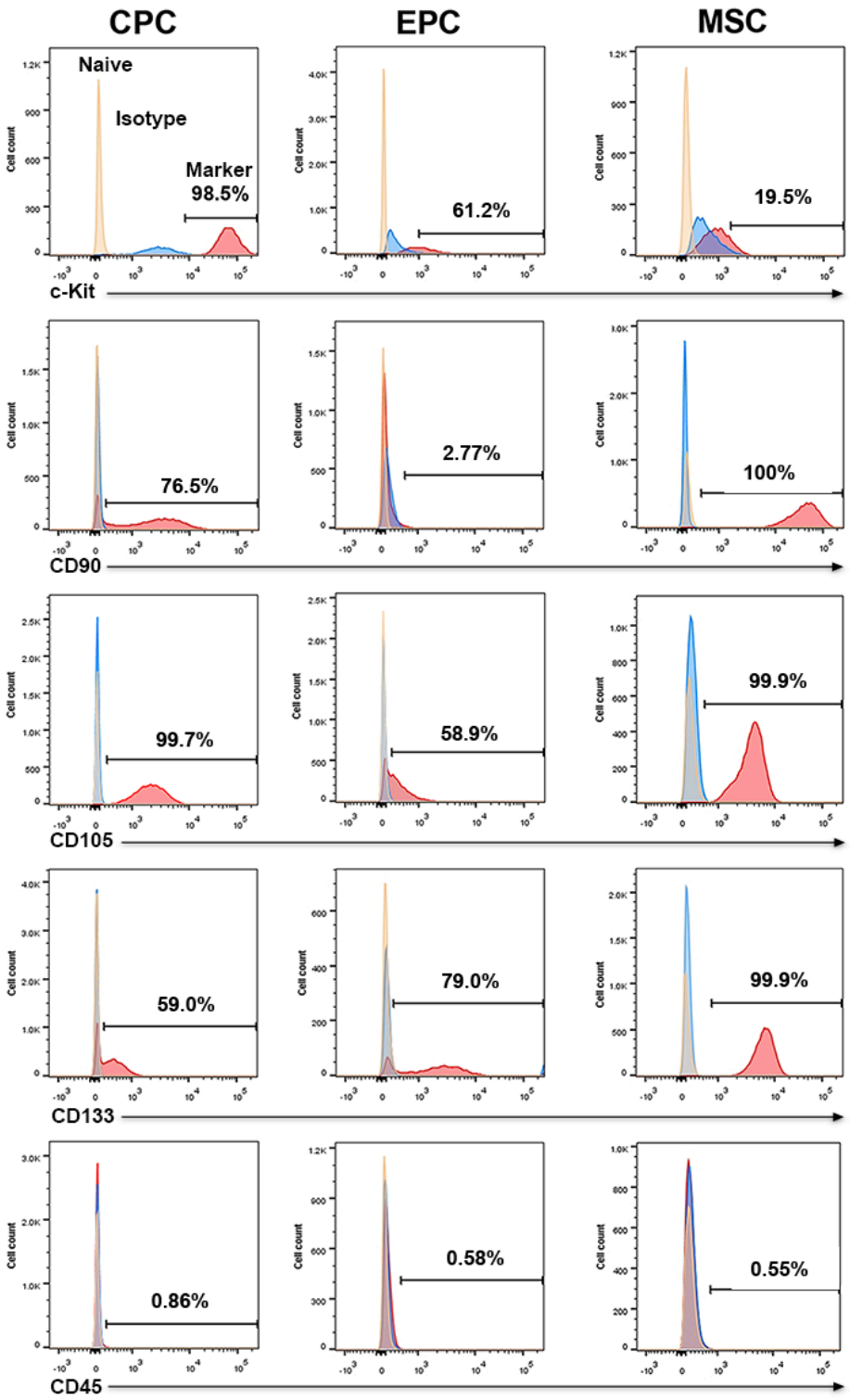

Figure 2.5. Flow cytometry analysis of stem cell markers
Representative flow cytometry plots analyze the percent of c-Kit, CD90, CD105, CD133, and CD45 expression in the three cardiac cell populations.

Figure 2.6. Analysis of markers used for stem cell isolation
A-C, Flow cytometry data from individual patient lines showing percent c-Kit, CD90, CD105, and CD133 expression in CPC (A), EPC (B), and MSC (C) fixed in 4% paraformaldehyde (PFA). D-F, Flow cytometry data from the same three patient lines showing percent of CD90, CD105, and CD45 expression of live CPC (D), EPC (E), and MSC (F).

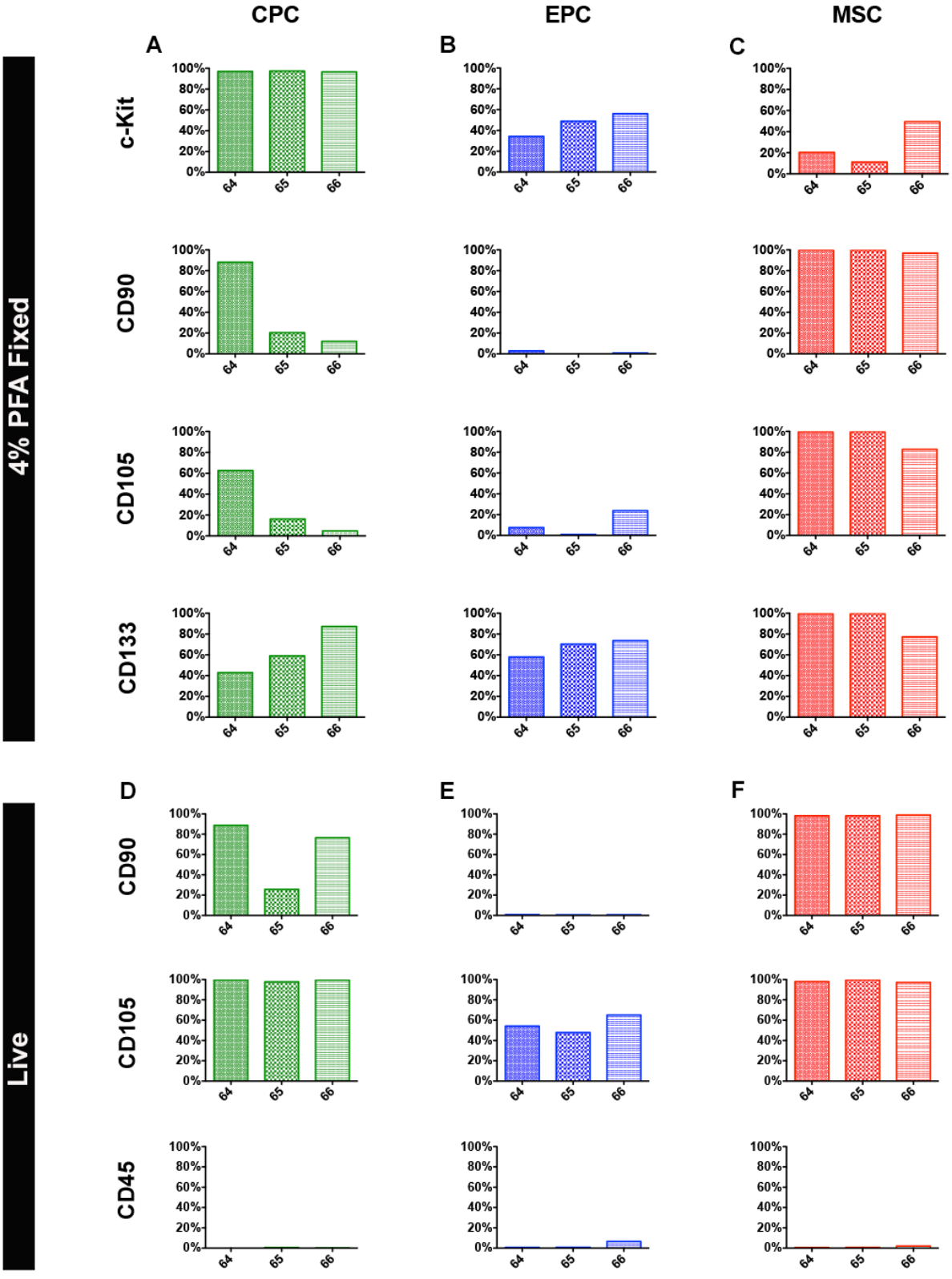
CPC
EPC
MSC
A
B
C
4% PFA Fixed
c-Kit
CD90
CD105
CD133
D
E
F
Live
CD90
CD105
CD45
100%
80%
60%
40%
20%
0%
64
65
66

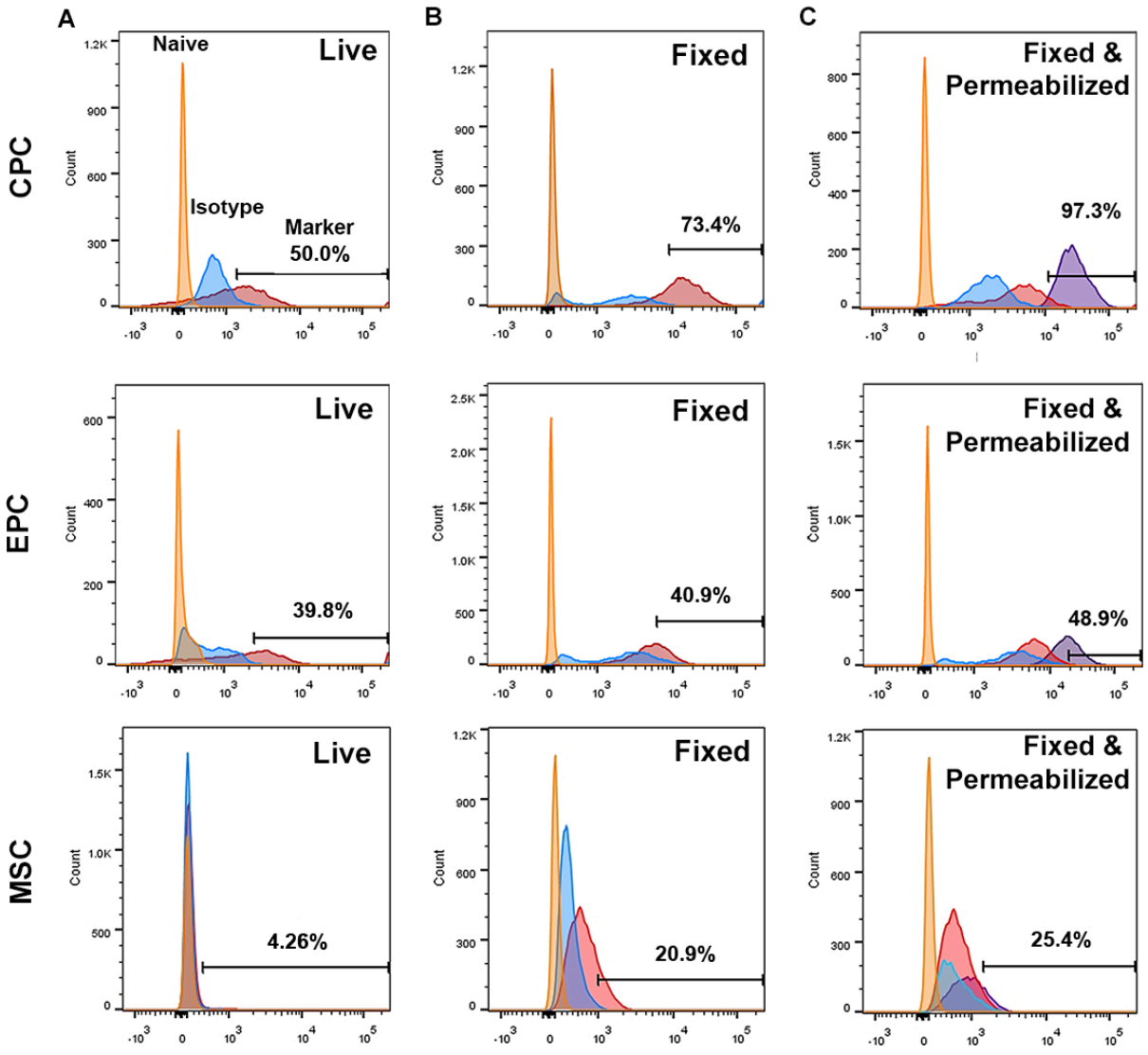

Figure 2.7. C-Kit Internalization occurs more readily in CPC than other cardiac stem cell populations A-C, Representative flow cytometry plots showing the percent of CPC, EPC, and MSC that express c-Kit when antibody labeling live cells (A), cells fixed in 4% paraformaldehyde (B), or cells that were both fixed and permeabolized (C).

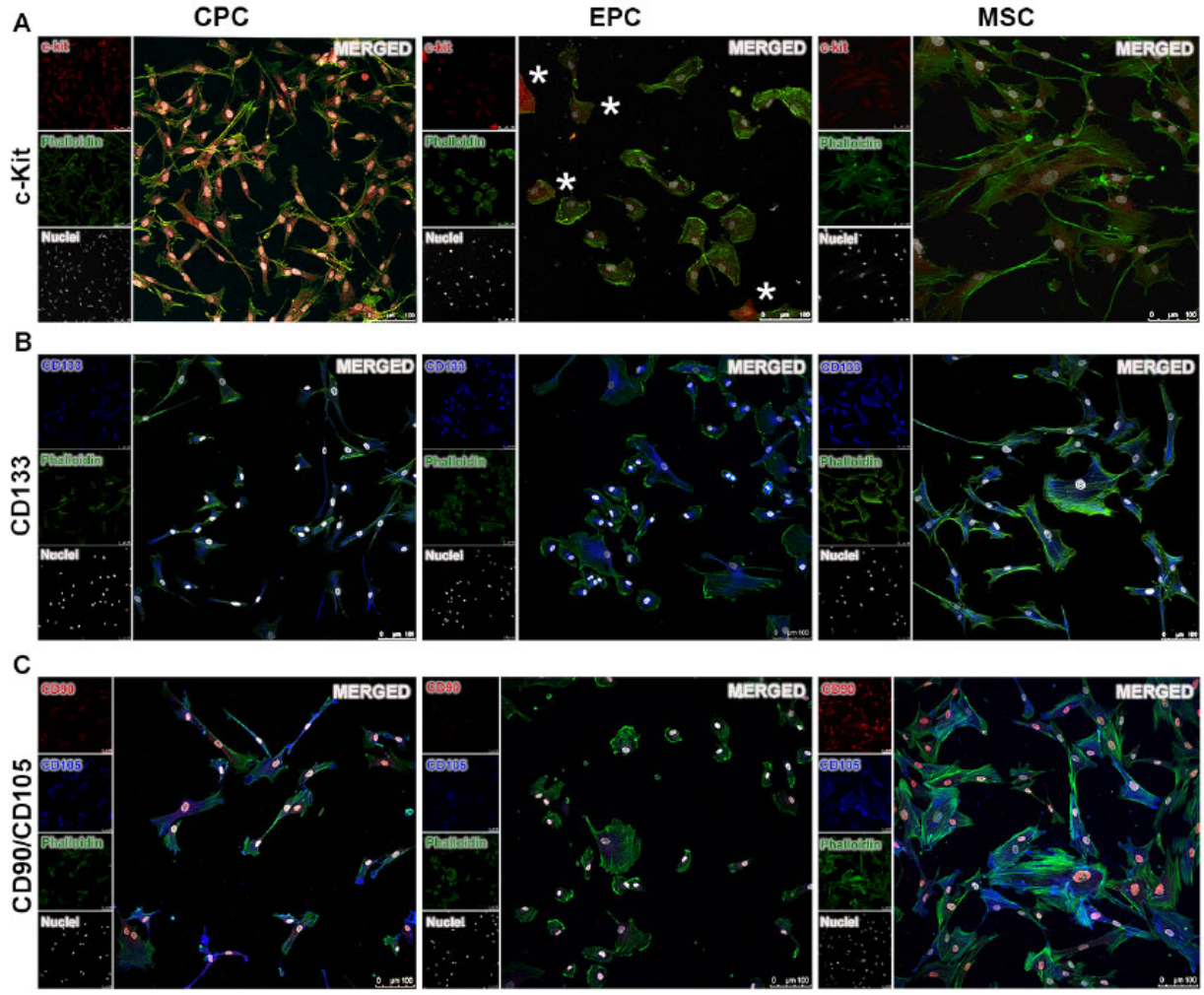

Figure 2.8. Immunofluorescence imaging of stem cell markers
A, Representative florescence microscopy showing c-Kit localization in CPC, EPC, and MSC (red, c-Kit; green, Phalloidin; white, Nuclei (DAPI)). B, Immunofluorescence labeling of the mesenchymal markers CD90 and CD105 showing varying degree of co-localization for these two markers in the three cell populations (red, CD90; blue, CD105; green, Phalloidin; white, Nuclei (DAPI)). C, CD133 expression revealed by immunofluorescence in the cardiac cells (blue, CD133; green, Phalloidin; white, Nuclei (DAPI)). Scale bar, 100 um. Asterisks (*) indicate cells positive for c-Kit.

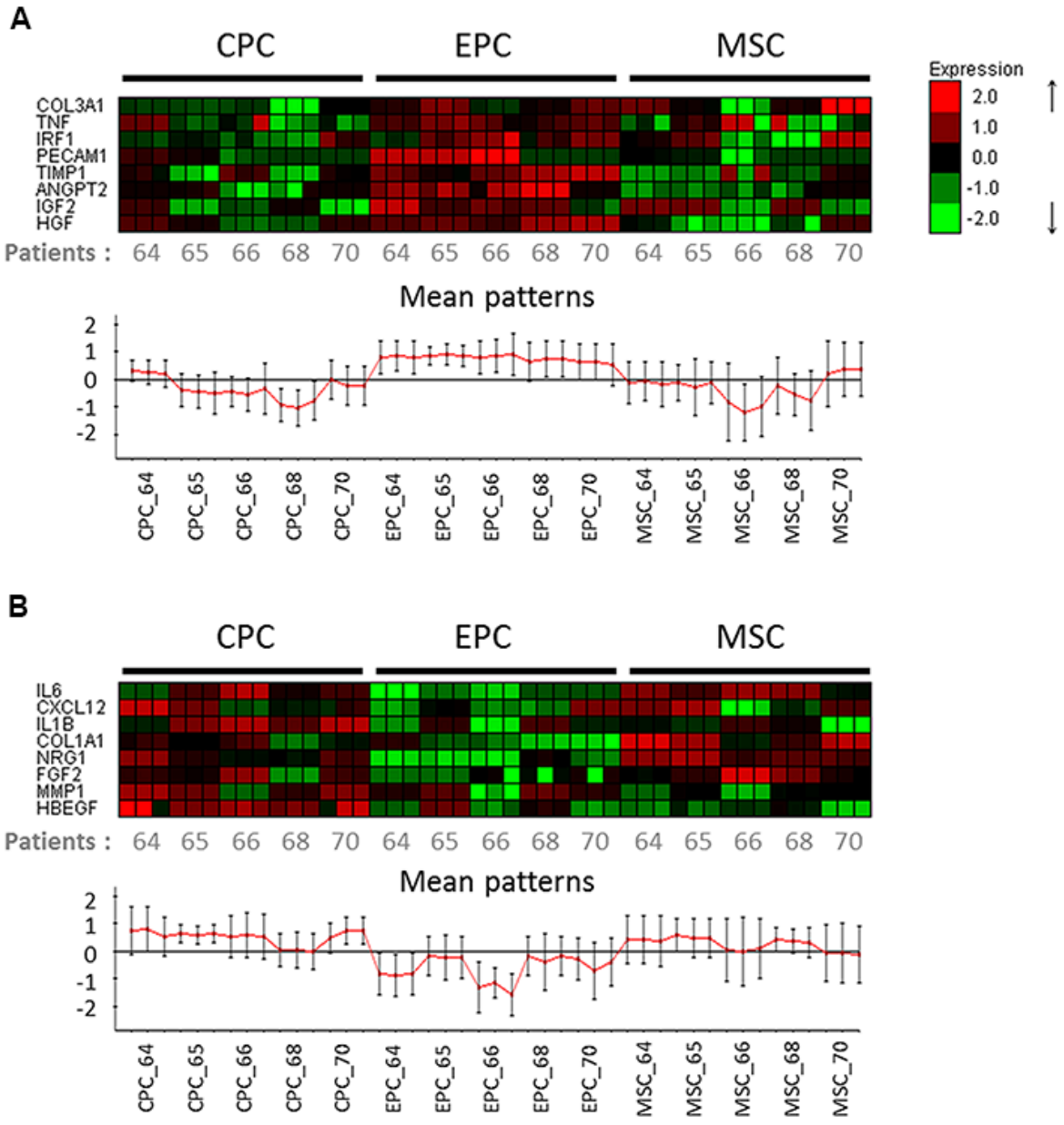

Figure 2.9. Supervised cluster analysis of gene expression levels in cardiac stem cells
A-B, Heatmaps representing differentially expressed genes in three different cell types. A, A cluster of genes showing specific up-regulation in EPC, but not CPC and MSC. B, A second cluster showing specific down-regulation in EPC, but not CPC and MSC (n=5 patients).

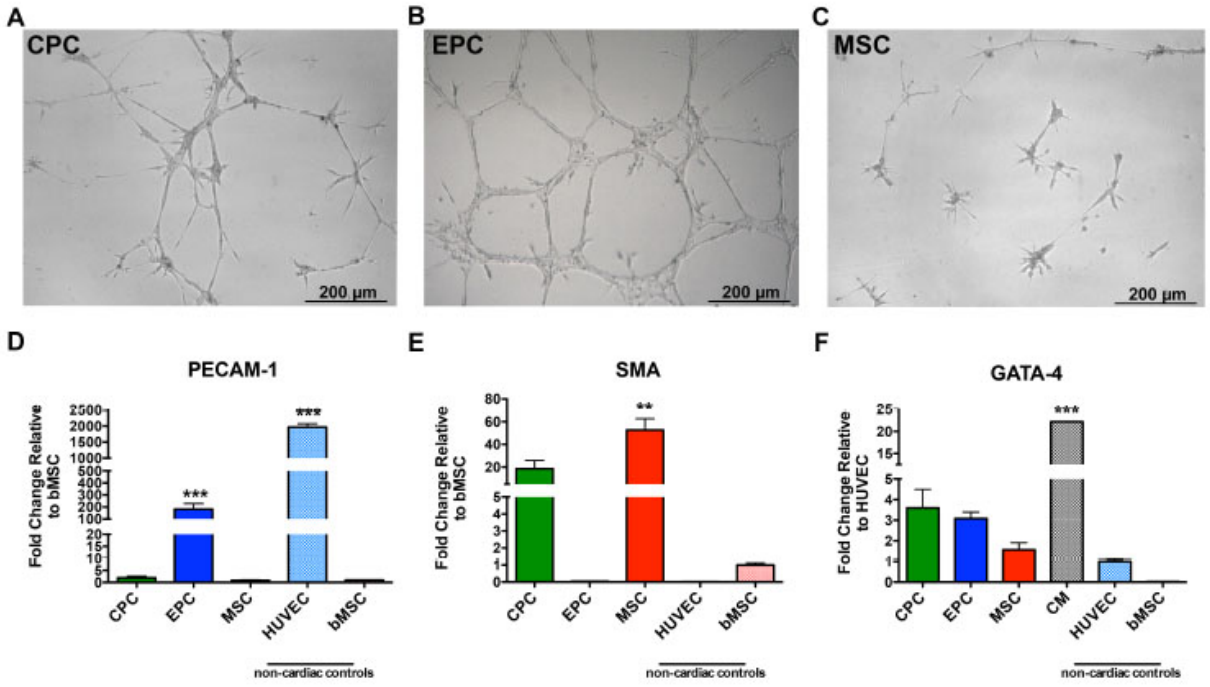

Figure 2.10. In vitro lineage assessment and comparison to established cell lines
A-C, Representative images of tubular network formation when plated on growth factor reduced matrigel for CPC (A), EPC (B), and MSC (C). D-F, Bar graphs using established cell lines, HUVECs, bMSCs and adult CM, to assess the potential of cardiac stem cells to commit to an angiogenic (D), smooth muscle (E), and cardiogenic fate (F) (n=3 patients). Data are presented as 1 Way ANOVA, **P<0.001, ***p<0.0001, versus cell type used for normalization. Scale bar, 200 um. CM indicates Cardiomyocytes; GATA4, GATA binding protein 4; PECAM-1, Platelet endothelial cell adhesion molecule; and SMA, a-smooth muscle actin (SMA).

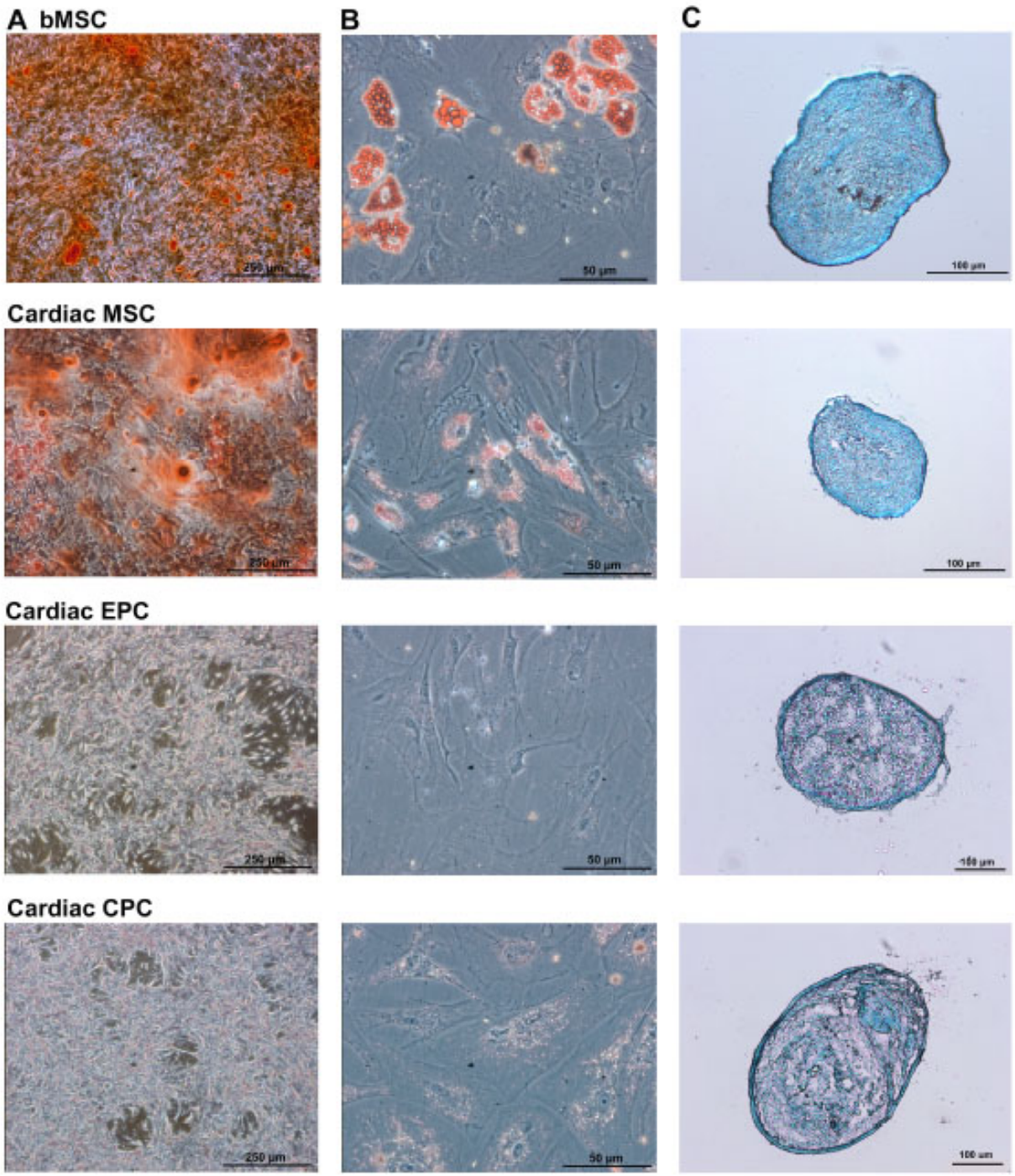

Figure 2.11. Mesenchymal stem cell differentiation potential
A-C, Differentiation potential for osteogenesis, adipogenesis, and chondrogenesis was assessed for the three cardiac stem cell populations relative to bMSC. For osteocyte differentiation cells were stained with Alizarian-Red Staining Solution (A), for adipocyte differentiation cells were stained with Oil Red O (B), and for chondrocyte differentiation cells were embedded in optimal cutting temperature (OCT) compound, cryosectioned and stained with Alcian-Blue Staining Solution (C) (n= 3 patients).

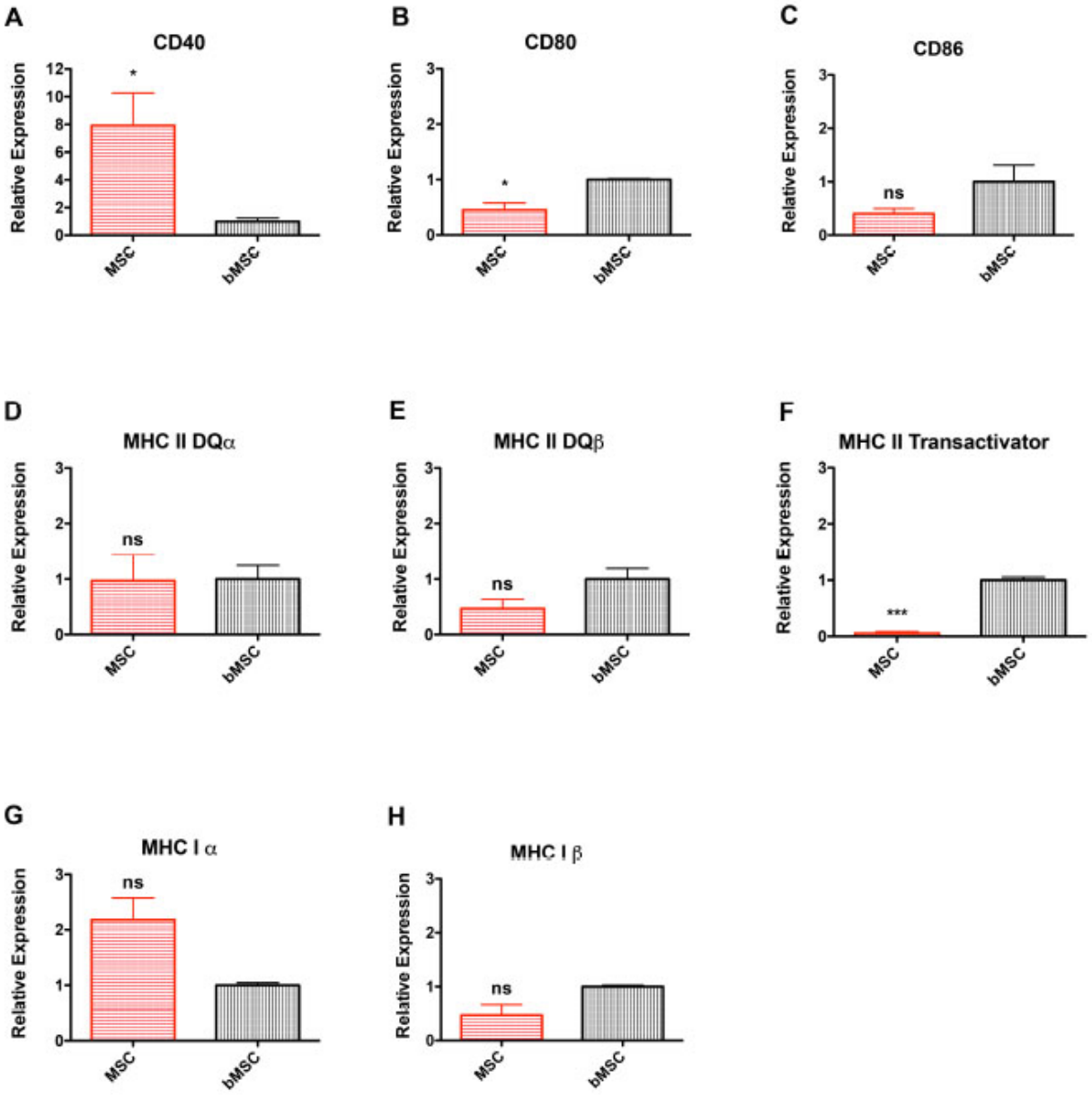

Figure 2.12. Expression levels of MHC Class I and Class II and co-stimulatory molecules A-H, Relative expression of cardiac derived MSC for co-stimulatory molecules CD40, CD80, and CD86 (A-C), MHC Class II molecules (D-F) and MHC Class I molecules (G and H) (n=5 patients) compared to control bMSCs. Data are presented as t test, *p<0.01, ***p<0.0001.

Chapter 2, with slight modifications, is a reprint of the material as it appears in Circulation Research, 2017. Concurrent Isolation of Three Distinct Cardiac Stem Cell Populations from a Single Human Heart Biopsy. Monsanto MM, White KS, Kim T, Wang BJ, Fisher K, Ilves K, Khalafalla FG, Casillas A, Broughton K, Mohsin S, Dembitsky WP, Sussman MA. The dissertation author was the primary author and investigator on this manuscript.

CHAPTER 3

Enhancing Myocardial Repair with CardioClusters

INTRODUCTION

Cellular therapy continues to be pursued as an experimental approach to treat cardiomyopathic damage following infarction in both preclinical animal models and human clinical trials[40, 42-45, 50, 78-80]. While promising, cellular therapy has been hindered by marginal improvement in cardiac function, in part due to low engraftment and persistence of the transplanted cells[38, 81]. As such, improving cell retention and survival has been a major area of research using a plethora of techniques, including biomaterials[8, 9], cytokines and growth factors[10], repeated administration of cells[54], or genetic enhancement with pro-survival and anti-apoptotic genes[11, 12]. Combinatorial cell therapies are an additional conceptual approach intended to promote additive or synergistic effects in myocardial repair[19, 82-84]; however, cell retention and survival remain poor whether single or combinatorial cell delivery is attempted. Furthermore, coincident delivery of multiple cell populations does not ensure effective cell interaction and cross talk following injection. Therefore, novel strategic approaches to prolong cell retention and survival are highly sought after, preferably also favoring cell phenotypic characteristics that promote short-term mitigation of injury and long-term recovery of myocardial structure and function.

Traditional monolayer culture, while both prevalent and convenient, promotes loss of cell identity and spatial organization, thereby impacting many cellular aspects, including cell morphology, proliferation, differentiation, viability, and transcriptome profile[85-87]. Approaches intended to mitigate deleterious effects of artificial *in vitro* environments through recreating native three dimensional (3D) architecture include engineered heart tissue grafts[88], organoids[89, 90], and 3D bioprinting.[91, 92] When grown in

3D cells aggregate and form complex cell-cell and cell-matrix interactions that mimic the natural environment found *in vivo,* allowing for cell differentiation and tissue organization not possible in conventional two-dimensional (2D) culture systems[93]. For example, cardiosphere formation[23, 24] enhances cellular communication through gap junction protein connexin 43 fostering signal propagation and cell differentiation[20, 25, 26]. However, cardiospheres are formed by random cell aggregation leading to inconsistent cell characterization markers[23, 24], variable sphere size, and muddled communication within the aggregate microenvironment[23, 24, 28]. A superior preferable methodology would utilize combinations of defined cell populations aggregated in 3D under controlled conditions that allow for intact delivery without dissociation of the spherical microenvironment to promote preservation of cellular phenotype and optimize cellular retention. This combination of desired features formed the rational basis for our novel methodological approach distinct in several critical aspects from cardiosphere-derived cell therapy.

A ‘next generation‘ conceptual approach for a deliverable cell therapeutic based upon the aforementioned literature precedents would involve 1) combinations of multiple cardiac-derived cell types, 2) *ex vivo* culture adaptation to a 3D microenvironment to maximize cellular interaction, 3) control over cell composition, cell number, and aggregate cell volume, and 4) capability to deliver *ex vivo* formed cell aggregate ‘niches’ intact to facilitate preservation of microenvironment biological properties and retention. Guided by these stipulated parameters to create a novel artificially engineered cell aggregate, inception began with essential methodological studies to isolate and expand three distinct cardiac-derived interstitial cell types from a single human heart biopsy as previously reported by our group[13]. Human cardiac tissue of varying age and gender

was used as source material to isolate c-Kit^{+} cardiac interstitial cells (cCIC), mesenchymal stem cells (MSCs), and endothelial progenitor cells (EPCs). Having isolated and characterized three distinct cardiac interstitial cell types each known to possess beneficial properties to blunt cardiomyopathic damage, a protocol was designed for spontaneous self-assembly of mixed cell populations into an optimal conceptual engineered solution that we have named “CardioClusters.”

CardioClusters harness the distinct phenotypic attributes of three well defined cardiac cell populations. MSCs support myocardial reparative activity through secretion of paracrine factors that activate endogenous cells, promote angiogenesis, protect cardiomyocytes, and reduce scar formation[14, 15]. MSCs also secrete cell adhesion molecules such as integrins and cadherins integral to cellular aggregation[36]. EPCs promote paracrine dependent vasculogenesis and angiogenesis and differentiate into mature endothelial cells[17, 18]. Prior studies demonstrate EPCs transplanted *in vivo* are capable of forming microvessels, but regress without MSCs to support vessel maturity[29, 94]. cCICs distributed in the CardioCluster contribute to support of myocardial homeostasis, response to injury, and remodeling. CardioCluster characteristics are particularly well suited to mediating myocardial repair in the wake of acute pathological damage by providing a more natural niche microenvironment for augmented delivery and extended functional activity to improve the outcome of cellular therapy.

CardioClusters advance the application of combinatorial cell therapy by integrating complementary and synergistic properties from multiple cardiac-resident cell types into a single injectable product. CardioCluster formation is a rapid, reproducible, and controllable process demonstrated in preclinical testing to mediate significant

improvements in myocardial structure and function following infarction injury. Enhancement of cell therapy with CardioClusters represents an important advance to improve clinical application of cell therapy for treatment of cardiomyopathic damage and disease.

METHODS

Human Cardiac Interstitial Cell Isolation

NIH guidelines for human research were followed as approved by IRB review (Protocol #120686). Neonatal heart tissue procured from post-mortem infants provided by a commercial source (Novogenix Laboratories) was used for isolation of human cardiac cells. The protocol detailing cardiac cell isolation can be found in our previous publication[13]. Briefly, fatty tissue was excised and remaining cardiac tissue was suspended in Basic Buffer (15 mL) and minced into 1 mm^3 pieces. After mincing, tissue and Basic Buffer were collected in 50 mL Falcon tube. Digestive solution containing collagenase, type II 225 U/mg dry weight (Worthington, catalog #LS004174, Bio Corp, Lakewood, NJ) was dissolved in Basic Buffer (2-2.5 mg/mL) and incubated with tissue pieces for 1.5-2 hours at 37°C with continuous shaking. Digestion solution was refreshed at the one-hour time point and resulting suspensions were centrifuged at 350 *g* and resuspended in cCIC media (see Table 1). Final suspension was filtered through a 100-µm filter (Corning, Inc., catalog #352360) followed by a 40-µm filter (Corning, Inc., catalog #352340) and centrifuged at 150 *g* for 2 minutes to collect CMs. The supernatant was collected and centrifuged at 350 *g* and resuspended in cCIC media and incubated overnight at 37°C in 5% CO_2 incubator. The following day, cells in suspension were collected in 50 mL Falcon tube. Any cells attached were dissociated using a 1:1 mixture of Cellstripper (Corning, catalog #25-056-CI) and TrypLE Express (1X) (Thermo Fisher Scientific, catalog #12604-013). Resulting suspension was filtered through a 40-µm filter, centrifuged at 350 *g*, and resuspended in wash buffer (PBS plus 0.5% bovine serum albumin).

To isolate c-Kit$^+$ cells, suspension was incubated with c-Kit–labeled beads (Miltenyi Biotec, catalog #130-091-332) and sorted according to the manufacturer's protocol. The c-Kit$^+$ fraction was divided as such: half the population was suspended in cCIC media (see Table 1) and the other half was suspended in EPC media (see Table 1). The c-Kit$^-$ population was further incubated with CD90/CD105–labeled beads and sorted according to the manufacturer's protocol (Miltenyi Biotec, catalog #130-096-253/130-051-201). Cells positive for CD90/CD105 were suspended in MSC media (see Table 1). To isolate an EPC population, at 1 week the c-Kit$^+$ population plated in EPC media was further sorted using CD133–labeled beads and sorted according to the manufacturer's protocol (Miltenyi Biotec, catalog #130-097-049). All cells were cultured at 37°C in 5% CO_2 incubator in their respective growth media. cCIC and EPC were split 1:2 when they reached 60-70% confluency. MSC were split 1:2 when they reached 90% confluency. All cells used in this study were mid-passage (passages 5–10).

CardioCluster Formation

CardioClusters are formed using 96 well, ultra-low attachment multiwell round-bottom plates (Corning, catalog #CLS7007) in a two-step process. Step 1 generates the inner core composed of cCICs and MSCs in a 1:2 ratio. The inner core of cCICs and MSCs is seeded in 100 µL/well MSC media for 24 hours at 37°C in 5% CO_2 incubator. Step 2 forms the outer EPC layer using a cell number equal to the number of cells used to create the central core. The EPCs are added in an additional 50 µL/well MSC media and incubated at 37°C in 5% CO_2 for an additional 24 hours until CardioCluster 3D

structure has formed. The radius of a CardioCluster is approximately 150 μm, composed of a total of 400±100 cells.

Flow Cytometry

For live cell analysis, single cells were suspended in 100 μL wash buffer and incubated with primary antibody (see Table 2 for dilutions) on ice for 30 minutes. Following, cells were washed with wash buffer and incubated with secondary antibody (1:100) for 20 minutes on ice. For fixed cell analysis, cells were suspended in 4% paraformaldehyde for 5 minutes at room temperature and then washed twice with wash buffer. For c-Kit analysis requiring permeabilization, cells were washed twice and resuspended in PBS plus 0.1% Triton X-100, 0.1 M Glycine for 3 minutes, then washed once. Fixed cells were suspended in 100 μL wash buffer and incubated with primary antibody on ice for 1 hour. Following, cells were washed twice and incubated with secondary antibody (1:100) for 30 minutes on ice. For both fixed and live cells a total of 300 μl wash buffer was added post secondary incubation and the cells were analyzed by flow cytometry with a BD FACS Canto instrument. Unstained and isotype controls were used to establish baseline fluorescence levels. Data was analyzed by Flow Jo software (BD Biosciences). A minimum of 10,000 cell counts was analyzed.

Quantitative Reverse-Transcriptase Polymerase Chain Reaction (qRT-PCR)

Total RNA was isolated using Quick-RNA MiniPrep kit (Zymo Research, catalog #R1055) according to manufacturer's protocol. RNA concentrations were determined using a Nanodrop 2000 spectrophotometer (Thermo Fisher Scientific, catalog #ND-

2000) with 500 ng concentration of RNA used to generate cDNA using an iScript cDNA Synthesis kit (Bio-Rad Laboratories, Inc, catalog #170-8891). The amplified cDNA was diluted at a ratio of 1:100 in DNase- and RNase- free water. Reactions were prepared in triplicate using 6.5 µL cDNA (equivalent to 3.25 ng total RNA) per reaction using iQ SYBER Green (Bio-Rad Laboratories, Inc, catalog #170-8882) on a CFX Real-Time PCR Detection System (Bio-Rad Laboratories, Inc, catalog #1855201). Samples were normalized to 18S and data were analyzed by $\Delta\Delta$Ct method. Primer sequences are listed in Supplemental Table 3.

Cell Morphology Measurement

Cardiac cell populations were imaged using a Leica DMIL inverted tissue culture phase contrast microscope. Cell morphology was measured by tracing the outline of the cells using Image J software. The three measurements analyzed were area, roundness, and length-to-width (L/W) ratios. L/W ratios were calculated by dividing feret/min feret measurements. A minimum of 30 cells was measured per cell line.

Cell Proliferation Assay

Cell populations were plated in quadruplicate (2,000 cells/well) in a 96-well black flat bottom plate with 100 µL/well of their respective growth media. Cell proliferation rate was determined using a CyQUANT Direct Cell Proliferation Assay (Thermo Fisher Scientific, catalog #C35011) on days 0, 1, 3 and 5.

Matrigel Tube Formation

Growth factor reduced matrigel (Corning, catalog #356231) was used to coat a 96-well flat bottom plate (50 µl/well) and incubated for 30 minutes at 37°C. Cell populations were plated in duplicate (5,000 cells/well) suspended in 100 µL per well of EPC basal medium (see Table 1) and incubated at 37°C in CO_2 incubator. Images of tubular networks were acquired using a Leica DMIL inverted tissue culture phase-contrast microscope 12 to 16 hours after plating.

Lentiviral Constructs and Cell Transduction

All cells used for CardioCluster formation were modified by expression of fluorescent-peptide fragment tags using a 3rd generation lentiviral vector. cCICs were modified with Lenti-PGK-eGFP (Addgene), MSCs were modified with PGK-Neptune-3XHA, EPCs were modified with PGK-mOrange-3Xmyc, all at multiplicity of infection (MOI) 25. Plasmid pLenti-PGK-eGFP was used as a backbone to sub-clone pLenti-PGK-mOrange-3xmyc and pLenti-PGK-Neptune-3xHA.

Cell Death Assay

Human cells were plated in a 6-well dish (30,000 cells per well) and incubated in starvation media (75% FBS depleted media) with 1% PSG for 24 hours. The cells were then treated with 40µM hydrogen peroxide for 4 hours. Cells were dissociated and labeled with Annexin V (BD Biosciences; 1:175) and Propidium Iodide (PI;10mg/ml) or Sytox Blue (Life Technologies; 1:1,000) to detect apoptosis and necrosis, respectively,

by flow cytometry. Data was acquired on a BD FACSAria instrument (BD Biosciences) and analyzed with FACS Diva 3 software (BD Biosciences).

CardioCluster Preservation in Liquid Nitrogen and Viability Testing

CardioClusters were collected, centrifuged at 150 *g* for 2 minutes, resuspended in cold freezing medium (10% DMSO in growth medium), aliquoted into cryogenic storage vials, and frozen in an isopropanol chamber stored at –80°C overnight. The following day vials were transferred to liquid nitrogen for a minimum of 24 hours prior to thaw and cell death analysis with propidium iodide (10mg/ml). Data was acquired on a BD FACSAria instrument (BD Biosciences) and analyzed with FACS Diva 3 software (BD Biosciences).

Co-culture of Neonatal Rat Cardiomyocytes (NRCMs) with Human Cardiac Cells

Neonatal rat hearts were excised and scissor minced prior to enzymatic digestion. Isolated NRCMs were plated in M199 media (Thermo Fisher Scientific, catalog #21157-029) with 15% FBS (Omega Scientific, Inc., catalog #FB-01) at a density of 200,000 cells per well of a 6-well culture dish. The following day, myocyte cultures were washed with PBS and incubated in M199 with 10% FBS for 24 hours. The next morning, the cells were subjected to serum starvation (0.5% FBS in M199) for 24 hours. After low serum conditions, human cardiac cells were added to the plate at a ratio of 1:10 (cCICs, EPC, MSCs, all 3 single cells combined [C+E+M], and CardioClusters) and allowed to incubate with NRCMs for an additional 24 hours in low serum conditions. Controls for NRCMs included leaving cells in 0.5% FBS M199, adding back 10% FBS

M199 (Serum Rescue) or maintaining NRCMS in 10% FBS M199 for the duration of the experiment. NRCM size was visualized by staining cardiomyocytes with sarcomeric actinin (Sigma-Aldrich; 1:100 dilution) and nuclei with TO-PRO-3 iodide (Molecular Probes; 1:10,000 dilution). NRCM relative size was measured using forward scatter on a BD FACSAria instrument (BD Biosciences). Separation of NRCMs and human cardiac cells was accomplished with fluorescent cell sorting of negative cells (NRCMs) versus eGFP+, mOrange+ or Neptune+ cells. After sorting, cells were centrifuged and resuspended in RNAse buffer for isolation and quantitation of mRNA from NRCMs or human cells.

Single-cell RNA-seq Preparation, Data Analysis, and Data Availability

Size distribution was quantified for single cell suspensions of cCIC, MSC, EPC and dissociated CardioClusters to verify cell size met droplet platform specifications. Cells were loaded on a Chromium™ Controller (10x Genomics) and single-cell RNA-Seq libraries were prepared using Chromium™ Single Cell 3’ Library & Gel Bead Kit v2 (10x Genomics) following manufacturer’s protocol. Each library was tested with Bioanalyzer (average library size: 450-490 bp). The sequencing libraries were quantified by quantitative PCR (KAPA Biosystems Library Quantification Kit for Illumina platforms P/N KK4824) and Qubit 3.0 with dsDNA HS Assay Kit (Thermo Fisher Scientific). Sequencing libraries were loaded at 2 pM on an Illumina HiSeq2500 with 2X75 paired-end kits using the following read length: 98 bp Read1, 8 bp i7 Index, and 26 bp Read2.

Raw sequencing data was processed with the Cell Ranger pipeline (10X Genomics; version 2.0). Sequencing reads were aligned to the human genome hg19. Cells with fewer than 1,000 genes or more than 10% of mitochondrial gene UMI count were filtered out and genes detected in fewer than three cells were filtered out using Seurat R Package (v2.3.4)[95]. The first 20 principal components were found to be significant to perform dimensionality reduction. Preparations derived from *in vitro* studies yielded 5659 barcoded cells for analysis, from which 1125, 1717, 1403 and 1414 corresponded to CardioClusters, cCICs, EPCs and MSCs, respectively. Approximately 2,029 variable genes were selected based on their expression and dispersion. The first 20 principal components were used for the t-SNE projection and unsupervised clustering[95]. Differential expression analysis was done using Wilcoxon rank sum test and selecting for an adjusted p-value ≤0.05 and a log (FC)>0.25. Global differential expression analysis was done using Loupe Cell Browser 2.0.0. Gene ontology analysis was performed using R package clusterProfiler[96].

scRNA-Seq data generated in this study has been uploaded to the Gene Expression Omnibus (GEO) database (GSE133832).

Myocardial Infarction and Intramyocardial Injection

Animal protocols and experimental procedures are approved by the Institutional Animal Care and Use Committee at San Diego State University. Animals were randomized for treatments that were blinded to personnel carrying out the surgical procedures, injections, and physiological function analysis. Appropriate animal sample size was determined using sample size calculator

(http://www.lasec.cuhk.edu.hk/sample-size-calculation.html). A total of 60 mice were used in this study. Myocardial infarctions were carried out on 8-week old NOD.CB17-Prkdc^{scid}/J female mice (The Jackson Laboratory, catalog #001303) under 2% isoflurane (Victor Medical, catalog #NDC 57319-474-06) as previously described[97]. Briefly, the 3rd and 4th ribs were separated enough to get adequate exposure of the operating region, but the ribs were kept intact. The heart was squeezed out by pressing the thorax lightly and the left anterior descending artery (LAD) was ligated at the distal diagonal branch with a 7-0 suture. Infarction was confirmed by blanching of anterior left myocardium wall. Following ligation, either CardioClusters (n=17), 2:3:1 ratio of cCIC+EPC+MSC (C+E+M; n=15), or a vehicle control (PBS plus 0.5% sodium alginate [NovaMatrix, catalog #4209001]; n=16) were delivered intramyocardially at 3 separate sites in the vicinity bordering the blanched area. A total of 90,000 cells per heart were introduced into CardioCluster and C+E+M animals. The hearts were immediately placed back into the intrathoracic space followed by muscle and skin closure. Animals in sham group (n=12) received a comparable surgical procedure without LAD ligation or injection. Each animal received 20 µL analgesic treatment with 0.3 mg/mL Buprenex (Victor Medical, catalog #12496-0757) at time of surgery and 12 hours post-surgery.

Echocardiography and Speckle-Tracking Based Strain Measurement

Transthoracic echocardiography was performed on lightly anesthetized mice under isoflurane (1.0-2.0%, Abbot Laboratories) using a Vevo 2100 (VisualSonics). Hearts were imaged in the 2D parasternal short-axis (SAX) view, and M-mode echocardiography of the mid-ventricle was recorded at the level of papillary muscles to

calculate fractional shortening (FS). From the recorded M-mode images the following parameters were measured: left ventricular (LV) anterior wall thickness (AWT), LV posterior wall thickness (PWT), LV internal diameter (LVID), and LV volume in diastole (index: d) and systole (index: s). An LV-Trace of hearts imaged in the 2D parasternal long-axis (PLAX) view was performed in B-mode to calculate ejection fraction (EF).

Strain analysis was conducted using a speckle-tracking algorithm provided by VisualSonics (VevoStrain, VisualSonics). In brief, B-mode loops were selected from echocardiographic images based on adequate visualization of the endocardial border. A minimum of 3 consecutive cardiac cycles was selected for analysis based on image quality. Semi-automated tracing of the endocardial and epicardial borders were performed and then corrected as needed to achieve good quality tracking throughout each cine loop. Tracked images were then processed for strain measurements. Strain measurements were averaged over time resulting in curvilinear strain data points. Each long-axis view of the LV was divided into 6 standard anatomic segments for regional speckle-tracking based strain analysis throughout the cardiac cycle. Global peak strain values were averaged across all 6 segments. Regional peak strain values averaged the area of injury using segments 3, 5 and 6.

Hemodynamic Analysis

Invasive hemodynamic data acquisition was performed with an ADVantage PV System (ADV500, Transonic Systems Inc.) using a 1.2F PV catheter (Transonic Systems Inc., catalog #FTH-1212B-4518). Animals were sedated using 1.2 mg/mL Ketamine (VetaKet CIII, Akorn Animal Health, Inc., catalog #59399-144-10), 0.5 mg/mL

Xylazine (Anased, Akorn Animal Health, Inc., catalog #59399-110-20) dosed at 10 µL/g body weight. PV catheter was pre-calibrated in 0.9% saline for at least 30 minutes at room temperature before each measurement. PV catheter was inserted through right carotid artery and advanced into LV chamber to record changes in LV pressure and volume. Hemodynamic data analysis was performed offline by LabScribe v3 software (iWorx). Mice after catheterization were immediately subjected to heart retroperfusion.

Tissue Section Preparation

Mice were infused with heparin (Sigma-Aldrich, catalog #H3393) at 10 U/g body weight and anesthetized using 3% chloral hydrate solution (Sigma-Aldrich, catalog #C-8383) dosed at 10 µL/g body weight. Hearts were arrested in diastole with 0.1 M CdCl2+KCl and perfused with either 1% paraformaldehydes (cryosectioned hearts) or formalin (paraffin embedded hearts) for 5 minutes at 80-100 mmHg via retrograde cannulation of abdominal aorta. Retroperfused hearts were removed from the thoracic cavity and weighed prior to fixation. Hearts were fixed overnight in either 1% paraformaldehyde at 4ºC (cryosectioned hearts) or formalin at room temperature (paraffin embedded hearts). Hearts fixed for cryosectioning were dehydrated in 30% sucrose overnight at 4°C followed by mounting in Neg50 frozen section medium (Thermo Fisher Scientific, catalog #6502) on dry ice. Tissues were cryosectioned at 20 µm thickness at -20ºC. Formalin fixed hearts were processed for paraffin embedding and sectioned at 7 µm thickness at room temperature.

Capillary Density Measurement

Paraffin sections were immunolabeled with isolectin GS-IB4 conjugated to Alexa Fluor 568 (Thermo Fisher Scientific, catalog # I21412**;** 1:100 dilution) to visualize vasculature, in combination with cardiac troponin T conjugated to Alexa Fluor 488 (Biocompare, catalog #bs-10648R-A488; 1:200 dilution) and 4′,6-diamidino-2-phenylindole (DAPI). Scans consisted of infarct, border and remote regions for each heart analyzed. The analysis software on a Leica TCS SP8 Confocal Microscope and Image J software were used to quantitate the number of positive cells in each field of view. A minimum of 3 independent fields of view per cardiac region was measured. The area of cardiac tissue in each field of view was measured and used to normalize capillary numbers per mm^2. N=4-6 hearts per group measured at week 20.

Cardiomyocyte Cross-sectional Area Measurement

Paraffin sections were immunolabeled with cardiac troponin T conjugated to Alexa Fluor 488 to visualize cardiomyocytes, wheat germ agglutinin conjugated to 680 (Thermo Fisher Scientific, catalog #W32465; 1:500 dilution) to outline cellular membranes, and DAPI to visualize nuclei. Cardiomyocytes were measured in the infarct, border, and remote regions. Cross-sectioned cardiomyocytes with a centrally located nucleus were considered. Approximately 50 cardiomyocytes from 3 independent fields of view per heart region were measured using the SP8 TCS Leica drawing tool to trace cardiomyocyte cross-sectional area. N=4-5 hearts per group measured at week 20.

Infarct Size Quantitation

Trichrome Stain (Masson) Kit (Sigma-Aldrich, catalog #HT15) was used to stain for collagen deposition in sham and infarcted hearts according to manufacturer's protocol. Staining was visualized using a Leica DMIL6000 microscope using XY stage tile scan and automatically stitched by Leica LAS X analysis software. Area of live versus dead myocardium was measured using the drawing tool in the SP8 TCS Leica Software using scar length over total LV length. Multiple heart sections from apex to mid-wall were averaged for scar quantification. N=4-5 hearts per group measured at week 20.

Statistical Analysis

Data are expressed as mean±SEM. Statistical analyses of multiple groups were assessed by 1-way ANOVA with Bonferroni post hoc test (comparison among all groups) or Dunnett's post hoc test (versus single group). Multiple groups over time were analyzed by 2-way ANOVA. Statistical analysis was performed using GraphPad Prism version 5.0 software. Experiments were performed in triplicate unless stated otherwise. A p-value of less than 0.05 was considered statistically significant.

RESULTS

Three distinct cardiac nonmyocyte cell types are used for CardioCluster formation

CardioClusters are comprised of three cardiac-resident cell populations concurrently isolated as previously described by our group with full phenotypic characterization[13]. Cell surface marker profiling of cell lines used to produce CardioClusters were similar to previous findings (cCIC express c-Kit^{high}, CD90^{high}, CD105^{low}, CD133^{low}, CD45^{neg}; EPC express CD133^{high}, CD105^{high}, c-Kit^{low}, CD90^{neg}, CD45^{neg}; and MSC express CD90^{high}, CD105^{high}, c-Kit^{low}, CD133^{low}, CD45^{neg}; data not shown). Commitment toward angiogenic and smooth muscle fates was assessed for the three cardiac-derived cell populations relative to control cell lines human umbilical vein endothelial cells (HUVECs) and bone marrow-derived MSCs (BM MSCs). Tube formation assays demonstrated robust angiogenic responses from both EPCs and HUVECs *in vitro* using growth factor-reduced Matrigel (data not shown). Transcript levels of endothelial-related genes *CD31* and *von Willebrand factor* (*vWF*) were elevated in HUVECs and EPCs ($p<0.001$ versus cCICs; data not shown). *Smooth muscle actin* (*SMA*) transcripts were highly expressed in BM MSCs and cardiac MSCs ($p<0.001$ versus cCICs), with both endothelial populations (EPC or HUVEC) expressing near undetectable levels ($p<0.05$ versus cCICs). *GATA4* was expressed by cCICs (1.0±0.05) and to a lesser extent by EPCs (0.87±0.03) and MSCs (0.33±0.01), with non-cardiac controls expressing undetectable levels (data not shown). Collectively, these three cardiac-derived cell populations recapitulate and validate previous results of phenotypic characterization for cell types obtained using our published protocol[13]. Distinct

phenotypic properties of these three cardiac-derived cell populations fulfills the conceptual design of combining multiple cell types for CardioClusters formation.

The three distinct cardiac derived cell populations were modified with lentiviral vectors to introduce fluorescent proteins for tracking purposes (eGFP tagged cCICs [green], mOrange tagged EPCs [blue], and Neptune tagged MSCs [red]; tagging efficiency 99.1±0.2%; Figure 3.1 and Figure 3.2, A-B). Distinct morphology for each cell population is evident in representative brightfield images with companion immunofluorescent images demonstrating corresponding fluorophore expression in cCICs (Figure 3.1A), EPCs (Figure 3.1B), and MSCs (Figure 3.1C). Cell morphology measurement of area, roundness, and L/W ratio for each cell type confirmed distinct phenotypes (Figure 3.1, D-F). MSCs were significantly larger (18,563±1,021) relative to both cCIC (3383±121) and EPC (3272±102) (Figure 3.1D). EPCs were significantly rounder (EPC, 0.55±0.012; cCIC, 0.19±0.0097; MSC, 0.36±0.015) (Figure 3.1E), while cCICs show increased L/W ratio (cCIC, 5.2±0.19; EPC, 2.1±0.063; MSC, 2.8±0.11) (Figure 3.1F). Morphometric parameters clustered by cell type, with minor variation between heart samples (data not shown). EPCs exhibited a proliferative rate similar to cCICs, with both populations showing increased proliferation over MSCs based on CyQuant proliferation assays (Figure 3.1G). EPCs were significantly more resistant to cell death and retained 92±0.76% cell viability, versus only 54±5.6% for cCIC and 79±1.5% for MSCs after 4 hours H_2O_2 treatment (Figure 3.1, H-J). Cumulatively, characterization showed phenotypic and biological distinctions between cardiac interstitial cell populations fundamental to CardioCluster design and utility, such as

elevated resistance to oxidative stress-induced cell death, high proliferative activity, and pro-angiogenic nature of EPCs.

Generation of CardioClusters

CardioClusters are formed in a two-step process (Figure 3.1K and Figure 3.2C). cCICs and MSCs are seeded to form the inner core, with EPCs added 24 hours later to provide an endothelial cell-enriched outer layer for the CardioCluster. The outer EPC layer provides enhanced resistance to oxidative stress relative to the more sensitive cCICs and MSCs within the CardioCluster core (Figure 3.1J). Individual cells within an assembled CardioCluster were readily visualized with their cognate fluorophore tags, obviating the need for antibody-mediated detection (Figure 3.1L and 3.1M). CardioCluster size reproducibly and predictably corresponds to cell number seeded per microwell (Figure 3.1N). CardioClusters ranging from 100-1000 cells were examined to determine changes in size and morphology over a 7 day time period (Figure 3.2D). CardioCluster diameter and area increased over 7 days, except for CardioClusters seeded with 1000 cells, whose diameter plateaued after day 3. This finding, also previously observed with 3D aggregated cells[98], is consistent with reduced oxygen and nutrient diffusion within dense cellular structures >200 μm[99, 100].

Preserving CardioCluster 3D structural integrity for intramyocardial delivery to promote intercellular contact and enhance retention is essential to improve upon typical approaches involving dissociated single cell suspensions. Intramyocardial injection for cell delivery in murine hearts uses a standard 30-gauge needle with a 159 μm internal diameter ([I.D.]), so CardioClusters were engineered for a diameter allowing for injection

to preserve 3D structure. The maximum number of cells that could comprise a CardioCluster and pass through a 30-gauge needle is 400 cells based on morphometric quantitative analysis (Figure 3.1O). EPC, cCICs and MSCs were combined in a 3:2:1 ratio, based upon the consideration of larger MSC size occupying relatively more volume relative to cCIC or EPC (Figure 3.1D). CardioCluster spontaneous self-assembly as revealed using time-lapse video microscopy shows the MSC population immediately migrating towards the central core (data not shown). cCIC/MSC interaction was allowed to progress for 24 hours, at which point EPCs were added to interact with established cCIC/MSC cores. Interestingly, EPCs initially form their own clusters instead of adhering to cCIC/MSC cores and then subsequently envelop the cCIC/MSC core (Figure 3.2D). Architecture of an MSC-enriched core was invariant regardless of seeding sequence, as plating of cCIC+EPCs prior to adding MSCs consistently resulted in MSCs migrating and localizing within the CardioCluster core rather than surface (data not shown) consistent with the preferential localization of MSC to hypoxic environments.[33, 34]. CardioCluster formation consistently occurs with MSCs in the core and cCIC/EPCs on the outer layers.

CardioClusters possess a high percentage of live cells maintained within the 3D structure (93.9-98% of cells alive; Figure 3.3). Robust vitality of CardioClusters was confirmed by recovery from long term liquid nitrogen storage, where the percentage of live cells was comparable to that of control non-frozen CardioClusters (Figure 3.3A and 3.3B). When cultured on standard tissue culture-treated plastic, cells adhered and migrated out from the CardioCluster whether frozen or not non-frozen with comparable cell morphology (Figure 3.3C). These findings support “off-the-shelf” feasibility of using

frozen banked CardioClusters for therapeutic purposes rather than necessitating *de novo* creation prior to use.

CardioCluster cells undergo reprogramming toward the transcriptome profile of freshly isolated cardiac interstitial cells

Transcriptional profiling of CardioClusters and their monolayer cultured parental counterparts reveals significant reprogramming consequential to 3D aggregation. Since CardioClusters are heterogeneous cell populations by design, single-cell RNA sequencing (scRNA-seq) was employed to reveal cellular transcriptome heterogeneity within the CardioCluster at the single cell level with a level of resolution not achievable with bulk population analysis. Quality control testing validated parameters of cell size distribution, sequence alignment and filtering of multiplets and dying cells (data not shown). Dimensionality reduction by t-SNE reveals segregation of CardioClusters (orange cluster) distinguished by a unique transcriptome profile separating them from their constituent parental populations, which form their own clusters (red, green, blue clusters representing MSCs, cCICs and EPCs respectively; Figure 3.4A). Differentially expressed genes (DEGs) are increased in the CardioCluster environment (620) relative to cCIC (296), EPC (167), or MSC (211) (Figure 3.4B, Supplemental Table 4). Taken together, these results demonstrate CardioClusters distinguishing themselves as a transcriptionally unique population diverged from parental cell lines.

Cellular identities of the three constituent parental lines comprising a CardioCluster are consistent with detected transcripts in each cell type. EPCs highly express ECSCR, ESM1, EGFL7 and RAC2, which are endothelial–related genes

important for neovasculature and the angiogenic response (Figure 3.4B and 3.4C). The highly specific marker vascular endothelial statin (VE-statin) referred to as EGFL7, exhibits near-exclusive expression and action upon endothelial cells[101] and is highly expressed in EPCs (Figure 3.4B). In contrast, many secreted angiogenic signaling molecules including vascular endothelial growth factor (VEGF) are expressed by nonendothelial cell types such as fibroblasts. MSC-enriched transcripts include the cell surface marker THY1 (also referred to as CD90) as well as Smooth muscle α-2 actin (ACTA2) (Figure 3.4B and 3.4C). Gene ontology analysis of MSCs reveals expression of extracellular matrix and adhesion molecules such as COL1A2, TIMP3 and FN1 (Figure 3.4B and 3.4D). Consistent with preference for hypoxia, MSCs are enriched for HIF1A, a transcription factor that plays a key role in response to hypoxic stimuli. Lastly, transcripts associated with cell proliferation and anti-apoptotic activity such as BIRC5 and HMGB1 are differentially expressed in cCICs, as well as the chemotactic signaling molecule CXCL12, commonly referred to as stromal derived factor-1 *(*SDF-1), and developmental genes DKK1 and FGF5 (Figure 3.4B). Collectively, these data highlight that the 3 parental populations are distinctly different from one another, with EPCs and MSCs expressing endothelial and stromal-associated genes.

Transcriptome profiling of CardioClusters by scRNA-seq reveals several features distinct from the three parental cell lines. CardioClusters are enriched for transcripts in multiple categories including stem cell-relevant factors (KLF4, LIF, JAK1, SMAD7, BAMBI, NOTCH3), adhesion/extracellular-matrix molecules (integrin-α2, laminin-γ1, type 1 collagen-α1, BMP1, MMP2), and cytokines (SOD2, SDF-1, FGF2). These aforementioned DEGs were similarly enriched in freshly isolated cardiac interstitial cells

(Figure 3.4, B-D, 3.4F), suggesting that CardioClusters adopt a transcriptome profile with features reminiscent of cardiac interstitial cells present in the myocardium rather than cultured cells. Indeed, 89 out of the 448 DEGs present in CardioClusters are also found in freshly isolated cardiac interstitial cells (Figure 3.4E and 3.4F), in stark contrast to the overlap with the 2D-cultured parental cell lines where only 7 DEGs are shared with freshly isolated cardiac interstitial cells (Figure 3.4E and 3.4F). This finding supports that standard tissue culture causes expanded cells to lose their identity, unlike cells within a 3D microenvironment. Consistent with this observation, the size of cells grown within a CardioCluster were smaller relative to 2D cultured parental counterparts ($p<0.01$; data not shown) resembling a size more similar to freshly isolated cells. Thus, the 3D microenvironment of a CardioCluster promotes a more native phenotype similar to endogenous or freshly isolated cardiac cells.

CardioClusters exert protective effects with serum starvation in vitro assay

Protective effects mediated by cCICs and MSCs are conferred upon serum starved neonatal rat cardiomyocytes (NRCMs) in co-culture[102]. Similarly, beneficial effects mediated by CardioClusters were assessed by co-culture with NRCMs in serum depleted conditions relative to effects conferred by cCIC, EPCs, MSCs, and a combined mixture of cCIC+EPC+MSC (C+E+M) (Figure 3.5A). NRCMs maintained in low serum (0.5%) were smaller relative to NRCMs maintained in high serum condition (10%) (Figure 3.5B and 3.5C, Figure 3.6). CardioCluster co-culture with low serum treated NRCMs restored cardiomyocyte size within 24 hours relative to all other treatments ($p<0.05$; Figure 3.5B and 3.5C, Figure 3.6) and also increased mRNA expression for

Desmin, a muscle-specific type III intermediate filament protein ($p<0.001$; Figure 3.5D). Furthermore, CardioCluster co-culture increased mRNA for *Sdf-1* ($p<0.05$; Figure 3.5E), a cardioprotective cytokine and chemotactic factor for MSCs that plays an additional role in recruitment of EPCs important for angiogenesis[103, 104]. Importantly, CardioClusters offered significantly greater protection upon NRCM than actions exerted by any individual parental population (cCICs, EPCs, MSCs) or the combined C+E+M mixed population. Collectively, these results demonstrate superior protective effects of CardioClusters for NRCM in response to serum starvation challenge.

Paracrine gene expression is increased in CardioClusters after NRCM in vitro co-culture

Paracrine factor action is considered a primary mechanism for cardioprotective[105], so mRNA transcript level expression for growth and immunomodulatory factors was assessed after CardioCluster co-culture for 5 days with serum depleted NRCM (Figure 3.7A). mRNA levels for CardioClusters, parental cells, and the C+E+M mixed population were measured by separating fluorescently tagged cells away from the NRCM population using flow cytometric sorting (Figure 3.6). mRNA transcript levels for *insulin-like growth factor* (*IGF*) and *interleukin-6* (*IL-6*) were highly elevated in CardioClusters co-cultured with NRCMS relative to any of the individual parental population (cCICs, EPCs, MSCs) or the combined C+E+M mixed population ($p<0.001$ and $p<0.05$ respectively, versus cCIC; Figure 3.7B and 3.7C). *IGF* exerts chemotactic and growth-stimulatory effects[105] in addition to anti-apoptotic properties[106-108]. Early release of anti-inflammatory cytokines such as *IL-6* after acute cardiac damage has been shown to be beneficial by signaling protective responses in local tissue and

initiating wound healing[109]. Additionally, the cardioprotective cytokines *SDF-1* and *hepatocyte growth factor* (*HGF*), both trended towards increased expression in CardioClusters following co-culture experiments (Figure 3.7D and 3.7E). *HGF* stimulates cell proliferation, motility, morphogenesis, angiogenesis and importantly tissue regeneration[108, 110]. Collectively these results show that at the transcript level CardioClusters induction of paracrine factors *IGF* and *IL-6* exceeds that of parental cell populations or C+E+M group when co-cultured with serum depleted NRCMs.

Several mRNAs associated with lineage specification were analyzed following co-culture of CardioClusters or parental cell populations with NRCMs. *GATA4* showed the highest expression in cCIC co-culture. Predictably, EPCs displayed the largest induction of endothelial marker *CD31*, whereas MSCs induced *SMA* gene expression after 5 days of co-culture with NRCMs (Figure 3.7, F-H). Neither *CD31* nor *SMA* were significantly upregulated in CardioCluster group (Figure 3.7G and 3.7H).

CardioClusters are resistant to oxidative stress by in vitro assay

CardioClusters were substantially more resistant to cell death induced by 4 hours of H_2O_2 treatment after overnight low serum culture (Figure 3.8). Dying cells were divided into groups of early apoptosis, late apoptosis, and necrosis based on Annexin V and Sytox Blue staining (Figure 3.9). CardioClusters showed significantly fewer cells in necrosis relative to any individual parental population (cCICs, EPCs, MSCs) ($p<0.05$ versus cCIC; Figure 3.8B and Figure 3.9F) as visually evidenced by fewer cells rounding up and detaching from the tissue culture dish (transparent arrows; Figure 3.8C and

3.8D). These results demonstrate superiority of CardioClusters to survive oxidative stress challenge *in vitro*.

CardioClusters improve myocardial structure and function following infarction injury

Therapeutic efficacy of CardioClusters was assessed in a murine experimental myocardial infarction injury model of permanent coronary artery occlusion. Xenogenic human cell treatment into NOD^{SCID} recipient mice was performed at the time of infarction with direct comparison between CardioClusters and the C+E+M combined population group administered as a single cell suspension mixture. Myocardial structure and function were assessed by parasternal long axis echocardiography for four experimental groups: non-injured sham, CardioCluster, C+E+M, and vehicle-treated (Figure 3.10A). All groups had comparable reduction in cardiac function at 1 week post injection (wpi) demonstrating consistency of infarction injury (Figure 3.10, B-D, F-G and Table 6) with average EF for all infarcted groups of approximately 30% (CardioCluster, 27±2.9%; C+E+M, 32±2.2%; Vehicle, 29±2.0%; Figure 3.11). The CardioCluster-treated group showed significant cardiac functional improvement starting 4 wpi, which was sustained throughout the 20-week time course, with increased fractional shortening (FS; Figure 3.10B) and ejection fraction (EF; Figure 3.10C) versus C+E+M treatment 4 and 8 wpi and was significant at study completion for EF. In comparison, EF and FS improvements in the C+E+M treated group only began to appear at 12 and 16 wpi, respectively (Figure 3.10B and 3.10C). Terminal EF measurements at 20 wpi show EF value is highest in the CardioCluster group relative to vehicle only or C+E+M groups (40±1.9% versus 16±1.0% or 30±4.5%, respectively; Figure 3.11, B-D). CardioCluster treatment shows a

45±7% improvement in EF at study completion relative to the starting value at week 1. In contrast, EF at study completion relative to week 1 for the C+E+M or vehicle only-treated groups decreased by 5±14% and 46±3%, respectively (Figure 3.10E). Furthermore, CardioCluster treatment group exhibits significantly smaller left ventricular internal diameter both in systole (LVID;s) and diastole (LVID;d), as well as reduction in LV end systolic and diastolic volumes (LV Vol;s and LV Vol;d). Heart rate was not significantly different among treatment groups (Figure 3.10, F-G and Figure 3.12, A-C). Structural and functional data are detailed in Table 6.

Speckle-tracking based strain analysis is a highly sensitive echocardiographic technique for assessing left ventricular (LV) function[111, 112]. LV function was similarly reduced in all infarcted mice at 1 wpi (Figure 3.13A). Progressive changes consistent with adverse ventricular remodeling occur in vehicle-treated animals in agreement with conventional echocardiographic measures of function (Figure 3.10). LV systolic deformation in the CardioCluster-treated group showed significant improvement starting at 8 wpi and progressing through 20 wpi compared to vehicle-treated animals ($p<0.001$; Figure 3.13, B-D). Radial strain measurements at 8 and 20 wpi confirmed significant functional benefit provided by CardioCluster treatment versus 2D cultured parental C+E+M mixed population ($p<0.01$; Figure 3.13C). Peak longitudinal strain was improved in the C+E+M treated group versus vehicle alone ($p<0.05$; Figure 3.13D). Regional strain measurements assessing the area of injury further demonstrate significant improvement in LV function for CardioCluster-treated animals (Figure 3.13E and 3.13F). In the area of injury, the absolute difference in radial strain (week 1-to-week 20) for CardioCluster-treated group was 7.59±1.28% which was significantly improved relative

to C+E+M and vehicle-treated groups (-1.56±1.96% and -1.88±1.61% respectively, $p<0.01$ versus CardioCluster group, Figure 3.13F). Similar improvement was seen for absolute difference in longitudinal strain 20 wpi.

CardioCluster superiority for restoring myocardial structure and function relative to the mixed population C+E+M is further reinforced by tissue morphometry and hemodynamic measurements. Cardiac hypertrophy was not a contributing factor to increasing anterior wall thickness (AWT) at 20 weeks in the CardioCluster-treated group (Figure 3.10D) as heart weight to tibia length ratios did not increase (HW/TL; Figure 3.10H) relative to the sham-operated control. In contrast, a significant increase in HW/TL is present in both vehicle control as well as C+E+M treatment groups. Fibrotic area is significantly smaller in CardioCluster-treated mice compared to vehicle at 20 wpi (38.4±4.5% of CardioCluster LV versus 55.3±4.3% of vehicle LV; Figure 3.10, I-M) although infarct size is not significantly different between hearts receiving C+E+M or CardioClusters. Invasive hemodynamic measurement validates functional superiority of the CardioCluster-treated group showing significantly improved developed pressure over time (dP/dT) versus vehicle (Figure 3.12D), in addition to increasing left ventricular developed pressure (LVDP) and P_{max}-P_{min} (Figure 3.12E). Collectively, these findings are evidence that CardioClusters offer significantly greater benefit for restoration of myocardial performance in this murine myocardial infarction injury model.

CardioClusters engraft and persist in the myocardial wall following intramyocardial injection

Characteristics of CardioClusters including multicellular 3D architecture and enhanced survival are attractive features to mediate increased persistence following delivery compared to dissociated single cell suspensions such as the C+E+M mixed population. CardioCluster persistence *in vivo* was longitudinally assessed over a 4-week period by confocal microscopy (Figure 3.14). CardioCluster localization was tracked with co-injection of DiI tracking beads in pilot studies to confirm the delivery site in tissue sections (Figure 3.14A). Cryosectioned hearts allowed for direct visualization of fluorophore tags without antibody labeling. All three constituent cell types were readily visualized in the myocardial wall, with MSCs at the center of the CardioCluster surrounded by a layer of cCICs and EPCs, similar to architecture observed *in vitro* (Figure 3.10H). With CardioCluster localization confirmed coincident with the injection site, subsequent injections and imaging were performed without DiI tracking beads for long-term functional studies. CardioClusters were clearly visible within the myocardium at serial time points: 1, 3, 7 and 28 days post injection (Figure 3.14, B-F). Antibody labeling confirmed CardioCluster persistence at day 7 and day 28 (Figure 3.14E and 3.14F).

CardioClusters increase capillary density in the infarct area

Capillary density was measured in the infarct, border zone, and remote regions at 20 wpi. Non-injured controls (sham) serve as the control group compared to injured hearts (Figure 3.15). Notably, the CardioCluster group exhibited significantly more isolectin labeled vessels in the infarct region at 20 wpi versus both vehicle and C+E+M-treated groups (Figure 3.15, A and E–G). CardioCluster group capillary density in the

infarct region increased 62% or 83% versus the C+E+M or vehicle only control, respectively. Within the infarct border zone at 20 wpi, both CardioCluster and C+E+M-treated groups trended toward increased capillary density versus vehicle control, but not achieving significance (Figure 3.15B). The remote region did not significantly increase capillary density in either CardioCluster or C+E+M groups relative to vehicle or sham (Figure 3.15C and 3.15D). Taken together, these data demonstrate a superior level of microvascularization prompted by CardioCluster treatment relative to dissociated mixed cell preparation or vehicle only control groups.

CardioCluster treatment antagonizes cardiomyocyte hypertrophy in the border and remote regions and preserves cardiomyocyte size in the infarct region

Cell therapy reduces hypertrophic remodeling following pathologic injury to blunt progression of heart failure after MI. Treatment groups receiving either CardioClusters or the C+E+M mixed population both exhibited normalized cardiomyocyte size in the infarct region nearly identical to uninjured sham control hearts at 20 wpi (Figure 3.16A). Cardiomyocytes within the border zone proximal to infarction or in remote regions from the injury site were significantly smaller in the CardioCluster treatment group compared to either C+E+M or vehicle only control groups ($p<0.001$; Figure 3.16, B-C and E-G). Indeed, cardiomyocyte size in remote regions was normalized in the CardioCluster group to values similar with non-injured controls (Figure 3.16C and 3.16D). Individual cardiomyocyte cross-sectional area was traced (Figure 3.17, A-C) along with average cardiomyocyte cross-sectional area for infarct, border zone, and remote regions (Figure 3.17, D-F). Collectively these data validate the action of CardioCluster treatment to blunt

hypertrophic cellular enlargement better than dissociated mixed cell preparation or vehicle only control groups.

DISCUSSION

The preceding decade of cardiac cell therapy has produced substantial knowledge regarding optimization as well as limitations of current therapeutic interventions. In a field sometimes overshadowed by contentious debate[113-117], it is important to remember that there are also many points of consensus. Specifically, all parties agree that inefficient cell delivery to the site of injury, low cell retention and modest efficacy of cells that do remain within the tissue are factors hampering advancement. Technical reinvention building upon prior success by incorporating 'next generation' approaches to surmount these established barriers represent the frontier of cell therapy research. CardioClusters introduced in this report are a novel and effective solution that integrates multiple cardiac-resident cell types into a single injectable product. The evolutionary advance offered by CardioClusters is mitigation of single cell delivery challenges through spherical self-assembly of a larger 3D structure, which provides enhanced retention to mediate repair after delivery. Inspiration for CardioClusters is drawn from prior studies showing superiority of combinatorial cell therapy[19, 82-84] and enhanced functional properties of cells grown in 3D environments[118-120]. The multicellular structure and composition of CardioClusters represents a distinctly unique *in vitro* engineered platform to enhance the outcome of cellular therapeutics as demonstrated in preclinical testing using an established murine infarction injury model treated with a xenograft of human cardiac-derived cells.

CardioClusters were deliberately designed with multiple features anticipated to enhance efficacy. Among these properties, the essential combination of multiple cardiac cell types was enabled by our prior methodological studies to isolate and expand three

distinct cardiac-derived interstitial cell types from patients with end-stage heart failure undergoing implantation of a left ventricular assist device (LVAD)[13]. End stage heart failure patients such as LVAD recipients represent likely candidates for interventional autologous therapy using cells derived from their own cardiac tissue. Combinatorial approaches harnessing beneficial attributes of multiple adult cell types are gaining acceptance as a method to enhance biological properties and efficacy based upon the tenets that: 1) no single cell population possesses all the requisite attributes for effective repair, and 2) both cardiomyogenic and non-cardiomyogenic cells contribute to myocardial repair and regeneration. Combining multiple cell types with complementary roles more efficiently mediates repair in preclinical experimental animal models of heart failure[19, 82-84] and is currently being assessed in the CONCERT clinical trial with patients receiving mixtures of MSCs and cardiac progenitor cells (cCIC)[121]. Similarly, induced pluripotent stem cell-derived cardiomyocytes combined with vascular cells[122] or MSCs[123] potentiates myocardial repair, likely due to enhanced stimulation of endogenous repair mechanisms. Efficient isolation and expansion of three distinct cardiac-resident non-myocyte populations brought together *ex vivo* to form CardioClusters is now technically feasible (Figure 3.1) [13]. CardioCluster biological variability depending upon the source, condition, and pathologic state of donor tissue is an important and intriguing unresolved issue to be addressed in follow-up studies based upon the proof-of-principle provided in the present report.

Another enabling feature of CardioClusters is the profound influence of aggregation upon phenotypic and biological properties of the constituent cell populations. Specifically, CardioClusters foster a transcriptional profile more consistent

with freshly isolated cardiac interstitial cells compared to their monolayer counterparts (Figure 3.4). Even relatively short-term *in vitro* expansion of cCIC in 2D monolayer culture results in loss of identity marker gene expression and decreased population heterogeneity by single cell RNA-Seq transcriptome profiling[87]. And although cells derived from typical 2D monolayer cultures are used to seed CardioClusters, the transcriptome signature of CardioCluster cells collectively resemble each other far more than original parental cells. The CardioCluster microenvironment promotes intercellular coordination initiated within a 3D environment, unlike traditional monolayer expansion[85-87]. Increased expression of collagen type I and III, integrins (ITGA2, ITGB1, ITGA11, ITGA1, ITGAV), fibronectin, and matrix remodeling enzymes (MMP-1, MMP-2, MMP-14, TIMP-1, TIMP-2) in CardioClusters is consistent with enhanced matrix remodeling capacity of cells maintained in a 3D microenvironment[124]. Transcript data for CardioClusters also showed elevated expression of Notch3 that exerts an important regulatory role in the contexts of development and tissue regeneration for maintenance of a progenitor pool and tissue homeostasis[125]. Elevated Notch expression and superiority of 3D aggregation culture relative to conventional 2D conditions is consistent with results using pediatric cCICs cultured in 3D spheres of approximately 1500 cells, wherein 3D aggregated cCICs exert enhanced repair with increased notch signaling compared with their 2D counterparts in a right ventricular heart failure model.[98] Restoring fresh and/or youthful characteristics to isolated cells expanded *in vitro*[52, 126-128] may be one way that CardioClusters provide functional benefits to the collective population.

A third enabling feature of CardioClusters is cardioprotective action, particularly under conditions of environmental stress. *In vitro* testing in co-culture assays is an established protocol to assess the potential of candidate cell types to inhibit cardiomyocyte death from pro-apoptotic challenge[102, 129]. Superior ability of CardioClusters to blunt NRCM death relative to single parental cell types supports the rationale for culturing the mixed cell population together in a 3D configuration (Figure 3.5). Cardioprotective action of CardioClusters is likely mediated by secreted factors such as *IL-6*, *IGF*, and *SDF-1* (3.7 and 3.8) known to exert pro-survival effects[123, 130, 131]. These findings establish the justification for subsequent *in vivo* testing and a potential paracrine mechanistic basis for CardioCluster action.

Superior restoration of structure and function following cardiomyopathic injury is evident from comparative testing with either CardioClusters or the dissociated cell mixture of C+E+M in xenogenic treatment of NOD^{SCID} mice (Figure 3.10). Empirical control of CardioCluster size to <160 μm (Figure 3.1N and 3.1O) allowed for injection through a 30-gauge needle without dissociation into single cells. Improvement in FS and EF was observed starting at week 4 and maintained during the entirety of the 20-week study, with CardioCluster-treated animals showing significantly improved myocardial wall structure compared to C+E+M-treated animals concomitant with increased capillary density (Figure 3.15) and preserved cardiomyocyte size (Figure 3.16). CardioClusters persisted within the myocardial wall, with the 3D structure clearly visible up to a week post-injection (Figure 3.14). Meta-analysis examining cardiac stem cell (CSC) and MSC ability to treat MI in animal models found that treatment culminated in an absolute difference in EF ranging from 8-10.7% compared to control animals[132, 133]. In

comparison, by 20 weeks CardioCluster treatment showed a 24.2% increase in EF compared with vehicle treatment. Our data shows the significant 2-fold improvement possible with CardioClusters versus traditional single cell therapy approaches. "Off-the-shelf" potential of CardioClusters preserved in liquid nitrogen demonstrated high viability and structural integrity indistinguishable from non-frozen counterparts (Figure 3.3). Frozen/thawed CardioCluster efficacy remains to be tested *in vivo*, but the ability to mass-produce and preserve CardioClusters in frozen storage is attractive for clinical implementation planning.

The conceptual framework of CardioClusters offers almost infinite possibilities for modification and optimization for therapeutic use, as well as basic investigation of cellular interactions. For example, parameters including cell ratios, cell types, cluster size, and number of CardioClusters to inject are all worthy of further consideration. CardioCluster contain approximately 300 cells crucial for injectability through the inner diameter of a 30-gauge needle, which constrained diameter to <160 μm (Figure 3.1O) in murine studies. However, a larger animal could tolerate a larger gauge needle and concomitantly scaled up CardioCluster size for a greater total number of cells to be injected. Alternatively, 'mini-CardioClusters' of 50-100 cells with smaller diameter would allow a greater number of individual clusters to be injected. Ability to fine-tune CardioCluster size is a benefit distinct from traditional 3D cell aggregates such as cardiospheres where diameter is not controllable, necessitating dissociation into single cell suspensions of cardiosphere-derived cells for clinical use. Additional strategies to further enhance the CardioCluster concept could involve incorporating genetically modified cells with pro-survival factors such as Pim-1[52, 134] or overexpression of

chemokine receptor (CCR1) to enhance migration, survival and engraftment[135]. Likewise, culture condition modification using hypoxia to favor cell growth and blunt senescence-associated characteristics[136] could dramatically alter CardioCluster biological properties. Cellular interactions occurring within 3D environments can also be tested, such as seeding the three C+E+M founder cell types together rather than sequentially, which appears to create a hollow CardioCluster (data not shown, Sussman lab). This may be attributable to EPC/MSC interaction allowing for internal cavity formation as seen during organ and tissue development[137, 138] or may be more similar to pericyte/MSC-like endothelial cell interactions[139]. With knowledge regarding combinatorial cell therapy at a rudimentary level [140-142] the 'next generation' CardioCluster approach will benefit from further investigation given the multiple possibilities for tweaking the system to enhance the outcome.

As with any novel technological approach, there are unknowns and limitations that need to be resolved for CardioCluster development. A benefit of CardioCluster design is the quick formation time of only 48 hours from start to finish, however creation of CardioClusters necessitates that the multiple composite founder cell types must be ready for utilization in sequence within a short time frame. Since CardioClusters could be conceived using a plethora of possible cells, the time required for expansion of the parental cells may differ depending on the cell types chosen, particularly if using cells isolated from aged patients suffering from cardiomyopathic disease. Allogeneic implementation for CardioClusters might incorporate immunosuppressive agents or assembly using 'universal' donor cells engineered by CRISPR-mediated genome editing[143]. Prospective preparation and freeze storage of either parental cells or

CardioClusters will help ease issues with timing for assembly and delivery. With respect to delivery, CardioClusters may present a safety concerns as microemboli if administered intravenously, so direct intramyocardial injection will be used, which would be the preferred approach regardless to enhance efficacy[144, 145].

This study presents the debut of CardioClusters as a novel technical 'next generation' approach to improve upon established protocols using dissociated single cell preparations proven to be safe for administration to patients but of limited efficacy. Unlike other tissue engineering microfabrication approaches, the spontaneously formed CardioCluster 3D structure maximizes cellular interaction and allows for defined cell ratios, controlled size, and facilitates injectability without dissociation. This combination of features makes CardioClusters unique among current cell therapeutic approaches with demonstrated superiority over single cell mixed suspensions in mitigation of myocardial infarction damage. This initial step toward enhanced cell therapy provides a readily manipulatable platform that will benefit from further research development with the goal of potentiating cell-based therapeutic efficacy to mediate myocardial repair.

TABLES

Table 3.1. List of Media

	Component	Catalog Number
Cardiac Interstitial Cell Medium	F12 HAM's (1x)	SH30026.01, HyClone
	10% ES FBS	16141079, Gibco
	1% Penicillin-Streptomycin-Glutamine (100X)	10378016, Gibco
	5 mU/mL human erythropoietin	E5627, Sigma-Aldrich
	10 ng/mL human recombinant basic FGF	HRP-0011, Biopioneer
	0.2 mM L-Glutathione	66013-256, Sigma-Aldrich
Endothelial Progenitor Cell Medium	EBM-2 Basal Medium	CC-3156, Lonza
	EGM-2 Kit Supplements and Growth Factors: • 0.5 mL Human Epidermal Growth Factor • 0.5 mL Insulin-Like Growth Factor-1 • 0.5 mL Vascular Endothelial Growth Factor • 0.5 mL HEPARIN • 0.5 mL Gentamicin Sulfate Amphotericin-B • 0.5 mL Ascorbic Acid • 2.0 mL Human Fibroblast Growth Factor-B • 2.0 Hydrocortisone • 10 mL FBS	CC-4176, Lonza
Mesenchymal Stem Cell Medium	10.1 g/L Minimum Essential Medium Eagle, Alpha Modification	M0644, Sigma-Aldrich
	20% FBS	FB-01, Omega Scientific, inc.
	1% Penicillin-Streptomycin-Glutamine (100X)	10378-016, Gibco
	Cell Culture Grade Water	
Basic Buffer	11 g/L Minimum Essential Medium Eagle, Joklik Modification	M0518, Sigma-Aldrich
	3 mM HEPES	H3375, Sigma-Aldrich
	1% Penicillin-Streptomycin-Glutamine (100X)	10378-016, Gibco
	10 mM Taurine	T0625, Sigma-Aldrich
	Insulin, solvate in 3% Acetic Acid/PBS	I-5500, Sigma-Aldrich
	1% Amphotericin B	15290-018, Invitrogen
	50 mg Gentamicin	G1397, Sigma-Aldrich
	Cell Culture Grade Water	

Table 3.2. List of Antibodies

Antibody	Vendor	Catalog Number	Dilution Flow	Dilution ICC/IHC
C-Kit (CD117)	R&D systems	AF1356	1:33	-
Thy-1 (CD90)	Biolegend	328109	1:33	-
Endoglin (CD105)	Biolegend	323203	1:33	-
Prominin-1 (CD133)	Thermo Fisher Scientific	PA5-38014	1:33	-
PTPRC (CD45)	Biolegend	368507	1:33	-
cTNT	Biocompare	bs-10648R-A488	-	1:200
Tropomyosin	Sigma-Aldrich	T 9283	-	1:200
eGFP	Molecular Probes	A-11122	-	1:100
mCherry	Thermo Fisher Scientific	M11240	-	1:100
Isolectin GS-IB4	Thermo Fisher Scientific	I21412	-	1:100
WGA	Thermo Fisher Scientific	W32465	-	1:500
Myc tag	Thermo Fisher Scientific	PA3-981		1:100
HA-prope	Santa Cruz Biotechnology	SC-7392	-	1:100
DAPI (4′,6-diamidino-2-phenylindole**)**	Sigma-Aldrich	D9542	-	1:10,000
Phalloidin	Thermo Fisher Scientific	A12379	-	1:1,000

Table 3.3. List of Primers

Target	Fwd Primer Sequence	Rev Primer Sequence
PECAM1	CCAAGCCCGAACTGGAATCT	CACTGTCCGACTTTGAGGCT
GATA4	CTCAGAAGGCAGAGAGTGTGTCAA	CACAGATAGTGACCCGTCCCAT
HGF	GGCTGGGGCTACACTGGATTG	CCACCATAATCCCCCTCACAT
IGF	GACCGCGGCTTCTACTTCAG	AAGAACTTGCCCACGGGGTAT
SMA	CCCAGCCAAGCACTGTCAGGAATCCT	TCACACACCAAGGCAGTGCTGTCC
CXCL12	CAGTCAACCTGGGCAAAGCC	AGCTTTGGTCCTGAGAGTCC
IL-6	TCGAGCCCACCGGGAACGAA	GCAGGGAAGGCAGCAGGCAA
18S	CGAGCCGCCTGGATACC	CATGGCCTCAGTTCCGAAAA

Table 3.4. Heart Rate and Echocardiographic Data

HEART RATE (bpm)

Heart Rate	SHAM			CardioCluster			C+E+M			Vehicle		
Week	Mean	SEM	N	Mean	SEM	N	Mean	SEM	N	Mean	SEM	N
Baseline	487.95	15.13	12	472.26	15.77	17	493.17	14.72	15	471.78	17.49	16
1	449.23	17.07	12	470.50	10.91	12	471.52	19.70	15	426.94	16.35	16
2	437.72	28.47	12	462.27	18.23	12	469.08	13.96	15	433.02	22.80	14
4	439.43	14.62	12	488.52	26.94	12	503.79	24.43	15	445.81	15.40	16
8	462.07	16.13	12	470.52	14.81	11	476.45	20.96	13	423.57	19.74	16
12	492.90	13.07	11	469.22	18.92	11	507.16	13.92	13	507.34	13.78	11
16	492.68	15.73	8	443.20	20.18	8	478.72	26.11	10	491.36	22.22	8
20	456.47	25.34	6	438.72	19.99	7	445.56	28.76	7	504.69	13.35	8

ANTERIOR WALL THICKNESS; SYSTOLE (mm)

LVAW;s	SHAM		CardioCluster		C+E+M		Vehicle	
Week	Mean	SEM	Mean	SEM	Mean	SEM	Mean	SEM
Baseline	1.16	0.05	1.16	0.04	1.07	0.04	1.21	0.04
1	1.27	0.07	0.72	0.10	0.67	0.06	0.87	0.09
2	1.13	0.06	0.60	0.07	0.62	0.07	0.58	0.03
4	1.21	0.07	0.53	0.07	0.51	0.04	0.52	0.03
8	1.22	0.05	0.62	0.08	0.54	0.08	0.45	0.04
12	1.29	0.06	0.71	0.09	0.54	0.06	0.51	0.03
16	1.18	0.07	0.69	0.08	0.48	0.05	0.36	0.04
20	1.34	0.09	0.68	0.02	0.49	0.06	0.38	0.05

ANTERIOR WALL THICKNESS; DIASTOLE (mm)

LVAW;d	SHAM		CardioCluster		C+E+M		Vehicle	
Week	Mean	SEM	Mean	SEM	Mean	SEM	Mean	SEM
Baseline	0.75	0.07	0.76	0.06	0.66	0.04	0.81	0.04
1	0.90	0.06	0.67	0.10	0.60	0.03	0.75	0.06
2	0.83	0.05	0.53	0.05	0.53	0.05	0.54	0.03
4	0.84	0.05	0.49	0.05	0.43	0.04	0.50	0.03
8	0.79	0.03	0.49	0.06	0.46	0.07	0.44	0.04
12	0.88	0.04	0.59	0.06	0.48	0.05	0.47	0.03
16	0.84	0.05	0.56	0.06	0.38	0.05	0.28	0.02
20	0.97	0.06	0.52	0.03	0.40	0.06	0.35	0.03

POSTERIOR WALL THICKNESS; SYSTOLE (mm)

LVPW;s	SHAM		CardioCluster		C+E+M		Vehicle	
Week	Mean	SEM	Mean	SEM	Mean	SEM	Mean	SEM
Baseline	1.23	0.06	1.39	0.04	1.50	0.05	1.32	0.05
1	1.27	0.08	1.25	0.07	1.28	0.12	1.25	0.09
2	1.29	0.06	1.22	0.09	1.18	0.10	1.26	0.10
4	1.05	0.09	1.11	0.06	1.01	0.09	1.12	0.07
8	1.08	0.06	0.83	0.12	1.00	0.08	0.96	0.08
12	1.10	0.06	1.17	0.09	1.32	0.09	0.96	0.08
16	1.16	0.09	1.13	0.09	1.06	0.15	0.99	0.16
20	1.20	0.07	1.34	0.10	1.03	0.06	1.20	0.15

POSTERIOR WALL THICKNESS; DIASTOLE (mm)

LVPW;d	SHAM		CardioCluster		C+E+M		Vehicle	
Week	Mean	SEM	Mean	SEM	Mean	SEM	Mean	SEM
Baseline	0.66	0.06	0.82	0.06	0.78	0.04	0.86	0.06
1	0.78	0.04	0.86	0.06	0.83	0.09	0.92	0.09
2	0.83	0.06	0.87	0.09	0.77	0.07	1.00	0.07
4	0.72	0.08	0.87	0.05	0.78	0.07	0.89	0.06
8	0.75	0.06	0.62	0.06	0.85	0.07	0.79	0.07
12	0.76	0.05	0.96	0.07	1.08	0.07	0.83	0.06
16	0.81	0.06	0.88	0.06	0.86	0.13	0.83	0.13
20	0.82	0.09	1.16	0.10	0.80	0.04	1.00	0.14

LEFT VENTRICULAR VOLUME; SYSTOLE (μL)

LV Vol;s	SHAM		CardioCluster		C+E+M		Vehicle	
Week	Mean	SEM	Mean	SEM	Mean	SEM	Mean	SEM
Baseline	14.45	1.66	13.30	1.18	12.93	1.38	13.33	0.90
1	10.81	0.90	37.98	5.44	37.63	4.19	41.07	3.59
2	12.46	1.23	42.28	3.22	45.18	4.15	45.85	3.16
4	13.22	1.41	41.83	5.20	51.40	4.58	56.60	6.31
8	11.84	0.59	45.20	5.41	54.85	6.06	64.57	7.43
12	11.71	0.67	46.84	8.88	56.34	8.24	71.03	10.05
16	11.94	1.64	40.78	5.58	56.15	10.42	71.52	9.07
20	9.72	1.37	37.64	4.29	64.76	11.04	80.37	8.77

LEFT VENTRICULAR VOLUME; DIASTOLE (μL)

LV Vol;d	SHAM		CardioCluster		C+E+M		Vehicle	
Week	Mean	SEM	Mean	SEM	Mean	SEM	Mean	SEM
Baseline	39.15	2.25	38.20	1.82	37.01	2.13	37.72	1.51
1	36.21	1.82	52.62	5.80	53.51	4.75	57.78	3.73
2	37.96	1.68	63.20	3.65	64.71	4.42	63.42	3.77
4	36.19	1.95	63.29	5.73	70.53	5.35	75.31	7.11
8	37.20	1.62	69.70	5.33	75.39	6.63	82.94	7.85
12	37.48	1.65	69.48	8.12	78.99	8.06	91.04	10.67
16	34.83	2.15	64.71	7.01	77.37	10.64	87.73	9.46
20	34.53	2.42	61.78	5.26	90.63	10.58	99.61	9.46

EJECTION FRACTION (%)

EF	SHAM		CardioCluster		C+E+M		Vehicle	
Week	Mean	SEM	Mean	SEM	Mean	SEM	Mean	SEM
Baseline	67.05	1.64	68.57	0.71	65.90	0.99	67.10	1.32
1	66.48	1.24	27.37	2.92	31.58	2.17	28.83	1.98
2	65.60	1.58	33.29	3.10	32.03	3.20	31.02	1.84
4	65.10	1.87	36.24	3.41	28.71	1.73	24.02	1.41
8	65.48	1.11	38.76	4.18	30.01	2.66	23.28	1.67
12	67.49	1.83	39.20	4.38	31.08	3.36	20.72	2.36
16	64.94	2.46	40.04	2.41	31.70	3.21	17.29	2.26
20	67.85	1.64	39.73	1.92	30.10	4.51	15.57	0.96

FRACTIONAL SHORTENING (%)

FS	SHAM		CardioCluster		C+E+M		Vehicle	
Week	Mean	SEM	Mean	SEM	Mean	SEM	Mean	SEM
Baseline	34.25	2.31	35.32	1.20	35.55	1.42	34.67	1.11
1	38.64	1.36	14.26	2.19	14.47	1.15	13.64	1.03
2	36.86	1.57	15.99	1.81	14.61	1.60	12.72	1.22
4	34.35	1.78	16.97	2.21	12.98	0.83	11.90	0.75
8	36.78	1.10	17.96	2.55	13.49	1.30	10.79	1.03
12	37.30	1.12	18.32	3.14	15.03	1.57	10.79	0.99
16	35.93	2.71	18.11	1.16	14.14	1.52	8.73	1.68
20	40.41	2.15	19.04	1.17	14.68	2.09	8.96	1.46

Echocardiographic data represented as mean ± SEM. Heart rate, anterior wall thickness, posterior wall thickness, left ventricular volume, ejection fraction and fractional shortening were measured at specified times after MI. (N) indicates the number of mice used in each group at the given time point

FIGURES

Figure 3.1. Three distinct cardiac cell types used to generate CardioClusters
A-C, Representative brightfield (BF) and immunofluorescent images for cCIC (eGFP^{+}) **(A)**, EPC (mOrange^{+}) **(B)** and MSC (Neptune^{+}) **(C)**. Scale bars: brightfield, 100 μm; immunofluorescent, 50 μm. DAPI to visualize nuclei (white). **D-F**, Cell morphometric parameters measuring area (a.u.: arbitrary units; **D**), roundness **(E)**, and length-to-width (L/W) ratio (**F;** n=3 human heart isolations; minimum of 30 cells traced per cell type, per heart). **G**, Cardiac cell proliferation measured using CyQuant assays at day 0, day 1, day 3, and day 5 (n=3). **H-J**, Annexin V/Sytox Blue labeling for apoptotic **(H)**, necrotic **(I)** and healthy **(J)** cells following cell death assay: 24 hours of low serum (75% serum reduction) followed by 4 hours treatment with 30 μM H_2O_2 in low serum medium (n=4). Data are presented as 1-way ANOVA, *p<0.05, **p<0.01, ***p<0.001. **K**, Schematic showing CardioCluster formation using three cell populations isolated from human heart tissue: MSC (red), cCIC (green), EPC (blue). **L**, Live CardioCluster visualized by endogenous fluorescent tags showing cCIC (eGFP; FITC channel; green), MSC (Neptune; APC channel; red) and EPC (mOrange; PE channel; blue). Scale bar, 75 μm. **M**, 3D cross section of a CardioCluster lightly fixed in 4% paraformaldehyde and stained with 4′,6-diamidino-2-phenylindole (DAPI; white) to visualize nuclei and cells exhibiting fluorescent tags without the need for antibody labeling. Scale bar, 75 μm. **N**, Representative brightfield images of CardioClusters ranging in size from 100-1000 cells cultured over a 7-day period. Scale bar, 100 μm. **O**, Determination of cell number enabling CardioClusters to pass through a 30-gauge needle, which has an inner diameter (I.D.) of 159 μm. Graph plot of CardioCluster diameters averaged over 3 days (n=4-7).

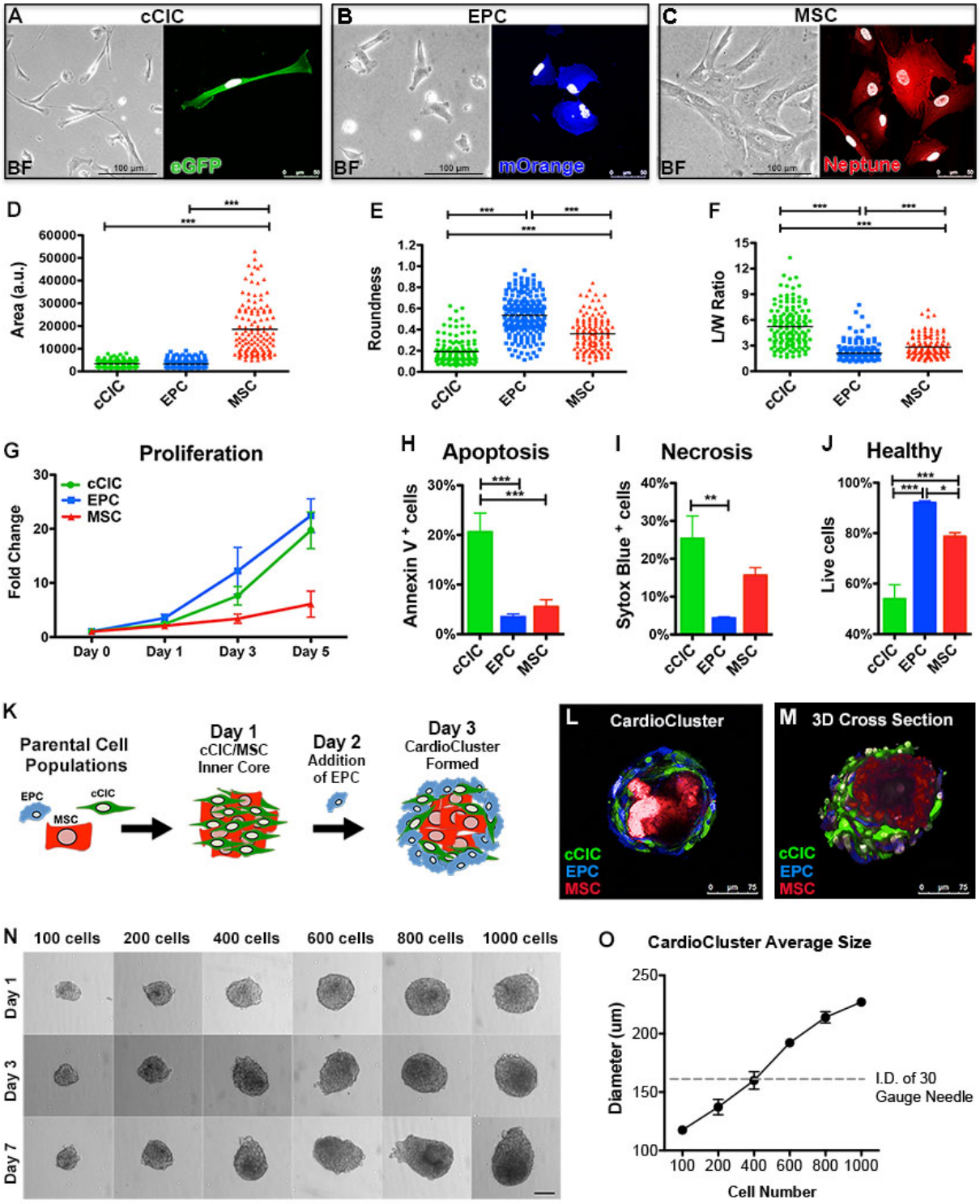
A
cCIC
BF
eGFP
B
EPC
BF
mOrange
C
MSC
BF
Neptune
D
Area (a.u.)
60000
50000
40000
30000
20000
10000
0
cCIC
EPC
MSC
E
Roundness
1.2
1.0
0.8
0.6
0.4
0.2
0.0
F
L/W Ratio
15
12
9
6
3
0
G
Proliferation
Fold Change
cCIC
EPC
MSC
Day 0
Day 1
Day 3
Day 5
H
Apoptosis
Annexin V + cells
30%
20%
10%
0%
I
Necrosis
Sytox Blue + cells
40%
30%
20%
10%
0%
J
Healthy
Live cells
100%
80%
60%
40%
K
Parental Cell Populations
EPC
cCIC
MSC
Day 1
cCIC/MSC
Inner Core
Day 2
Addition
of EPC
Day 3
CardioCluster
Formed
L
CardioCluster
cCIC
EPC
MSC
M
3D Cross Section
cCIC
EPC
MSC
N
100 cells
200 cells
400 cells
600 cells
800 cells
1000 cells
Day 1
Day 3
Day 7
O
CardioCluster Average Size
Diameter (um)
250
200
150
100
I.D. of 30
Gauge Needle
100
200
400
600
800
1000
Cell Number

Figure 3.2. CardioCluster formation and characterization
A, Human phosphorglycerate kinase (hPGK) lentiviral backbones of fluorescent protein tags used to transduce parental cell lines. cCIC express eGFP, EPC express mOrange (with a 3x myc tag), and MSC express Neptune (with a 3x HA tag). **B**, Representative flow cytometry plots showing the percentage of cells expressing their respective fluorescent proteins. **C**, CardioClusters are formed using 96 well, ultra-low attachment round bottom plates in a two-step process. The first step generates the inner core composed of cCIC and MSC, and the second step forms the outer EPC layer. The inner core of cCIC and MSC is seeded for 24 hours. The EPC are added the following day and resulting cell mixture is incubated for an additional 48-72 hours prior to experimentation. Schematic adapted from previous publication[146]. **D**, CardioCluster morphometric parameters measuring area (a.u.: arbitrary units.), roundness, and length-to-width (L/W) ratio over a 7 day time course for CardioClusters ranging from 100-1000 cells. **E**, Still frame images from a video showing CardioCluster formation.

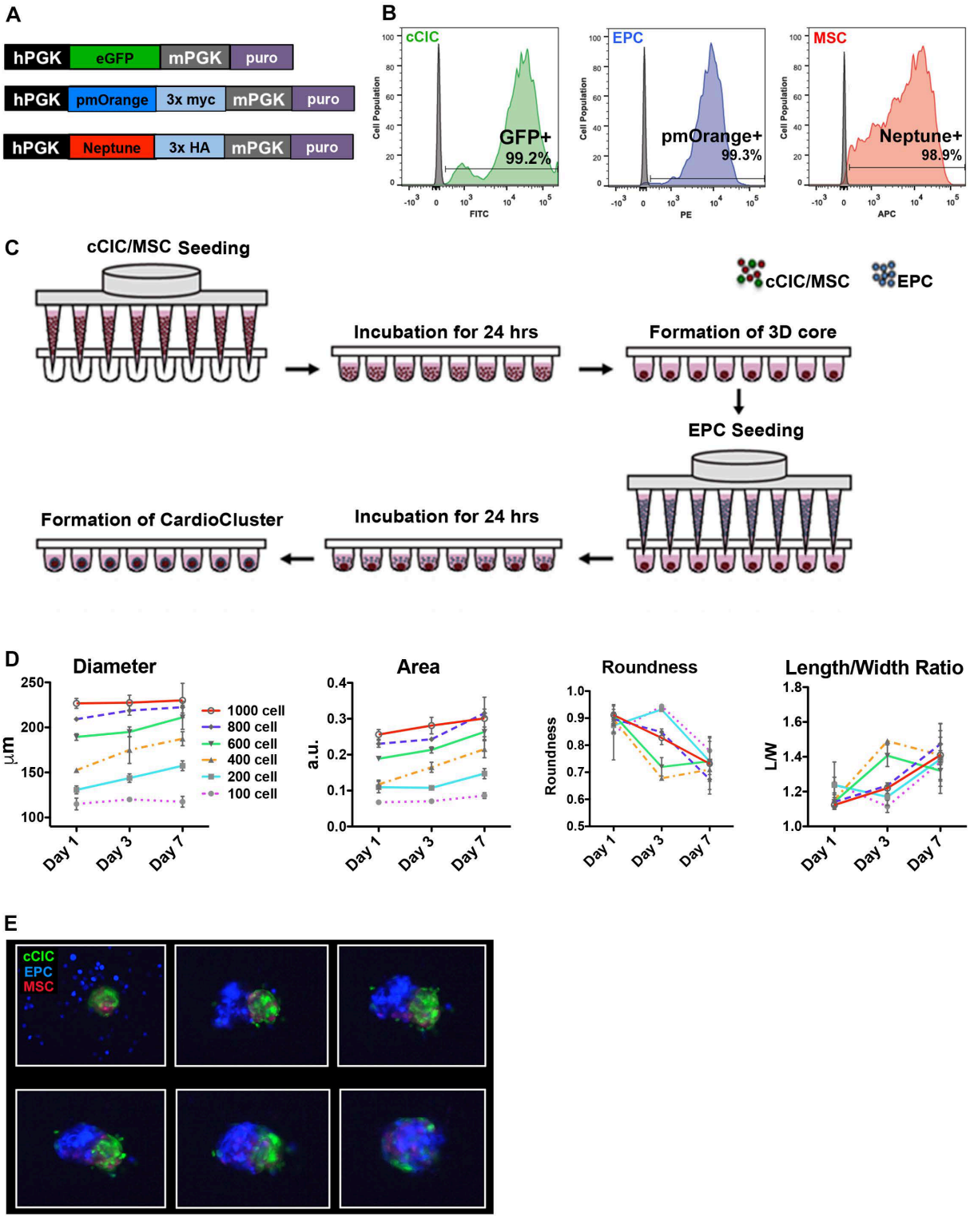
A
hPGK
eGFP
mPGK
puro
hPGK
pmOrange
3x myc
mPGK
puro
hPGK
Neptune
3x HA
mPGK
puro
B
cCIC
GFP+
99.2%
EPC
pmOrange+
99.3%
MSC
Neptune+
98.9%
Cell Population
FITC
PE
APC
C
cCIC/MSC Seeding
cCIC/MSC
EPC
Incubation for 24 hrs
Formation of 3D core
EPC Seeding
Incubation for 24 hrs
Formation of CardioCluster
D
Diameter
Area
Roundness
Length/Width Ratio
μm
a.u.
Roundness
L/W
1000 cell
800 cell
600 cell
400 cell
200 cell
100 cell
Day 1
Day 3
Day 7
E
cCIC
EPC
MSC

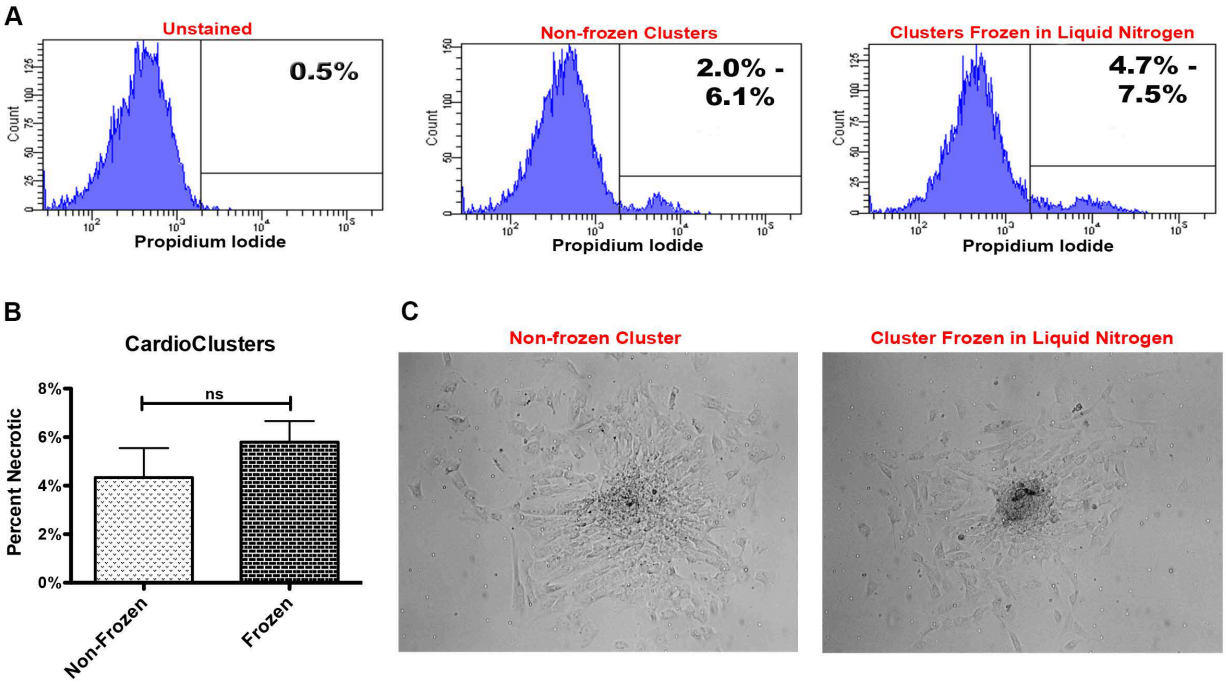

Figure 3.3. CardioClusters frozen in liquid nitrogen maintain structural integrity and viability

A, Representative flow cytometry plots showing propidium iodide (PI) gating strategy used in freezing assay. **B**, Brightfield images showing cell outgrowth of non-frozen versus liquid nitrogen frozen CardioClusters. **C**, Quantification of percent necrotic (PI^+) cells from non-frozen versus liquid nitrogen frozen experimental groups. Data are presented as 1-way ANOVA, *p<0.05, **P<0.01, ***p<0.001, versus non-frozen CardioClusters. ns indicates not statically significant.

Figure 3.4. CardioCluster single cell RNA-Seq reveals transcriptional profile acquisition with increased similarity to freshly isolated cardiac interstitial cells

A-F, Transcriptional profiling on CardioClusters and parental cells using scRNA-seq. **A**, t-SNE map showing cells grown within a 3D CardioCluster (orange) predominately cluster together, while cCICs (green), EPCs (blue), and MSCs (red) primarily cluster into their own individual groups. **B**, Heatmap of differentially expressed genes (DEGs) among CardioClusters and parental cells. Selected DEGs for each group are color-coded and shown on the right. **C**, Violin plots of expression distribution for selected DEGs. **D**, Gene Ontology (GO) term analysis of molecular functions that are enriched based on DEGs. **E-F**, DEGs compared to genes expressed by freshly isolated mouse cardiac interstitial cells (mFreshCIC) represented in a Venn diagram **(E)** and heatmap of the gene set coexpressed by freshly isolated cells in comparison to CardioCluster and parental cell populations **(F)**. hParental indicates human parental cells; hCardioCluster, human CardioCluster cells; BAMBI, BMP and activin membrane bound inhibitor; LIF, leukemia inhibitory factor; CXCL12, C-X-C motif chemokine 12 or stromal cell-derived factor 1 (SDF1); ACTA2, smooth muscle alpha (α)-2 actin; C. Cluster, CardioCluster.

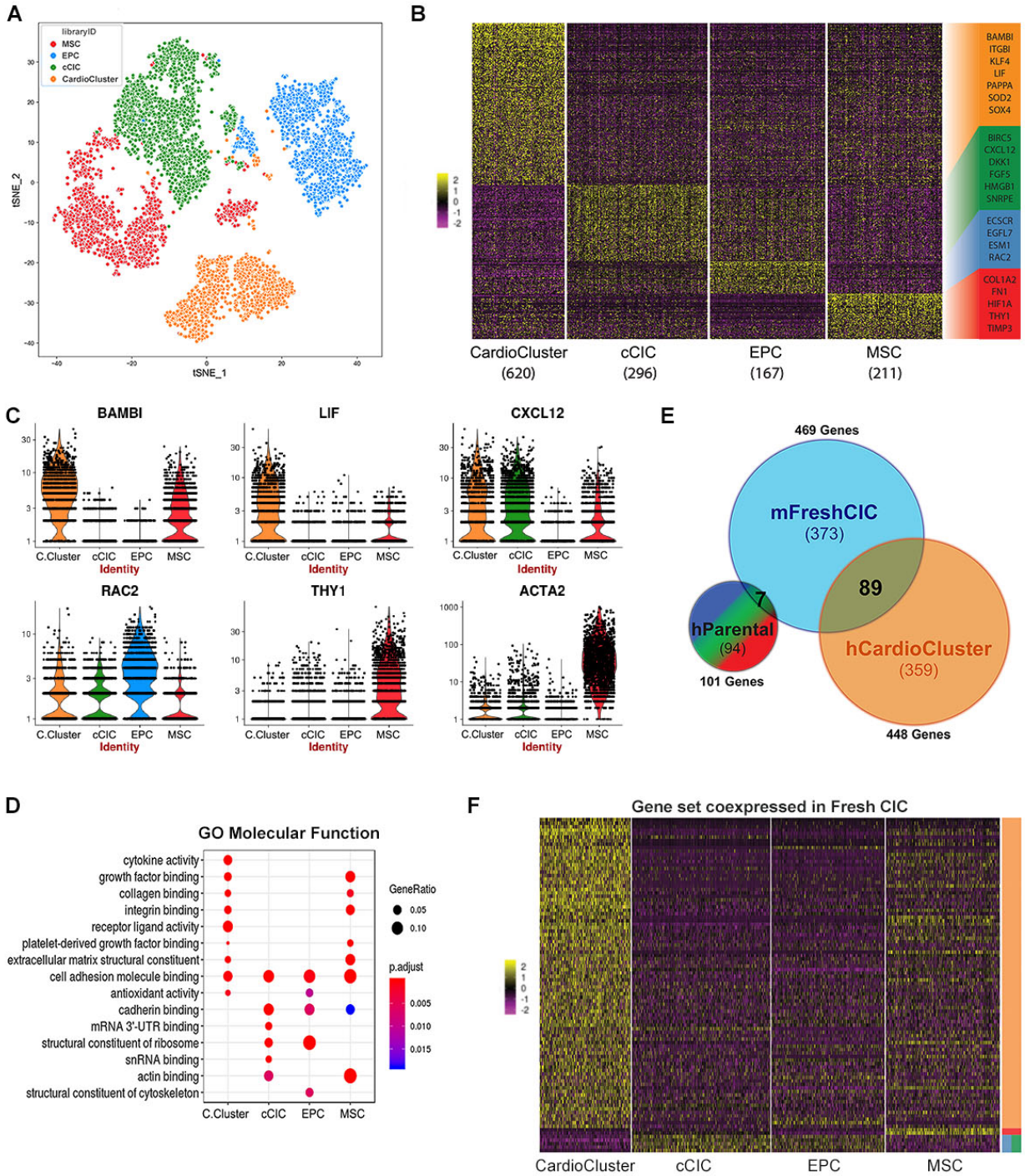
A
libraryID
MSC
EPC
cCIC
CardioCluster
tSNE_2
tSNE_1
B
BAMBI
ITGBI
KLF4
LIF
PAPPA
SOD2
SOX4
BIRC5
CXCL12
DKK1
FGF5
HMGB1
SNRPE
ECSCR
EGFL7
ESM1
RAC2
COL1A2
FN1
HIF1A
THY1
TIMP3
CardioCluster (620)
cCIC (296)
EPC (167)
MSC (211)
C
BAMBI
LIF
CXCL12
RAC2
THY1
ACTA2
C.Cluster
cCIC
EPC
MSC
Identity
D
GO Molecular Function
cytokine activity
growth factor binding
collagen binding
integrin binding
receptor ligand activity
platelet-derived growth factor binding
extracellular matrix structural constituent
cell adhesion molecule binding
antioxidant activity
cadherin binding
mRNA 3'-UTR binding
structural constituent of ribosome
snRNA binding
actin binding
structural constituent of cytoskeleton
GeneRatio
0.05
0.10
p.adjust
0.005
0.010
0.015
E
469 Genes
mFreshCIC
(373)
89
7
hParental
(94)
101 Genes
hCardioCluster
(359)
448 Genes
F
Gene set coexpressed in Fresh CIC
CardioCluster
cCIC
EPC
MSC

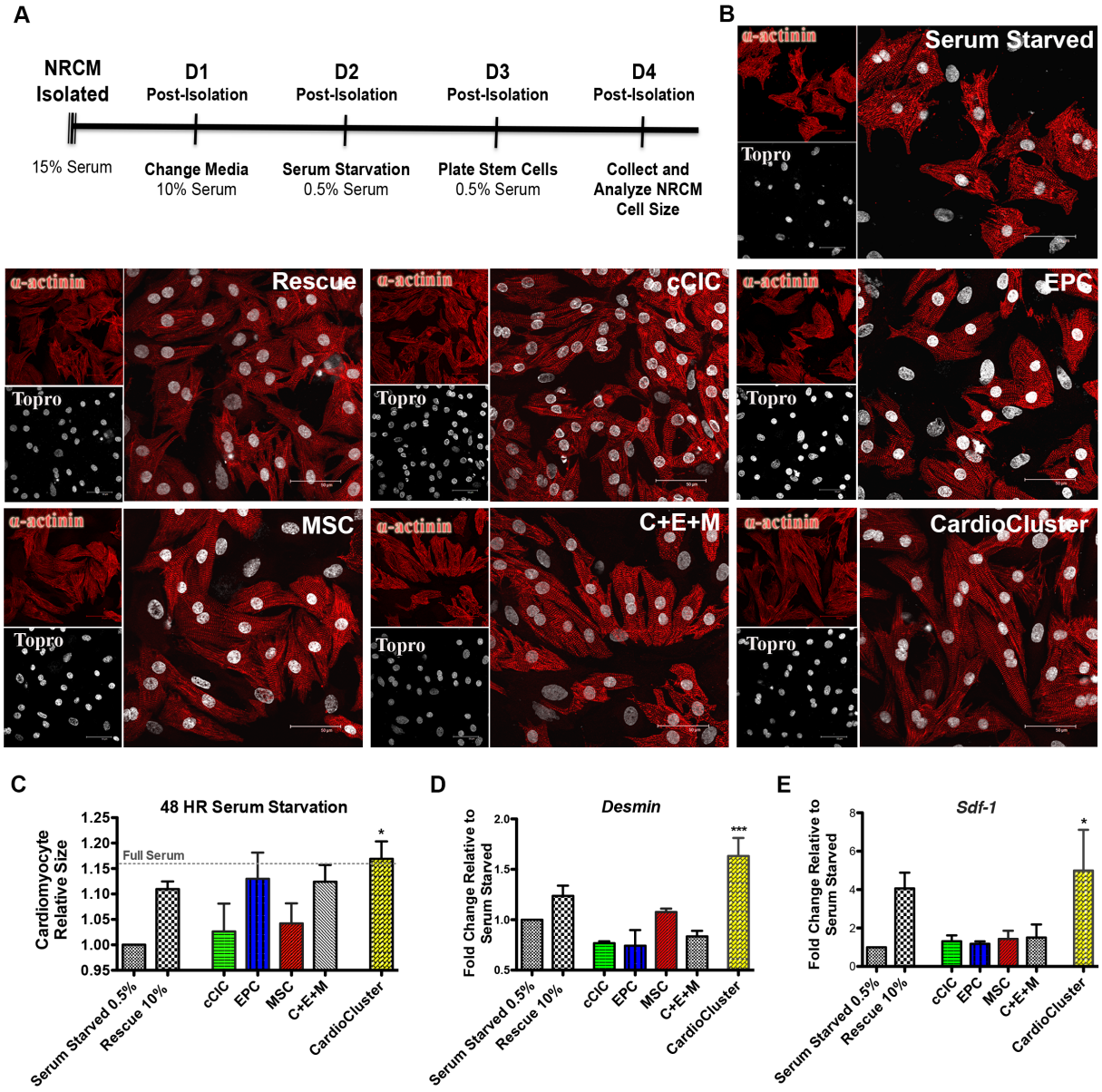

Figure 3.5. CardioClusters protect cardiomyocytes against low serum conditions *in vitro* **A**, Timeline for neonatal rat cardiomyocyte (NRCM) low serum assay over a 4-day (D) period. **B**, Representative images of NRCM conditions: serum starved (48 hours of 0.5% serum), rescued (24 hours of 0.5% serum with 10% serum added for additional 24 hours), and experimental groups (24 hours of 0.5% serum with addition of either cCIC, EPC, MSC, C+E+M, or CardioCluster for additional 24 hours). Cardiomyocytes visualized by staining with sarcomeric actinin (α-actinin; red). TO-PRO-3 iodide (Topro; white) used to visualize nuclei. Scale bar, 50 μm. **C**, Quantitation of cardiomyocyte size relative to serum starved control. **D**-**E**, Gene expression of *desmin* **(D)** and *sdf-1* **(E)** in cardiomyocytes with and without the addition of cells. Data are presented as 1-way ANOVA, *p<0.05 and ***p<0.001, versus serum starved control (n=3).

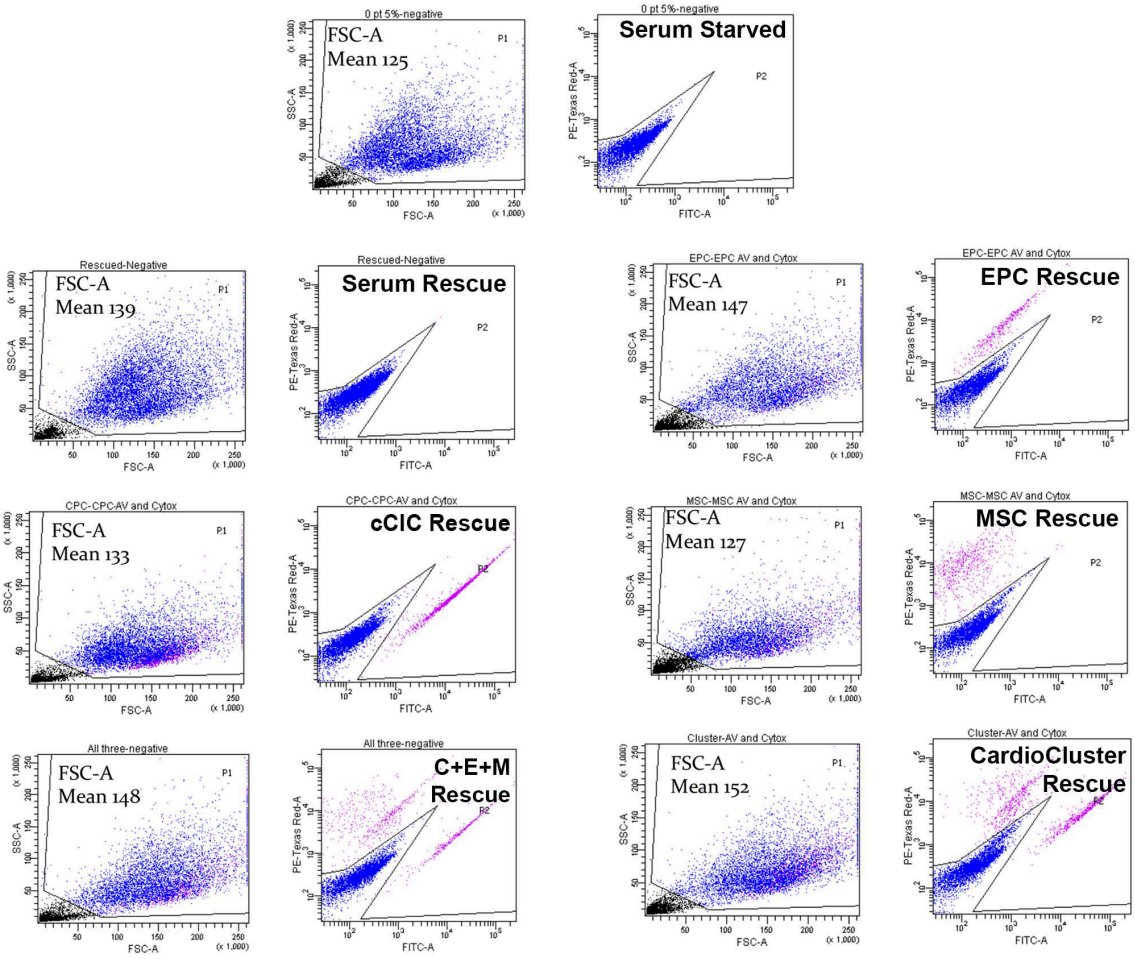

Figure 3.6. CardioClusters restore NRCM morphology following serum starvation
Representative flow cytometry plots showing forward scatter (FSC-A) used to quantitate neonatal rat cardiomyocyte (NRCM) mean area. Human cardiac cell populations are excluded from analysis by gating out fluorescently tagged cells (represented by pink cells in plots). NRCMs included in analysis are represented in blue.

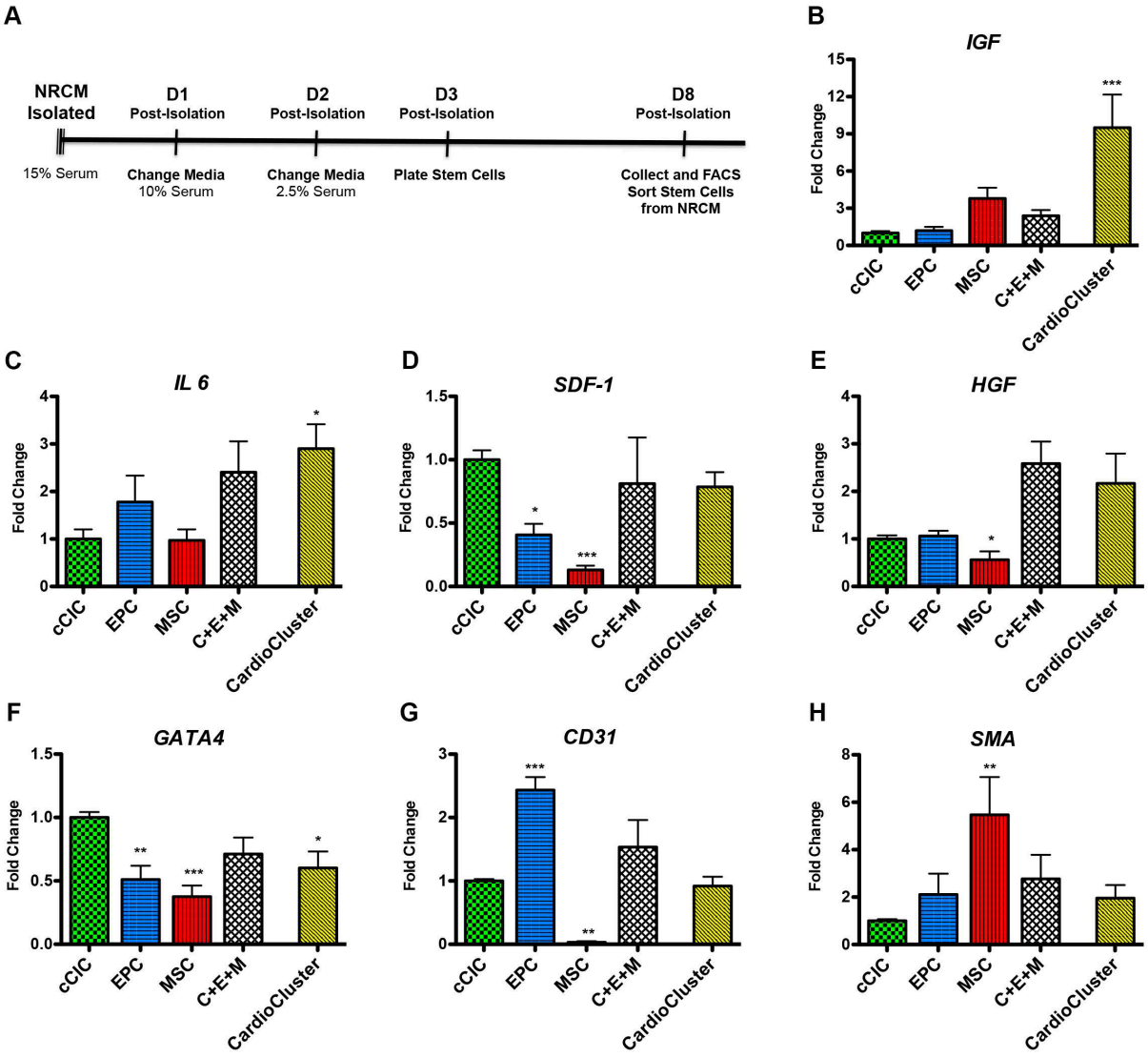

Figure 3.7. CardioClusters have increased paracrine and commitment gene expression after *in vitro* co-culture with cardiomyocytes

A, Timeline for NRCM co-culture commitment assay. **B-H**, Gene expression in interstitial cells after a 7-day co-culture with NRCMs. **B**, *IGF* **C**, *IL-6* **D**, *SDF-1* **E**, *HGF* **F**, *GATA4* **G**, *CD31* and **H**, *SMA* gene expression (n=3 NRCM preps). Data are presented as 1-way ANOVA, *p<0.05, **p<0.01, ***p<0.001, versus cCIC.

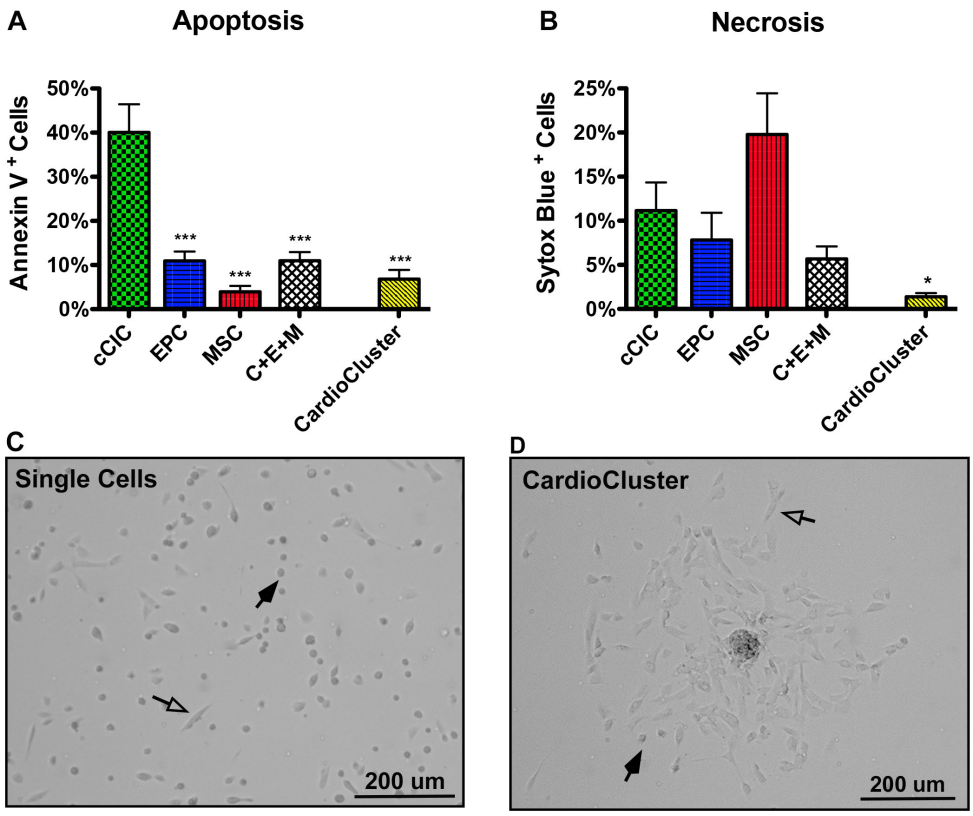

Figure 3.8. CardioClusters exhibit increased protection from oxidative stress
A-D, Cell death assay performed on cardiac cell populations under 24 hours of low serum (75% serum reduction), followed by 4 hours of treatment with 30 μM H_2O_2 in low serum medium. **A-B**, Apoptosis visualized by Annexin V **(A)** and necrosis visualized by Sytox Blue **(B)**. Data are presented as 1-way ANOVA, *p<0.05, **p<0.01, ***p<0.001, versus cCIC (n=3-5). **C-D**, Brightfield images of single cells **(C)** and CardioClusters **(D)** 4 hours after H_2O_2 treatment. Transparent arrows highlight adherent (healthy) cells and black arrows highlight cells that have rounded up and detached from the tissue culture surface, presumably undergoing cell death.

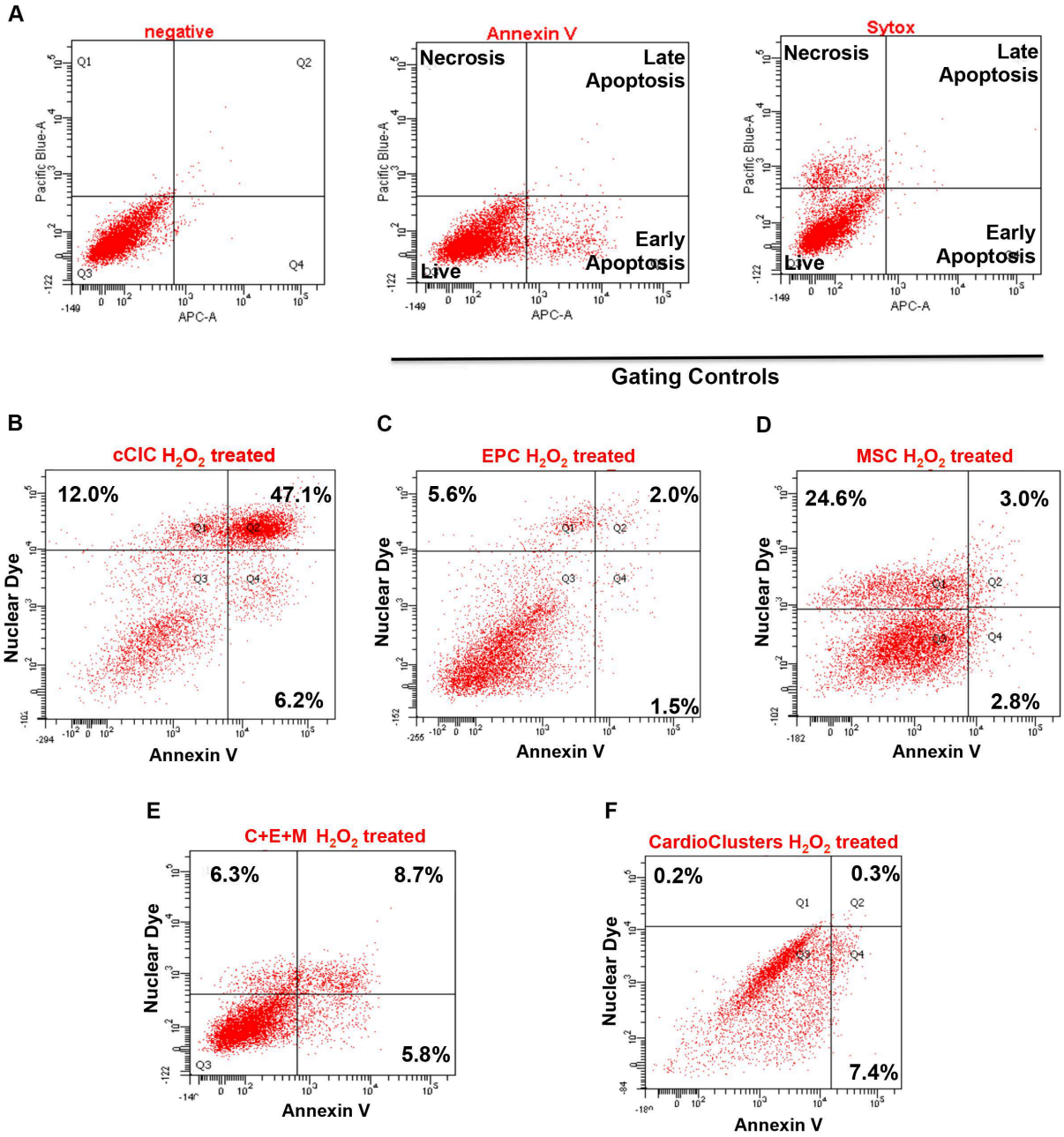

Figure 3.9. Representative staining for markers of apoptosis and necrosis
A, Representative flow cytometry plots showing Annexin V/Sytox Blue gating strategy used in cell death assay. **B-F**, Representative flow cytometry plots showing Annexin V/Sytox Blue labeling following cell death assay on cardiac cell populations under 24 hours of low serum (75% serum reduction) and 4 hours of treatment with 30 μM H_2O_2 in low serum medium for cCIC **(B)**, EPC **(C)**, MSC **(D)**, C+E+M **(E)**, and CardioCluster **(F)**.

Figure 3.10. CardioCluster treatment improves left ventricular wall structure and cardiac function after myocardial injury

A, Representative 2D echocardiography images (M-mode) at study completion (week 20). Parasternal short-axis view showing LV anterior wall and posterior wall movement. **B-D**, Longitudinal assessment of LV fractional shortening (FS, %) **(B),** ejection fraction (EF, %) **(C)**, and anterior wall thickness in systole (LVAW;s, mm) **(D)** over 20 weeks. Data are presented as 1-way ANOVA, analyzed per timepoint, **p<0.01 and ***p<0.001, CardioCluster versus vehicle. $^{+}$p<0.05 and $^{+++}$p<0.001, C+E+M versus vehicle. $^{\$}$p<0.05, CardioCluster versus C+E+M. Sample size specified in Supplemental Table 6. **E**, Percent change in EF from week 1 to week 20. Data are presented as 1-way ANOVA, ***p<0.001, versus CardioCluster. $^{++}$p<0.01, versus C+E+M (n=7–8 mice per group). **F-G**, Bar graph showing LV volume in systole (Vol;s, µl; **(F)** and in diastole (Vol;d, µl; **(G**). Data are presented as 1 Way ANOVA, *p<0.05, **p<0.01, ***p<0.001, versus CardioCluster. Sample size specified in Supplemental Table 6. **H**, Heart weight to tibia length ratio (HW/TL; mg/mm) at week 20. Data are presented as 1-way ANOVA, *p<0.05, **p<0.01, versus sham (n=4–5 mice per group). I**-M**, Masson's Trichrome staining used to evaluate LV fibrotic area. Percentage of fibrotic LV in CardioCluster, C+E+M and vehicle-treated hearts **(I)**. Data are presented as 1-way ANOVA, *p<0.05, versus CardioCluster (n=4–5 mice per group). Representative histology sections of sham **(J)**, vehicle **(K)**, CardioCluster **(L)**, and C+E+M **(M)** treated hearts 20 weeks after MI. Collagen-rich areas (scar tissue) are colored in blue and healthy myocardium in red.

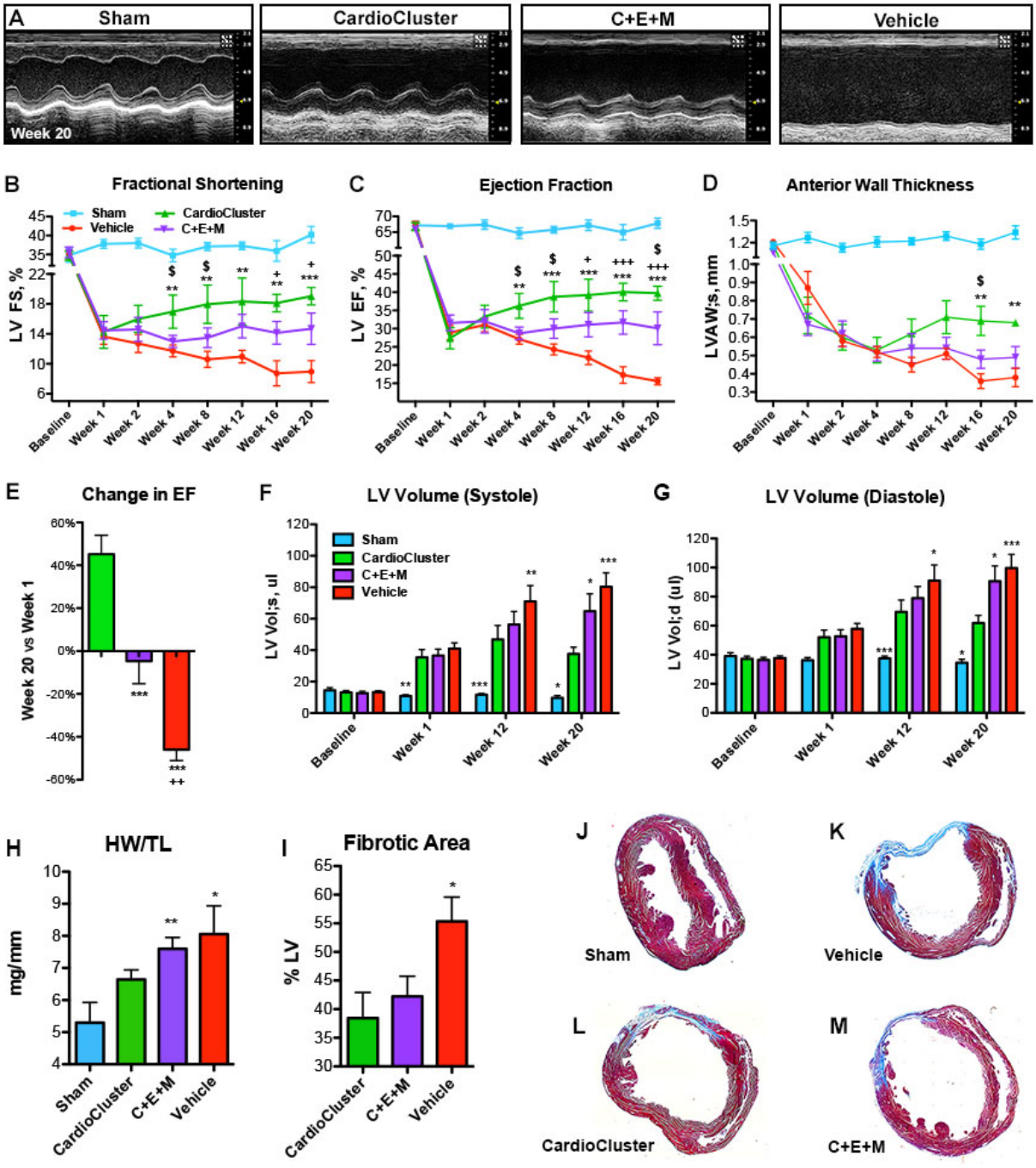
A
Sham
CardioCluster
C+E+M
Vehicle
Week 20
B
Fractional Shortening
LV FS, %
Sham
Vehicle
CardioCluster
C+E+M
Baseline
Week 1
Week 2
Week 4
Week 8
Week 12
Week 16
Week 20
C
Ejection Fraction
LV EF, %
D
Anterior Wall Thickness
LVAW;s, mm
E
Change in EF
Week 20 vs Week 1
F
LV Volume (Systole)
LV Vol;s, ul
G
LV Volume (Diastole)
LV Vol;d (ul)
H
HW/TL
mg/mm
I
Fibrotic Area
% LV
J
Sham
K
Vehicle
L
CardioCluster
M
C+E+M

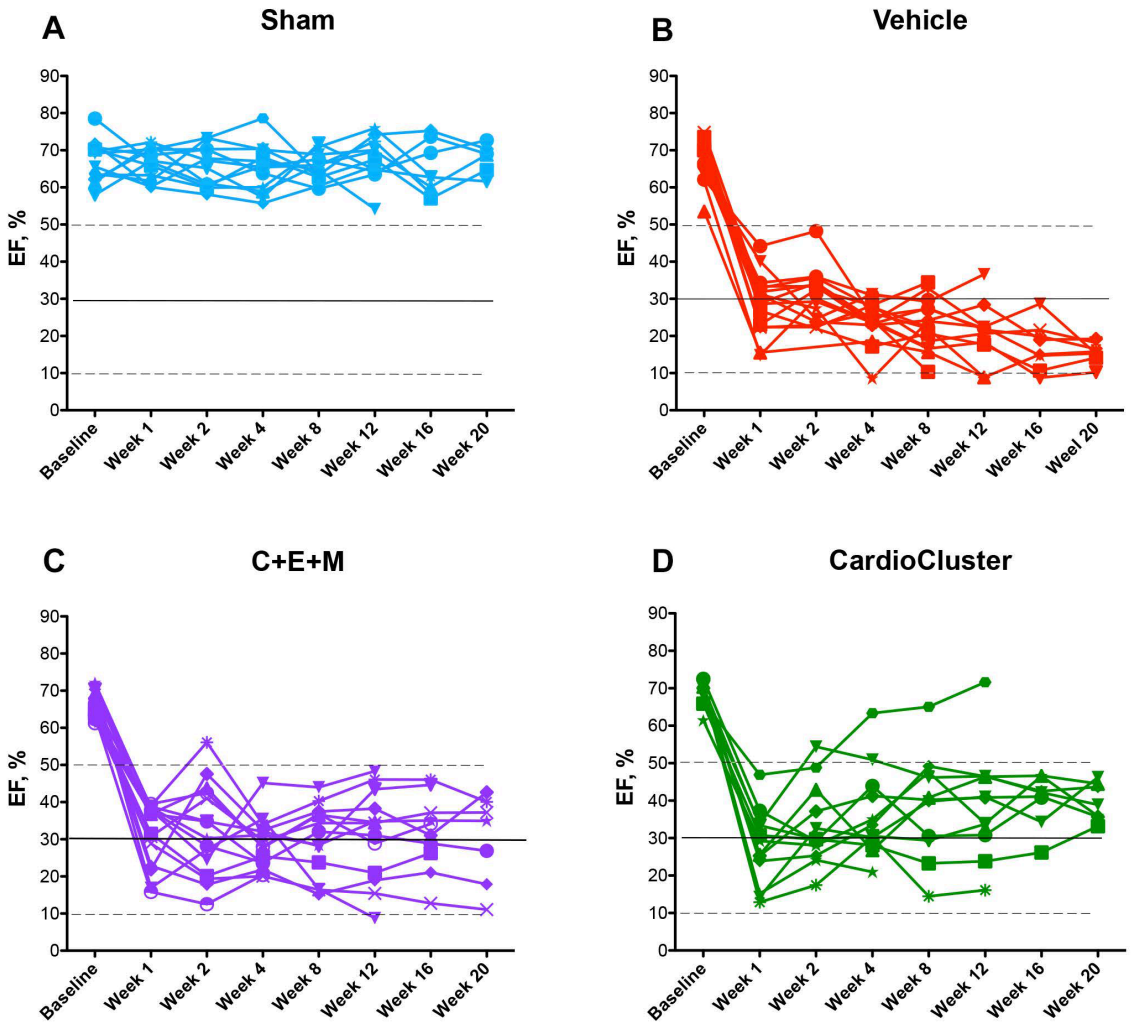

Figure 3.11. Ejection fraction for individual mice grouped by surgery
A-D, Longitudinal assessment of ejection fraction (EF, %) over 20 weeks for individual mice by surgery type: sham **(A)**, vehicle **(B)**, C+E+M **(C)**, and CardioCluster **(D)**.

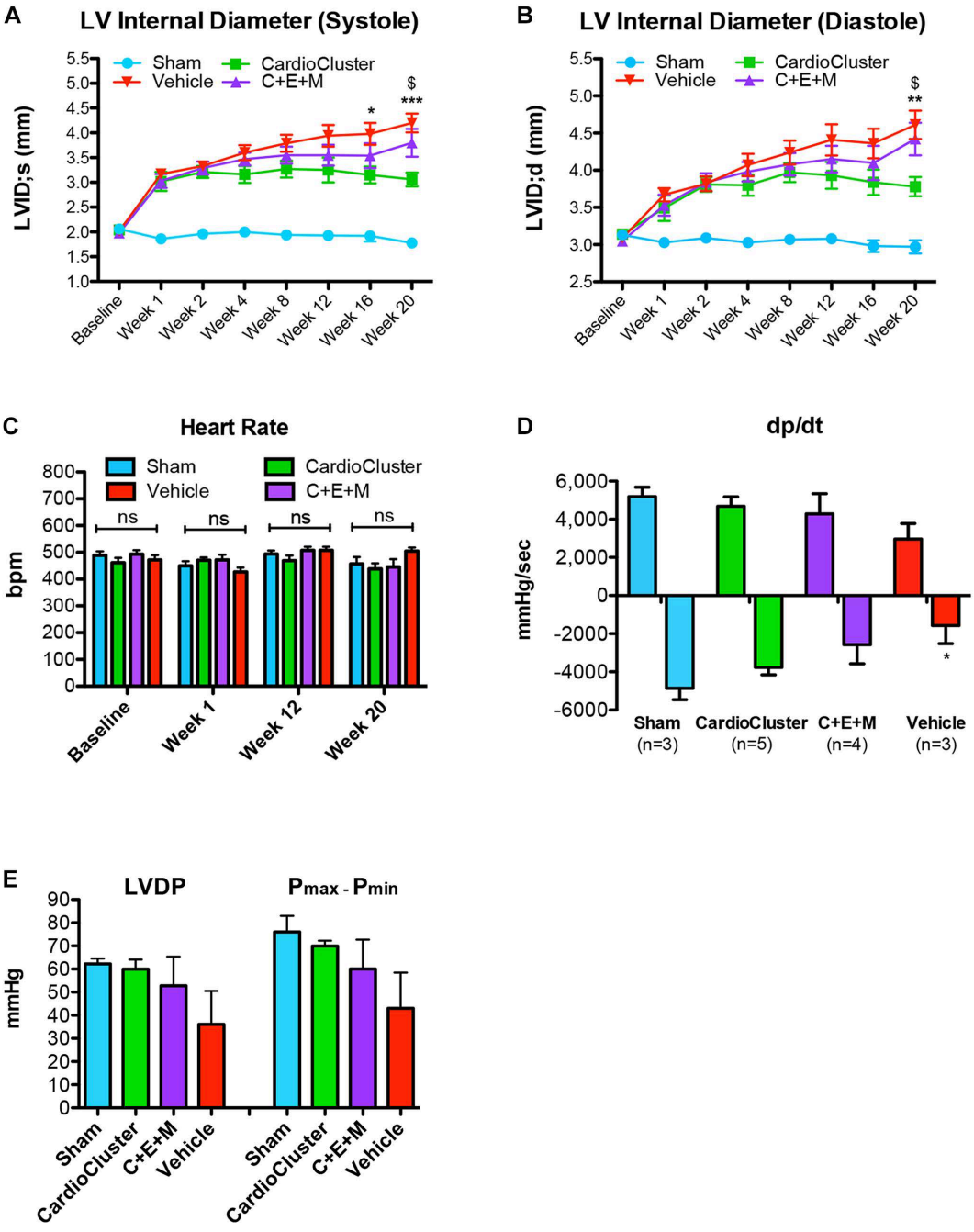

Figure 3.12. Hemodynamic data confirms CardioCluster treatment preserves cardiac function

A-B, LV internal diameter (LVID) in systole (LVID;s; **A**) and diastole (LVID;d; **B**). Sample size specified in Supplemental Table 6. **C,** Heart rates (beats per minute [bpm]) for sham, CardioCluster, C+E+M, and vehicle treatment groups shown at baseline, week 1, week 12 and week 20. Sample size specified in Supplemental Table 6. **D-E**, Hemodynamic analysis showing developed pressure over time (dP/dt, mmHg/sec; **D**) and left ventricular developed pressure (LVDP, mmHg) and pressure max minus pressure min (P_{max}-P_{min}, mmHg) shown at week 20 (**E**; n=3-5 mice per group). Data are presented as 1-way ANOVA, *p<0.05, versus sham.

Figure 3.13. Impact of CardioClusters on cardiac function measured by cardiac strain
A-B, Representative images of long-axis echocardiography recording (left panel), with cross-sectional segment synchronicity map (middle panels), and radial and longitudinal strain curves (right panels) at week 1 **(A)** and week 20 **(B)**. Strain curves (representing strain measures over time) are generated for the 6 standard myocardial regions, with a 7th line (shown in black) denoting the average strain. **C-D**, Speckle tracking echocardiography analysis used to determine global peak radial strain (%) **(C)** and global peak longitudinal strain (%) **(D)** at week 1, week 8, and week 20. Data are presented as 2-way ANOVA, *p<0.05, **p<0.01, ***p<0.001, versus sham. $^{+}$p<0.01, $^{++}$p<0.05, $^{+++}$p<0.001, versus CardioCluster. $^{\$}$p<0.05, versus C+E+M (n=6–8 mice per group). **E**, Speckle tracking echocardiography analysis used to determine regional peak radial and longitudinal strain (%) in the area of injury at week 1 and week 20. Data are presented as 2-way ANOVA, **p<0.01, versus vehicle. $^{+++}$p<0.001, versus CardioCluster. $^{\$}$p<0.05, versus C+E+M (n=6–9 mice per group). **F**, Total change in regional radial and longitudinal strain from week 1 to week 20 in the area of injury. Data are presented as 1-way ANOVA, *p<0.05, **p<0.01, ***p<0.001, versus CardioCluster (n=6–9 mice per group).

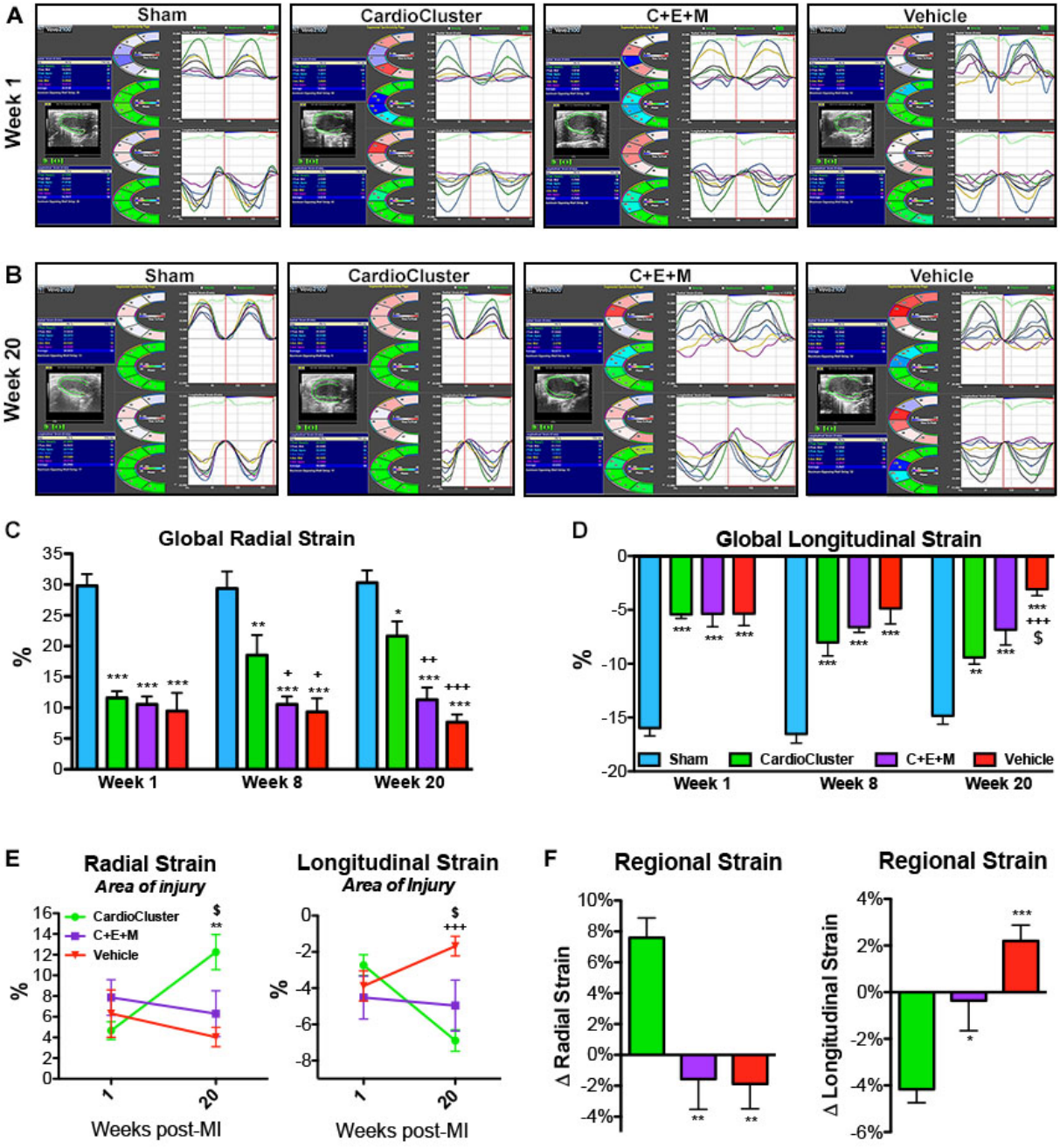
A
Sham
CardioCluster
C+E+M
Vehicle
Week 1
B
Sham
CardioCluster
C+E+M
Vehicle
Week 20
C
Global Radial Strain
%
Week 1
Week 8
Week 20
D
Global Longitudinal Strain
%
Sham
CardioCluster
C+E+M
Vehicle
Week 1
Week 8
Week 20
E
Radial Strain
Area of injury
CardioCluster
C+E+M
Vehicle
%
Weeks post-MI
Longitudinal Strain
Area of Injury
%
Weeks post-MI
F
Regional Strain
Δ Radial Strain
Regional Strain
Δ Longitudinal Strain

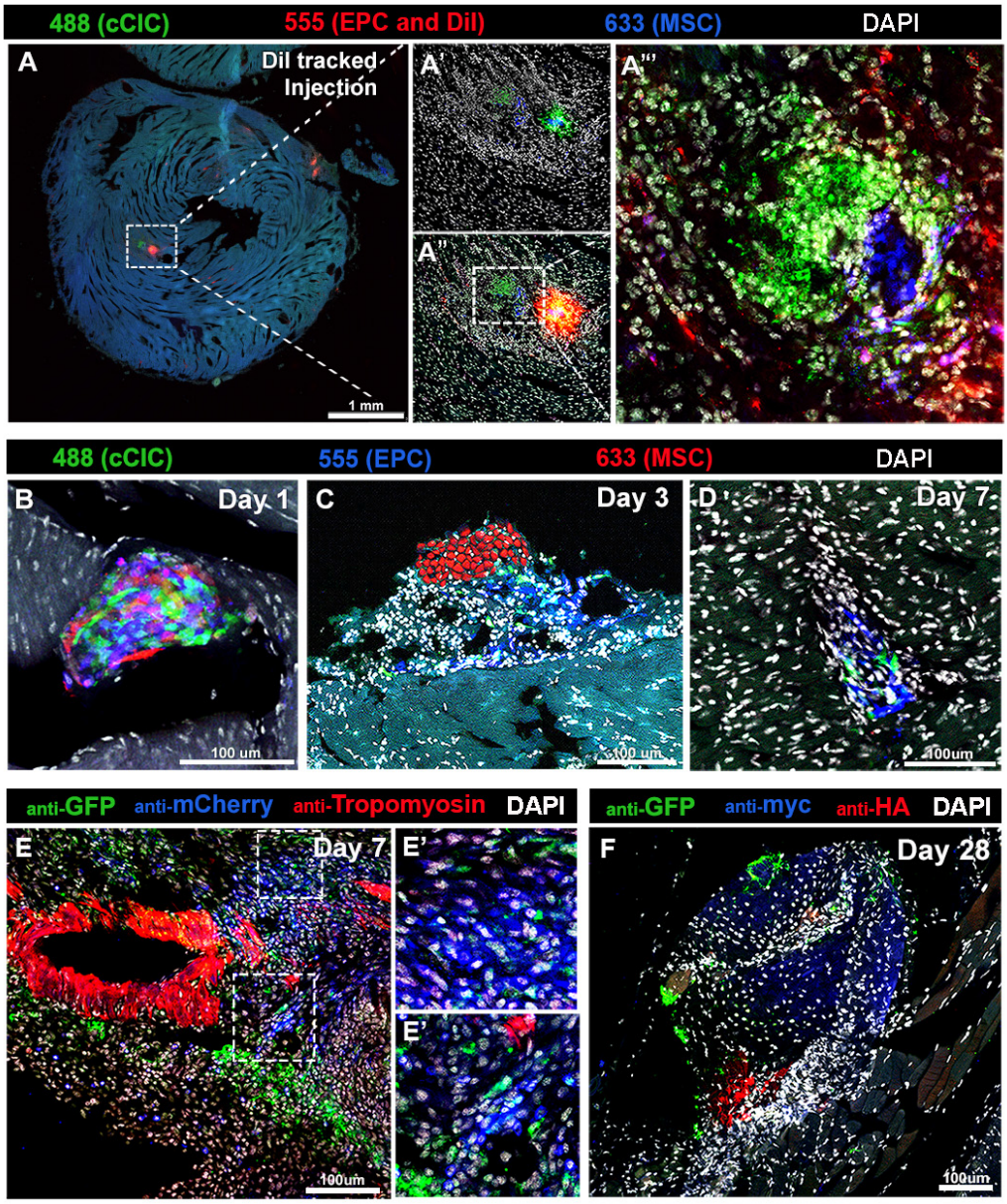

Figure 3.14. CardioCluster show enhanced engraftment and persistence in the myocardial wall

A, Immunofluorescent tile scan of a cryosectioned heart from an animal injected with CardioClusters day 3 post-surgery tracked by DiI beads with no antibody labeling required for visualization of cells. **A'-A'''**, Higher magnification of areas with white dotted boxes. **A'**, Illustrates the removal of the 555nm channel in order to better visualize cCIC (green) and MSC (blue), without DiI beads. **A''- A'''**, 555nm channel restored **(A'')** and field of view magnified **(A''')**. **B-D**, Immunofluorescent images from cryosectioned MI hearts injected with CardioClusters at day 1 **(B)**, day 3 **(C)**, and day 7 **(D)** . **E-F**, Antibody labeled immunofluorescent images from MI hearts injected with CardioClusters at day 7 **(E)** and day 28 **(F)**. **E'**, Higher magnification of areas with white dotted boxes. Antibody labeling: anti-GFP labels CCIC, anti-mCherry labels EPC and MSC (E); anti-GFP labels CCIC, anti-myc labels EPC and anti-HA labels MSC (F). Scale bars: 1mm (A); 100μm (B-F).

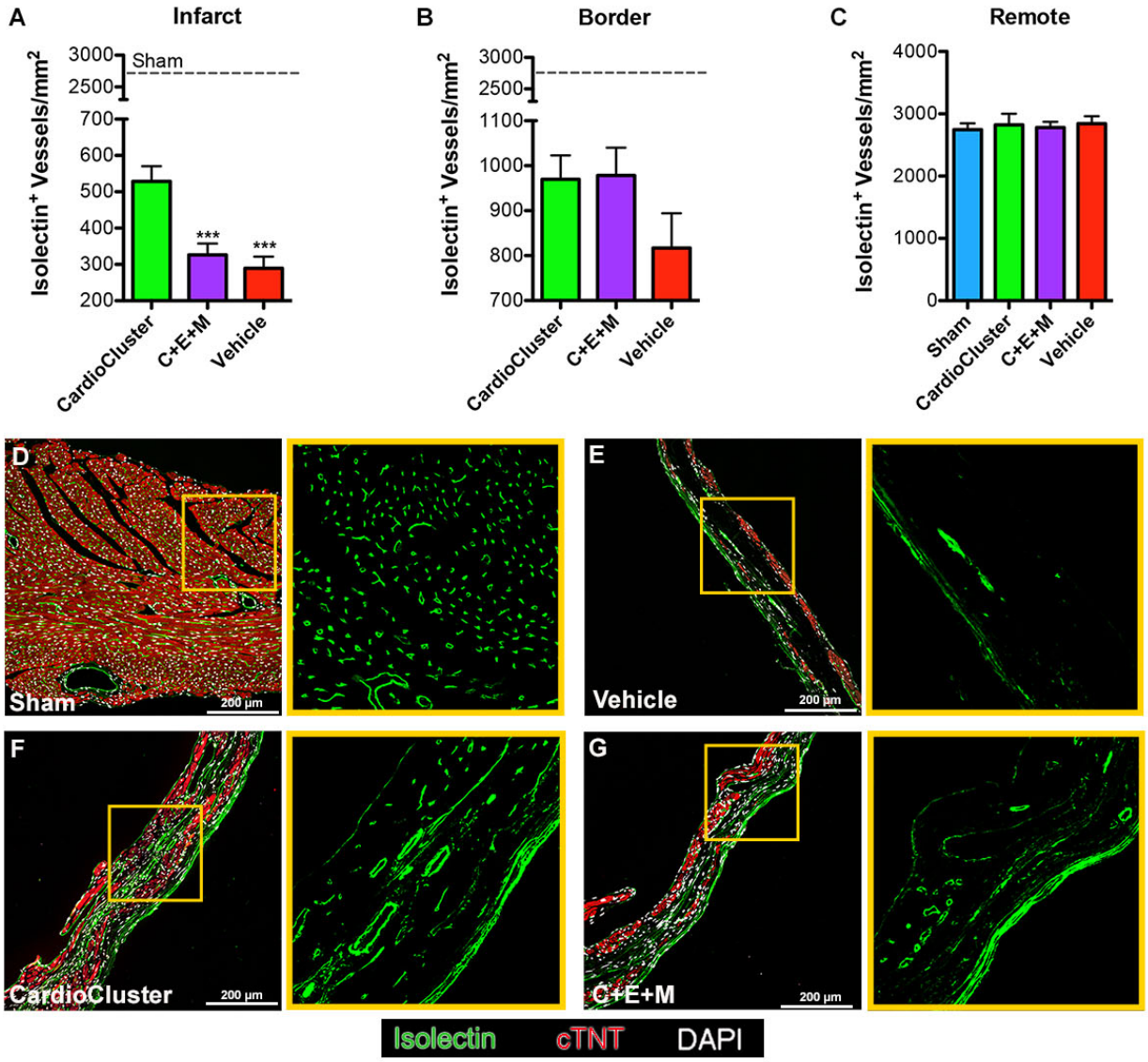

Figure 3.15. CardioCluster treatment increases capillary density in the infarct region
A-C, Quantitative analysis represents measurement of capillary density in the infarct **(A)**, border zone **(B)**, and remote **(C)** heart regions (n= 4-6 mice per group). Dashed line: mean capillary density of sham group. **D-G**, Representative image of isolectin$^+$ vessels in sham **(D)** and infarct regions of Vehicle **(E)**, CardioCluster **(F)**, and C+E+M **(G)** used to quantitate capillaries (isolectin B4; green), cardiac troponin T (cTNT; red), and nuclei (DAPI; white). Right panels show higher magnification of isolectin$^+$ vessels from areas highlighted by yellow boxes. Scale bar, 200 µm. Data are presented as 1-way ANOVA, ***p<0.001, versus CardioCluster.

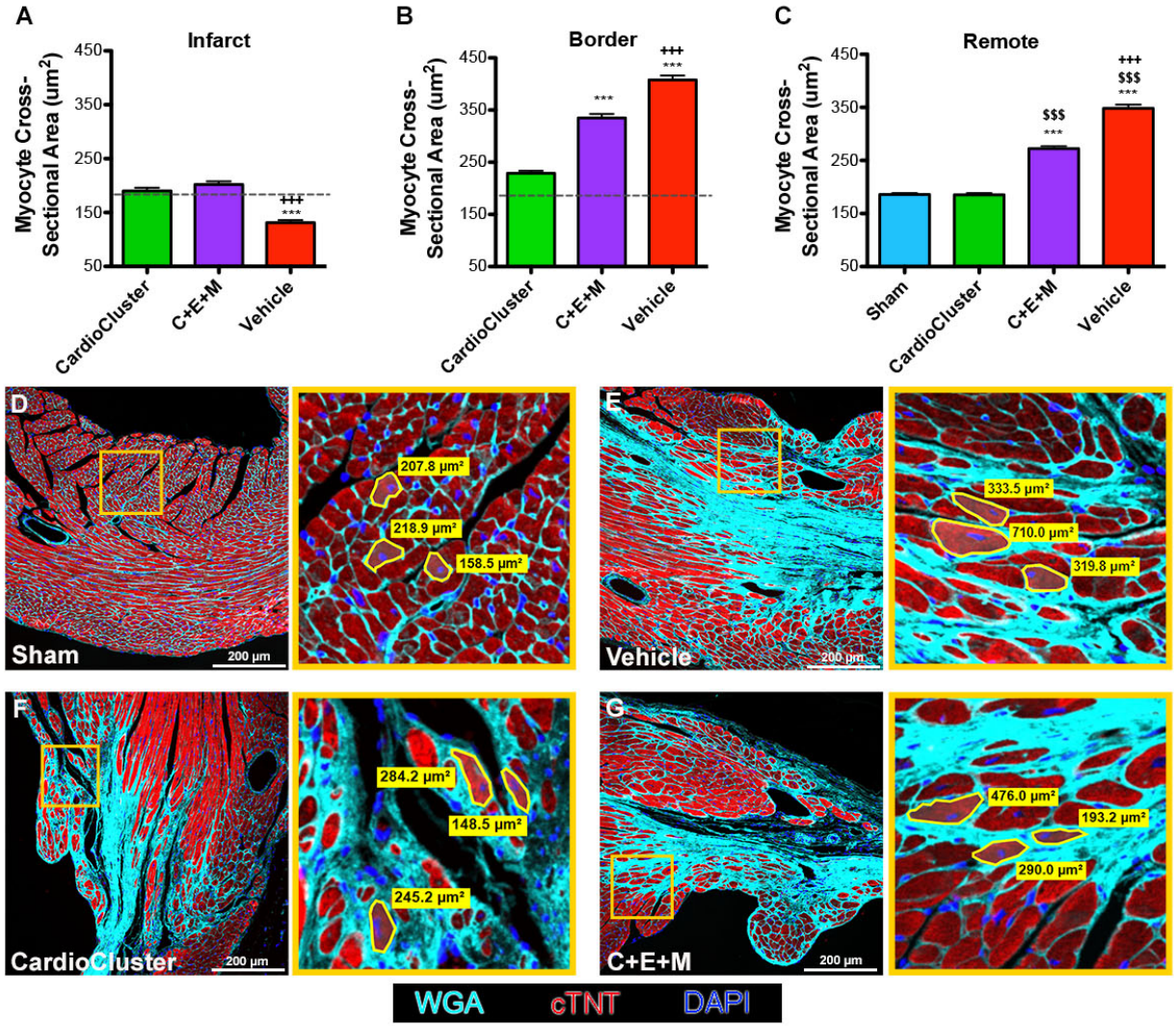

Figure 3.16. CardioCluster treatment antagonizes cardiomyocyte hypertrophy in the border and remote region and preserves cardiomyocyte size in the infarct region
A-C, Quantitative analysis represents measurement of cross-sectional area of cardiomyocytes from infarct **(A)**, border zone **(B)**, and remote **(C)** heart regions (n=4-5 mice per group). Dashed line: mean cross-sectional area of sham group. **D-G**, Representative image from sham **(D)** and border zone regions of vehicle **(E)**, CardioCluster **(F)**, and C+E+M **(G)** used to quantitate cardiomyocyte cross-sectional area (wheat germ agglutinin [WGA]; cyan), cardiac troponin T (cTNT; red), and nuclei (DAPI; blue). Right panels show higher magnification of areas highlighted by yellow boxes. The area of three traced cardiomyocytes per region are shown within magnified view. Scale bar, 200 µm. Data are presented as 1-way ANOVA, ***p<0.001, versus CardioCluster. $^{+++}$p<0.001, versus C+E+M. $^{\$\$\$}$p<0.001, versus sham.

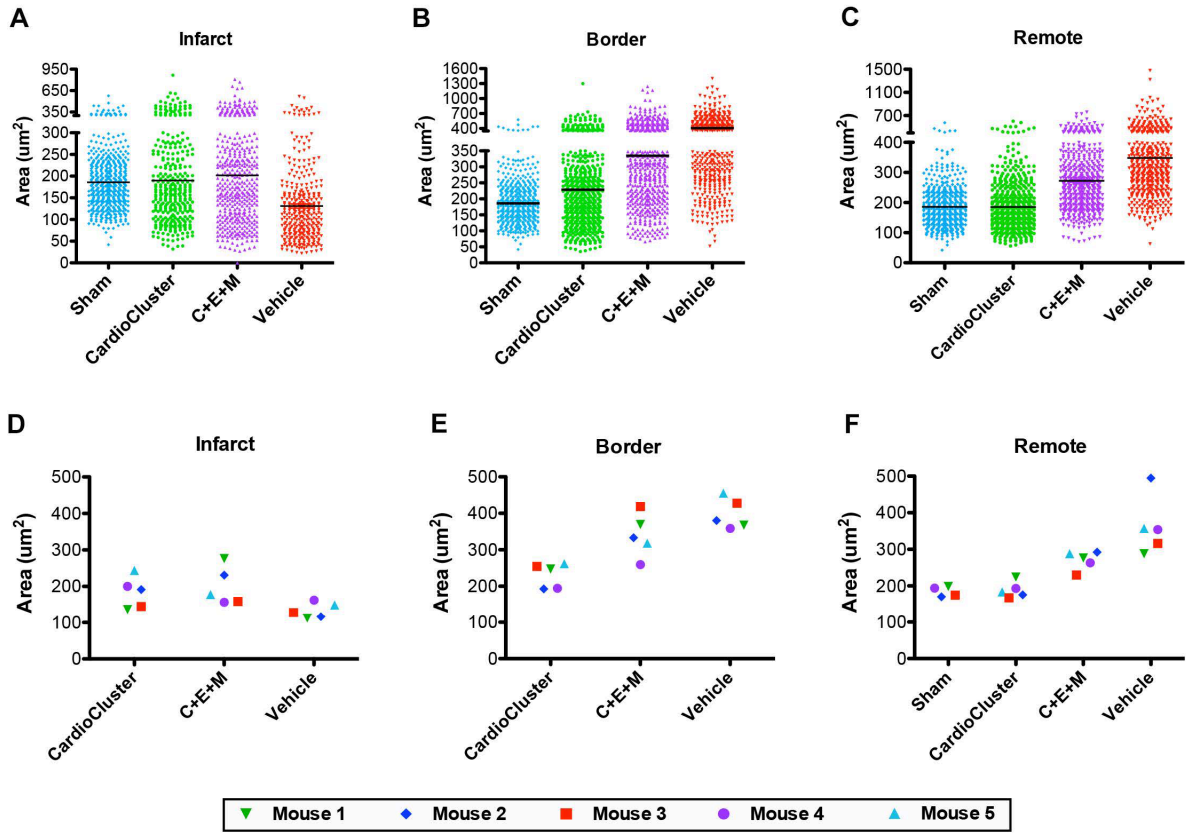

Figure 3.17. CardioCluster treatment antagonizes cardiomyocyte hypertrophy in the border and remote region and preserves cardiomyocyte size in the infarct region
A-C, Scatter plots showing cardiomyocyte cross-sectional area for each individually traced cell in the infarct **(A)**, border **(B)**, and remote **(C)** heart regions. **D-F**, Individual mean for each mouse used to quantify cardiomyocyte cross-sectional area in the infarct **(D)**, border **(E)**, and remote **(F)** heart regions shown by scatter plots (n=4-5 mice per group).

Chapter 3, with slight modifications, has been submitted for publication. Enhancing Myocardial Repair with CardioClusters. Monsanto MM, Wang BJ, Ehrenberg ZR, White KS, Alvarez R, Echeagaray OH, Fisher K, Sengphanith S, Gude N, Sussman MA. The dissertation author was the primary author and investigator on this manuscript.

CHAPTER 4

Conclusion of the Dissertation

The restorative impact of cell therapy to regenerate damaged myocardium is muddled by multiple unresolved issues including inefficient cell delivery to the site of injury, low cell retention and the seemingly weak effectiveness of the cells that do remain within the tissue. These inherent problems likely contribute to the rather modest efficacy thus far. The CardioCluster approach presented in this dissertation is intended to overcome some of these issues by integrating multiple cardiac-resident cell types into a single injectable product, overcoming single cell delivery challenges through spherical self-assembly of a larger 3D structure which provides enhanced retention to mediate repair after delivery. The restorative impact of cell therapy is hotly debated and remains to be fully understood and appreciated[113-117]. Increased knowledge of cardiac cell biology emerges from the use and application of three cardiac-derived cells patterned into 3D CardioClusters.

The development of this therapeutic approach began through methodological studies in which three distinct cardiac-derived interstitial cell types were successfully isolated and expanded from patients with end-stage heart failure undergoing implantation of a left ventricular assist device LVAD[13]. This is the profile patient population that would benefit most from interventional cell therapy, and we wanted to develop an approach to utilize three cardiac-resident interstitial cell populations found within their heart tissue. Combinatorial approaches harnessing the beneficial attributes of multiple cell types have generated interest in the field[19, 82-84]. It is recognized that the heart is composed of multiple cell populations that must work synergistically to mediate repair. Straightforward and reproducible protocols to isolate, expand and characterize this heterogeneous non-myocyte cell population will help to elucidate their biological

significance. We effectively formulated such a protocol in our previous publication[13] and utilizing this method we routinely isolate CPCs, EPCs, and MSCs. What was initially referred to as cardiac progenitor cells (CPCs) has later been referred to as cardiac interstitial cells (CICs) due to controversy in the field regarding the potential for CPCs to differentiate into full fledge cardiomyocytes[113-117]. Due to this controversy interstitial cells isolated based on c-Kit expression are currently being referred to as CIC as done in Chapter 3 and onward of this Dissertation.

Aggregating the three cardiac interstitial cells as a CardioCluster influences their biological properties. Transcriptional profiling showed that single cells grown as 3D CardioClusters preserved a more native phenotypic signature than their monolayer counterparts. Increased expression of collagen type I and III, integrins (ITGA2, ITGB1, ITGA11, ITGA1, ITGAV), fibronectin, and matrix remodeling enzymes (MMP-1, MMP-2, MMP-14, TIMP-1, TIMP-2) in the CardioCluster is indicative of enhanced matrix remodeling capacity of cells maintained in a 3D microenvironment[124]. Moreover, cells grown as a CardioCluster collectively resemble each other far more than original parental cells, suggesting strong environmental influences and intercellular coordination initiated within a 3D environment, unlike traditional monolayer expansion[85-87]. Restoring isolated cells to a more native state[87, 147] may be one way that 3D clustering improves cell performance upon injection. Many of the genes expressed by CardioClusters were also found to be highly expressed in freshly isolated cardiac cells. This suggests that standard tissue culture causes expanded cells to lose their identity, which can be reversed by culturing the cells within a 3D microenvironment.

Transcript data showed that CardioClusters highly expressed Notch3. Given the role of Notch during development and tissue regeneration, this is an important mechanism for aspects such as maintenance of a progenitor pool and tissue homeostasis[125]. This finding is in agreement with a recent study[98] that found pediatric CICs cultured in 3D spheres of approximately 1500 cells increased notch signaling. In their right ventricular heart failure model, the 3D aggregated CICs were found to repair cardiac injury significantly more than their 2D counterparts, in what the authors believe to be a notch-dependent manner. In our scRNA-seq data analyzing CardioClusters we also found high expression of two inhibitory SMADs (SMAD6/7) known to negatively regulate TGF-β signaling[148, 149]. Inhibition of TGF-β signaling reduces fibrosis following myocardial injury[150], and could be a potential mechanism for the smaller scar size seen in CardioCluster-treated animals. One additional thought-provoking observation from single cell profiling was the upregulation of various heat shock proteins (HSPs) in CICs (HSPE1, HSP90AA1, HSPD1, HSP90AB1), EPCs (HSP90AA1, HSPD1), and MSCs (HSPB7), while CardioClusters were not found to highly express a single HSPs. HSPs are a family of proteins produced by cells in response to exposure to stressful conditions. Their decreased expression in CardioCluster suggests a decreased need for cells grown in 3D to express HSPs compared to cells isolated and introduced to monolayer culture, an environment completely foreign to the freshly isolated cells, once again confirming 3D aggregation is beneficial to cells expanded in culture and helps to maintain a homeostatic environment.

The ability to promote cardiomyocyte survival under stress conditions is a critical aspect of cell therapy. The ability of CardioClusters to promote cardiomyocyte survival

is demonstrated by the *in vitro* co-culture assay. This assay has previously been used to show cardioprotective effects with other cell types[102]. Stress from serum deprivation and acute exposure to hydrogen peroxide showed the protective effects of CardioClusters. The cardioprotective effect of CardioClusters is likely mediated by secreted factors such as *IL-6*, *IGF*, and *SDF-1*. These factors have previously been shown to exert pro-survival effects[123, 130, 131]. The ability of CardioClusters to promote survival better than the single cell mixes demonstrated the superiority of CardioClusters for potentiating the protective effect of cell therapy *in vitro* and also reinforces the benefits of culturing the mixed cell population together in a 3D configuration.

Studies have shown that combining multiple cell types generates better results, however, there still has not been a specific combination that has had adequate regenerative capacity for clinical translation. In this report, we demonstrate a novel 3D approach by using CardioClusters to enhance cellular communication and retention upon myocardial delivery. CardioClusters injected into acutely damaged NOD^{SCID} hearts improved cardiac function and reduced infarct size. Improvement in FS and EF was observed starting at week 4 and maintained during the entirety of the 20-week study, with CardioCluster-treated animals showing notable improvements relative to their 2D-cultured single cell counterparts (C+E+M). Specifically, CardioClusters significantly improved myocardial wall structure compared to C+E+M-treated animals, concomitant with increased capillary density and preserved cardiomyocyte size. Being able to control CardioCluster size to <160 μm allowed the cluster to be directly injected through a 30-gauge needle without the need to dissociate the 3D structure into single cells.

CardioClusters persisted within the myocardial wall, with the 3D structure clearly visible up to a week post-injection.

Cell therapy to treat ischemic heart disease has been investigated in clinical trials for nearly 20 years[151]. While multiple cell types have been examined, bone marrow mononuclear cells, MSCs, and cardiac stem cells (CSCs) are the most commonly investigated. Meta-analysis examining a total of 80 papers using CSC therapy to treat MI in both large and small animals[133] found that CSC treatment culminated in an absolute difference in EF of 10.7% compared with control animals. Pooled observations made from large animal studies using MSC and bone marrow mononuclear cell therapy show similar results (8.0% and 7.6%, respectively)[132]. In comparison, at 4 weeks we saw a 12.2% difference in EF between CardioCluster-treated animals and vehicle control animals, which was significantly greater than the 4.7% difference between C+E+M versus vehicle control animals. By 20 weeks CardioCluster treatment had pulled ahead to a 24.2% difference in EF compared with vehicle treatment (14.5% difference between C+E+M and vehicle). Our data showed the significant improvement possible with CardioClusters versus traditional single cell therapy approaches.

In a feasibility study to confirm off-the-shelf potential of CardioClusters, clusters were frozen in liquid nitrogen. The percentage of dead cells was insignificantly different from fresh, non-frozen, CardioClusters. Additionally, frozen CardioClusters maintained structural integrity when cultured on tissue culture-treated plastic plates, visibly indistinguishable from non-frozen counterparts. From a future clinical perspective, the ability to mass-produce and preserve CardioClusters frozen in liquid nitrogen is

desirable. Testing for comparable efficacy of frozen/thawed CardioClusters in our *in vivo* model system remains to be determined in future studies.

The highly amenable platform of the CardioCluster can be utilized to better understand cellular interactions occurring within 3D environments. An example already initiated in our laboratory includes seeding the three cell types at once, which appears to create a hollow CardioCluster. This may be attributable to EPC/MSC interaction allowing for internal cavity formation as seen during organ and tissue development[137, 138] or may be more similar to pericyte/MSC-like endothelial cell interactions[139]. While the exact pathways are as yet elusive, what is known is that cells aggregate in a 3 step process: (1) formation of loose cell aggregates via integrin-ECM binding; (2) a delay period for cadherin expression and accumulation; (3) formation of compact 3D microenvironments through homophilic cadherin-cadherin interactions[152]. With this understanding, we have begun trying to resolve how EPCs form an exclusively endothelial cluster during initial phases of CardioCluster formation. Identification of which surface receptors and/or integrins is part of ongoing studies and will help to elucidate cardiac cell biology and predict how cells bind to the extracellular matrix and interact in a non-cell-autonomous fashion. Potential ways to further enhance the CardioCluster concept would be to genetically modify the cells with pro-survival factors such as done previously in our laboratory with Pim-1[52, 134] or in other studies such as with the overexpression of chemokine receptor (CCR1) that was shown to enhance migration, survival and engraftment of murine MSCs[135]. Likewise, other applications could include varying culture conditions, as we have done previously using hypoxia versus normoxia culture[136] to study altered phenotypic changes resulting from changes

in oxygen concentration. RNA-Seq would be utilized to assess the impact of changing conditions upon transcriptional reprogramming.

There are several limitations with the use of CardioClusters. For example, due to their larger size vascular delivery is not feasible with CardioClusters. This being said, several studies have shown direct intramyocardial injection is the preferred approach to enhance efficacy anyway. Another potential problem is the fact that CardioClusters are composed of multiple cells types that must be ready for utilization at the same time. Clusters can be formed using a plethora of cells, and depending on the cell types chosen, the length required for expansion of the parental cells may differ. To circumvent this problem freezing either the parental cells or the CardioClusters once formed are feasible options. A benefit of CardioCluster design is the quick formation time of only 48 hours from start to finish. There is also potential for allogeneic use by combining clusters with immunosuppressive agents or the more recent idea of creating a 'universal' donor cell such as was done with the CRISPR-mediated genome editing of an immortalized human erythroblast cell line to create 'universal' donor cells for patients with sickle cell disease[143] .

Given the highly adaptable nature of CardioClusters there are many aspects that can be optimized, such as the best cell ratios, best cell types, optimal cluster size, and number of CardioClusters to inject. While the CardioClusters in our study contained approximately 300 cells, other applications could include creating mini-CardioClusters of 50-100 cells. Their smaller diameter would allow a greater number of individual clusters to be injected intramyocardially. This ability to fine-tune CardioCluster size is a benefit distinct from traditional 3D cell aggregates, such as Cardiospheres, where

diameter is not controllable, and the 3D organization is broken down to CDCs. In our murine animal study CardioCluster cell number was crucial. The inner diameter of a 30-gauge needle constrained CardioCluster diameter to <160 μm. For a larger animal system, CardioClusters size could be scaled up to allow for a greater total number of cells to be injected. In future studies it will be interesting to see how changes to CardioCluster size or cell patterning affect cell interactions and ultimately regenerative ability. There is a lot of room for improvement and optimization of the technique. With limited knowledge of how combinatorial cell therapy works[140-142] this 'next generation' approach requires substantial investigation given the multiple possibilities for tweaking the system to enhance the outcome.

This dissertation work presents the first step of many to show clinical utility of CardioClusters. CardioClusters were found to greatly restore cardiac function in a MI murine model system and this therapeutic effect was found to be long-term, as established by continued perseveration during the 20-week time course. Unlike current microfabrication approaches, CardioClusters represent a 3D structure that maximizes cellular interaction and allows for defined cell ratios, controlled size, and enabled injectability. We were able to demonstrate the superiority of this combinatorial cell therapy as a 'next generation' approach. Overcoming current limitations plus enhancing cell biological properties will be required to advance the field from current status. Promising approaches of combining cell therapy with bioengineering in novel ways is a practical and tractable way to implement improvement of cell therapy.

REFERENCES

1. Losordo DW, Henry TD, Davidson C, Sup Lee J, Costa MA, Bass T, Mendelsohn F, Fortuin FD, Pepine CJ, Traverse JH, Amrani D, Ewenstein BM, Riedel N, Story K, Barker K, Povsic TJ, Harrington RA and Schatz RA. Intramyocardial, autologous CD34+ cell therapy for refractory angina. *Circ Res*. 109:428-36.

2. Wang S, Cui J, Peng W and Lu M. Intracoronary autologous CD34+ stem cell therapy for intractable angina. *Cardiology*. 117:140-7.

3. Bolli R, Chugh AR, D'Amario D, Loughran JH, Stoddard MF, Ikram S, Beache GM, Wagner SG, Leri A, Hosoda T, Sanada F, Elmore JB, Goichberg P, Cappetta D, Solankhi NK, Fahsah I, Rokosh DG, Slaughter MS, Kajstura J and Anversa P. Cardiac stem cells in patients with ischaemic cardiomyopathy (SCIPIO): initial results of a randomised phase 1 trial. *Lancet*. 378:1847-57.

4. Chugh AR, Beache GM, Loughran JH, Mewton N, Elmore JB, Kajstura J, Pappas P, Tatooles A, Stoddard MF, Lima JA, Slaughter MS, Anversa P and Bolli R. Administration of cardiac stem cells in patients with ischemic cardiomyopathy: the SCIPIO trial: surgical aspects and interim analysis of myocardial function and viability by magnetic resonance. *Circulation*. 126:S54-64.

5. Hare JM, Fishman JE, Gerstenblith G, DiFede Velazquez DL, Zambrano JP, Suncion VY, Tracy M, Ghersin E, Johnston PV, Brinker JA, Breton E, Davis-Sproul J, Schulman IH, Byrnes J, Mendizabal AM, Lowery MH, Rouy D, Altman P, Wong Po Foo C, Ruiz P, Amador A, Da Silva J, McNiece IK and Heldman AW. Comparison of allogeneic vs autologous bone marrow-derived mesenchymal stem cells delivered by transendocardial injection in patients with ischemic cardiomyopathy: the POSEIDON randomized trial. *JAMA*. 308:2369-79.

6. Trachtenberg B, Velazquez DL, Williams AR, McNiece I, Fishman J, Nguyen K, Rouy D, Altman P, Schwarz R, Mendizabal A, Oskouei B, Byrnes J, Soto V, Tracy M, Zambrano JP, Heldman AW and Hare JM. Rationale and design of the Transendocardial Injection of Autologous Human Cells (bone marrow or mesenchymal) in Chronic Ischemic Left Ventricular Dysfunction and Heart Failure Secondary to Myocardial Infarction (TAC-HFT) trial: A randomized, double-blind, placebo-controlled study of safety and efficacy. *Am Heart J*. 161:487-93.

7. Anversa P, Rota M, Urbanek K, Hosoda T, Sonnenblick EH, Leri A, Kajstura J and Bolli R. Myocardial aging--a stem cell problem. *Basic Res Cardiol*. 2005;100:482-93.

8. Fujita J, Itabashi Y, Seki T, Tohyama S, Tamura Y, Sano M and Fukuda K. Myocardial cell sheet therapy and cardiac function. *Am J Physiol Heart Circ Physiol*. 303:H1169-82.

9. Cheng K, Blusztajn A, Shen D, Li TS, Sun B, Galang G, Zarembinski TI, Prestwich GD, Marban E, Smith RR and Marban L. Functional performance of human cardiosphere-derived cells delivered in an in situ polymerizable hyaluronan-gelatin hydrogel. *Biomaterials*. 33:5317-24.

10. Beohar N, Rapp J, Pandya S and Losordo DW. Rebuilding the damaged heart: the potential of cytokines and growth factors in the treatment of ischemic heart disease. *J Am Coll Cardiol*. 56:1287-97.

11. Fischer KM, Cottage CT, Wu W, Din S, Gude NA, Avitabile D, Quijada P, Collins BL, Fransioli J and Sussman MA. Enhancement of myocardial regeneration through genetic engineering of cardiac progenitor cells expressing Pim-1 kinase. *Circulation*. 2009;120:2077-87.

12. Mohsin S, Khan M, Toko H, Bailey B, Cottage CT, Wallach K, Nag D, Lee A, Siddiqi S, Lan F, Fischer KM, Gude N, Quijada P, Avitabile D, Truffa S, Collins B, Dembitsky W, Wu JC and Sussman MA. Human Cardiac Progenitor Cells Engineered With Pim-I Kinase Enhance Myocardial Repair. *J Am Coll Cardiol*.

13. Monsanto MM, White KS, Kim T, Wang BJ, Fisher K, Ilves K, Khalafalla FG, Casillas A, Broughton K, Mohsin S, Dembitsky WP and Sussman MA. Concurrent Isolation of 3 Distinct Cardiac Stem Cell Populations From a Single Human Heart Biopsy. *Circulation research*. 2017;121:113-124.

14. Bernstein HS and Srivastava D. Stem cell therapy for cardiac disease. *Pediatr Res*. 71:491-9.

15. Gnecchi M, Zhang Z, Ni A and Dzau VJ. Paracrine mechanisms in adult stem cell signaling and therapy. *Circulation research*. 2008;103:1204-19.

16. Aggarwal S and Pittenger MF. Human mesenchymal stem cells modulate allogeneic immune cell responses. *Blood*. 2005;105:1815-22.

17. Jujo K, Ii M and Losordo DW. Endothelial progenitor cells in neovascularization of infarcted myocardium. *Journal of molecular and cellular cardiology*. 2008;45:530-44.

18. Thal MA, Krishnamurthy P, Mackie AR, Hoxha E, Lambers E, Verma S, Ramirez V, Qin G, Losordo DW and Kishore R. Enhanced angiogenic and cardiomyocyte differentiation capacity of epigenetically reprogrammed mouse and human endothelial progenitor cells augments their efficacy for ischemic myocardial repair. *Circ Res*. 111:180-90.

19. Williams AR, Hatzistergos KE, Addicott B, McCall F, Carvalho D, Suncion V, Morales AR, Da Silva J, Sussman MA, Heldman AW and Hare JM. Enhanced effect of combining human cardiac stem cells and bone marrow mesenchymal stem cells to reduce infarct size and to restore cardiac function after myocardial infarction. *Circulation*. 127:213-23.

20. Leri A, Kajstura J and Anversa P. Role of cardiac stem cells in cardiac pathophysiology: a paradigm shift in human myocardial biology. *Circ Res*. 109:941-61.

21. Anversa P, Kajstura J, Rota M and Leri A. Regenerating new heart with stem cells. *J Clin Invest*. 123:62-70.

22. Fuchs E, Tumbar T and Guasch G. Socializing with the neighbors: stem cells and their niche. *Cell*. 2004;116:769-78.

23. Messina E, De Angelis L, Frati G, Morrone S, Chimenti S, Fiordaliso F, Salio M, Battaglia M, Latronico MV, Coletta M, Vivarelli E, Frati L, Cossu G and Giacomello A. Isolation and expansion of adult cardiac stem cells from human and murine heart. *Circ Res*. 2004;95:911-21.

24. Chimenti I, Smith RR, Li TS, Gerstenblith G, Messina E, Giacomello A and Marban E. Relative roles of direct regeneration versus paracrine effects of human cardiosphere-derived cells transplanted into infarcted mice. *Circ Res*. 106:971-80.

25. Cho HJ, Lee HJ, Youn SW, Koh SJ, Won JY, Chung YJ, Yoon CH, Lee SW, Lee EJ, Kwon YW, Lee HY, Lee SH, Ho WK, Park YB and Kim HS. Secondary sphere formation enhances the functionality of cardiac progenitor cells. *Mol Ther*. 20:1750-66.

26. Smith RR, Barile L, Cho HC, Leppo MK, Hare JM, Messina E, Giacomello A, Abraham MR and Marban E. Regenerative potential of cardiosphere-derived cells expanded from percutaneous endomyocardial biopsy specimens. *Circulation*. 2007;115:896-908.

27. Makkar RR, Smith RR, Cheng K, Malliaras K, Thomson LE, Berman D, Czer LS, Marban L, Mendizabal A, Johnston PV, Russell SD, Schuleri KH, Lardo AC, Gerstenblith G and Marban E. Intracoronary cardiosphere-derived cells for heart regeneration after myocardial infarction (CADUCEUS): a prospective, randomised phase 1 trial. *Lancet*. 379:895-904.

28. Lee ST, White AJ, Matsushita S, Malliaras K, Steenbergen C, Zhang Y, Li TS, Terrovitis J, Yee K, Simsir S, Makkar R and Marban E. Intramyocardial injection of autologous cardiospheres or cardiosphere-derived cells preserves function and minimizes adverse ventricular remodeling in pigs with heart failure post-myocardial infarction. *J Am Coll Cardiol*. 57:455-65.

29. Lee WY, Wei HJ, Wang JJ, Lin KJ, Lin WW, Chen DY, Huang CC, Lee TY, Ma HY, Hwang SM, Chang Y and Sung HW. Vascularization and restoration of heart function in rat myocardial infarction using transplantation of human cbMSC/HUVEC core-shell bodies. *Biomaterials*. 33:2127-36.

30. Pittenger MF, Mackay AM, Beck SC, Jaiswal RK, Douglas R, Mosca JD, Moorman MA, Simonetti DW, Craig S and Marshak DR. Multilineage potential of adult human mesenchymal stem cells. *Science*. 1999;284:143-7.

31. Wang W, Itaka K, Ohba S, Nishiyama N, Chung UI, Yamasaki Y and Kataoka K. 3D spheroid culture system on micropatterned substrates for improved differentiation efficiency of multipotent mesenchymal stem cells. *Biomaterials*. 2009;30:2705-15.

32. Hwang HJ, Chang W, Song BW, Song H, Cha MJ, Kim IK, Lim S, Choi EJ, Ham O, Lee SY, Shim J, Joung B, Pak HN, Kim SS, Choi BR, Jang Y, Lee MH and Hwang KC. Antiarrhythmic potential of mesenchymal stem cell is modulated by hypoxic environment. *J Am Coll Cardiol*. 60:1698-706.

33. Tang YL, Zhu W, Cheng M, Chen L, Zhang J, Sun T, Kishore R, Phillips MI, Losordo DW and Qin G. Hypoxic preconditioning enhances the benefit of cardiac progenitor cell therapy for treatment of myocardial infarction by inducing CXCR4 expression. *Circ Res*. 2009;104:1209-16.

34. Yan F, Yao Y, Chen L, Li Y, Sheng Z and Ma G. Hypoxic preconditioning improves survival of cardiac progenitor cells: role of stromal cell derived factor-1alpha-CXCR4 axis. *PLoS One*. 7:e37948.

35. Saleh FA, Whyte M and Genever PG. Effects of endothelial cells on human mesenchymal stem cell activity in a three-dimensional in vitro model. *Eur Cell Mater*. 22:242-57; discussion 257.

36. Wagner W, Roderburg C, Wein F, Diehlmann A, Frankhauser M, Schubert R, Eckstein V and Ho AD. Molecular and secretory profiles of human mesenchymal stromal cells and their abilities to maintain primitive hematopoietic progenitors. *Stem Cells*. 2007;25:2638-47.

37. Saleh FA, Whyte M, Ashton P and Genever PG. Regulation of mesenchymal stem cell activity by endothelial cells. *Stem Cells Dev*. 20:391-403.

38. Sanganalmath SK and Bolli R. Cell therapy for heart failure: a comprehensive overview of experimental and clinical studies, current challenges, and future directions. *Circ Res*. 2013;113:810-34.

39. Dixit P and Katare R. Challenges in identifying the best source of stem cells for cardiac regeneration therapy. *Stem Cell Res Ther*. 2015;6:26.

40. Assmus B, Schachinger V, Teupe C, Britten M, Lehmann R, Dobert N, Grunwald F, Aicher A, Urbich C, Martin H, Hoelzer D, Dimmeler S and Zeiher AM. Transplantation of Progenitor Cells and Regeneration Enhancement in Acute Myocardial Infarction (TOPCARE-AMI). *Circulation*. 2002;106:3009-17.

41. Clifford DM, Fisher SA, Brunskill SJ, Doree C, Mathur A, Watt S and Martin-Rendon E. Stem cell treatment for acute myocardial infarction. *Cochrane Database Syst Rev*. 2012:CD006536.

42. Hare JM, Fishman JE, Gerstenblith G, DiFede Velazquez DL, Zambrano JP, Suncion VY, Tracy M, Ghersin E, Johnston PV, Brinker JA, Breton E, Davis-Sproul J, Schulman IH, Byrnes J, Mendizabal AM, Lowery MH, Rouy D, Altman P, Wong Po Foo C, Ruiz P, Amador A, Da Silva J, McNiece IK, Heldman AW, George R and Lardo A. Comparison of allogeneic vs autologous bone marrow-derived mesenchymal stem cells delivered by transendocardial injection in patients with ischemic cardiomyopathy: the POSEIDON randomized trial. *JAMA*. 2012;308:2369-79.

43. Mills JS and Rao SV. REPAIR-AMI: stem cells for acute myocardial infarction. *Future Cardiol*. 2007;3:137-40.

44. Traverse JH, Henry TD, Ellis SG, Pepine CJ, Willerson JT, Zhao DX, Forder JR, Byrne BJ, Hatzopoulos AK, Penn MS, Perin EC, Baran KW, Chambers J, Lambert C, Raveendran G, Simon DI, Vaughan DE, Simpson LM, Gee AP, Taylor DA, Cogle CR, Thomas JD, Silva GV, Jorgenson BC, Olson RE, Bowman S, Francescon J, Geither C, Handberg E, Smith DX, Baraniuk S, Piller LB, Loghin C, Aguilar D, Richman S, Zierold C, Bettencourt J, Sayre SL, Vojvodic RW, Skarlatos SI, Gordon DJ, Ebert RF, Kwak M, Moye LA, Simari RD and Cardiovascular Cell Therapy R. Effect of intracoronary delivery of autologous bone marrow mononuclear cells 2 to 3 weeks following acute myocardial infarction on left ventricular function: the LateTIME randomized trial. *JAMA*. 2011;306:2110-9.

45. Menasche P, Alfieri O, Janssens S, McKenna W, Reichenspurner H, Trinquart L, Vilquin JT, Marolleau JP, Seymour B, Larghero J, Lake S, Chatellier G, Solomon S, Desnos M and Hagege AA. The Myoblast Autologous Grafting in Ischemic Cardiomyopathy (MAGIC) trial: first randomized placebo-controlled study of myoblast transplantation. *Circulation*. 2008;117:1189-200.

46. Leri A, Kajstura J and Anversa P. Role of cardiac stem cells in cardiac pathophysiology: a paradigm shift in human myocardial biology. *Circulation research*. 2011;109:941-61.

47. Beltrami AP, Barlucchi L, Torella D, Baker M, Limana F, Chimenti S, Kasahara H, Rota M, Musso E, Urbanek K, Leri A, Kajstura J, Nadal-Ginard B and Anversa P. Adult cardiac stem cells are multipotent and support myocardial regeneration. *Cell*. 2003;114:763-76.

48. Bearzi C, Rota M, Hosoda T, Tillmanns J, Nascimbene A, De Angelis A, Yasuzawa-Amano S, Trofimova I, Siggins RW, Lecapitaine N, Cascapera S, Beltrami AP, D'Alessandro DA, Zias E, Quaini F, Urbanek K, Michler RE, Bolli R, Kajstura J, Leri A and Anversa P. Human cardiac stem cells. *Proceedings of the National Academy of Sciences of the United States of America*. 2007;104:14068-73.

49. Lyngbaek S, Schneider M, Hansen JL and Sheikh SP. Cardiac regeneration by resident stem and progenitor cells in the adult heart. *Basic Res Cardiol*. 2007;102:101-14.

50. Makkar RR, Smith RR, Cheng K, Malliaras K, Thomson LE, Berman D, Czer LS, Marban L, Mendizabal A, Johnston PV, Russell SD, Schuleri KH, Lardo AC, Gerstenblith G and Marban E. Intracoronary cardiosphere-derived cells for heart regeneration after myocardial infarction (CADUCEUS): a prospective, randomised phase 1 trial. *Lancet*. 2012;379:895-904.

51. Bolli R, Chugh AR, D'Amario D, Loughran JH, Stoddard MF, Ikram S, Beache GM, Wagner SG, Leri A, Hosoda T, Sanada F, Elmore JB, Goichberg P, Cappetta D, Solankhi NK, Fahsah I, Rokosh DG, Slaughter MS, Kajstura J and Anversa P. Cardiac stem cells in patients with ischaemic cardiomyopathy (SCIPIO): initial results of a randomised phase 1 trial. *Lancet*. 2011;378:1847-57.

52. Mohsin S, Khan M, Nguyen J, Alkatib M, Siddiqi S, Hariharan N, Wallach K, Monsanto M, Gude N, Dembitsky W and Sussman MA. Rejuvenation of human cardiac progenitor cells with Pim-1 kinase. *Circulation research*. 2013;113:1169-79.

53. Kulandavelu S, Karantalis V, Fritsch J, Hatzistergos KE, Loescher VY, McCall F, Wang B, Bagno L, Golpanian S, Wolf A, Grenet J, Williams A, Kupin A, Rosenfeld A, Mohsin S, Sussman MA, Morales A, Balkan W and Hare JM. Pim1 Kinase Overexpression Enhances ckit+ Cardiac Stem Cell Cardiac Repair Following Myocardial Infarction in Swine. *Journal of the American College of Cardiology*. 2016;68:2454-2464.

54. Tokita Y, Tang XL, Li Q, Wysoczynski M, Hong KU, Nakamura S, Wu WJ, Xie W, Li D, Hunt G, Ou Q, Stowers H and Bolli R. Repeated Administrations of Cardiac Progenitor Cells Are Markedly More Effective Than a Single Administration: A New Paradigm in Cell Therapy. *Circulation research*. 2016;119:635-51.

55. Williams AR, Hatzistergos KE, Addicott B, McCall F, Carvalho D, Suncion V, Morales AR, Da Silva J, Sussman MA, Heldman AW and Hare JM. Enhanced effect of combining human cardiac stem cells and bone marrow mesenchymal stem cells to reduce infarct size and to restore cardiac function after myocardial infarction. *Circulation*. 2013;127:213-23.

56. Bernstein HS and Srivastava D. Stem cell therapy for cardiac disease. *Pediatr Res*. 2012;71:491-9.

57. Miyahara Y, Nagaya N, Kataoka M, Yanagawa B, Tanaka K, Hao H, Ishino K, Ishida H, Shimizu T, Kangawa K, Sano S, Okano T, Kitamura S and Mori H. Monolayered mesenchymal stem cells repair scarred myocardium after myocardial infarction. *Nature medicine*. 2006;12:459-65.

58. Malgieri A, Kantzari E, Patrizi MP and Gambardella S. Bone marrow and umbilical cord blood human mesenchymal stem cells: state of the art. *Int J Clin Exp Med*. 2010;3:248-69.

59. Dominici M, Le Blanc K, Mueller I, Slaper-Cortenbach I, Marini F, Krause D, Deans R, Keating A, Prockop D and Horwitz E. Minimal criteria for defining multipotent mesenchymal stromal cells. The International Society for Cellular Therapy position statement. *Cytotherapy*. 2006;8:315-7.

60. Kuraitis D, Ruel M and Suuronen EJ. Mesenchymal stem cells for cardiovascular regeneration. *Cardiovasc Drugs Ther*. 2011;25:349-62.

61. Hare JM, Traverse JH, Henry TD, Dib N, Strumpf RK, Schulman SP, Gerstenblith G, DeMaria AN, Denktas AE, Gammon RS, Hermiller JB, Jr., Reisman MA, Schaer GL and Sherman W. A randomized, double-blind, placebo-controlled, dose-escalation study of intravenous adult human mesenchymal stem cells (prochymal) after acute myocardial infarction. *Journal of the American College of Cardiology*. 2009;54:2277-86.

62. Asahara T, Murohara T, Sullivan A, Silver M, van der Zee R, Li T, Witzenbichler B, Schatteman G and Isner JM. Isolation of putative progenitor endothelial cells for angiogenesis. *Science*. 1997;275:964-7.

63. Peichev M, Naiyer AJ, Pereira D, Zhu Z, Lane WJ, Williams M, Oz MC, Hicklin DJ, Witte L, Moore MA and Rafii S. Expression of VEGFR-2 and AC133 by circulating human CD34(+) cells identifies a population of functional endothelial precursors. *Blood*. 2000;95:952-8.

64. Gehling UM, Ergun S, Schumacher U, Wagener C, Pantel K, Otte M, Schuch G, Schafhausen P, Mende T, Kilic N, Kluge K, Schafer B, Hossfeld DK and Fiedler W. In vitro differentiation of endothelial cells from AC133-positive progenitor cells. *Blood*. 2000;95:3106-12.

65. Handgretinger R, Gordon PR, Leimig T, Chen X, Buhring HJ, Niethammer D and Kuci S. Biology and plasticity of CD133+ hematopoietic stem cells. *Annals of the New York Academy of Sciences*. 2003;996:141-51.

66. Lee WY, Wei HJ, Wang JJ, Lin KJ, Lin WW, Chen DY, Huang CC, Lee TY, Ma HY, Hwang SM, Chang Y and Sung HW. Vascularization and restoration of heart function in rat myocardial infarction using transplantation of human cbMSC/HUVEC core-shell bodies. *Biomaterials*. 2012;33:2127-36.

67. Sharan R, Maron-Katz A and Shamir R. CLICK and EXPANDER: a system for clustering and visualizing gene expression data. *Bioinformatics*. 2003;19:1787-99.

68. Ridzuan N, Al Abbar A, Yip WK, Maqbool M and Ramasamy R. Characterization and Expression of Senescence Marker in Prolonged Passages of Rat Bone Marrow-Derived Mesenchymal Stem Cells. *Stem Cells Int*. 2016;2016:8487264.

69. Shaer A, Azarpira N, Aghdaie MH and Esfandiari E. Isolation and characterization of Human Mesenchymal Stromal Cells Derived from Placental Decidua Basalis; Umbilical cord Wharton's Jelly and Amniotic Membrane. *Pak J Med Sci*. 2014;30:1022-6.

70. Aliborzi G, Vahdati A, Mehrabani D, Hosseini SE and Tamadon A. Isolation, Characterization and Growth Kinetic Comparison of Bone Marrow and Adipose Tissue Mesenchymal Stem Cells of Guinea Pig. *Int J Stem Cells*. 2016;9:115-23.

71. Shi H, Drummond CA, Fan X, Haller ST, Liu J, Malhotra D and Tian J. Hiding inside? Intracellular expression of non-glycosylated c-kit protein in cardiac progenitor cells. *Stem Cell Res*. 2016;16:795-806.

72. Chen CL, Faltusova K, Molik M, Savvulidi F, Chang KT and Necas E. Low c-Kit Expression Level Induced by Stem Cell Factor Does Not Compromise Transplantation of Hematopoietic Stem Cells. *Biol Blood Marrow Transplant*. 2016;22:1167-72.

73. Babina M, Rex C, Guhl S, Thienemann F, Artuc M, Henz BM and Zuberbier T. Baseline and stimulated turnover of cell surface c-Kit expression in different types of human mast cells. *Exp Dermatol*. 2006;15:530-7.

74. Mohsin S, Khan M, Toko H, Bailey B, Cottage CT, Wallach K, Nag D, Lee A, Siddiqi S, Lan F, Fischer KM, Gude N, Quijada P, Avitabile D, Truffa S, Collins B, Dembitsky W, Wu JC and Sussman MA. Human cardiac progenitor cells engineered with Pim-I kinase enhance myocardial repair. *Journal of the American College of Cardiology*. 2012;60:1278-87.

75. Sitte N, Saretzki G and von Zglinicki T. Accelerated telomere shortening in fibroblasts after extended periods of confluency. *Free Radic Biol Med*. 1998;24:885-93.

76. Butura A, Johansson I, Nilsson K, Warngard L, Ingelman-Sundberg M and Schuppe-Koistinen I. Differentiation of human hepatoma cells during confluence as revealed by gene expression profiling. *Biochem Pharmacol*. 2004;67:1249-58.

77. Nowbar AN, Mielewczik M, Karavassilis M, Dehbi HM, Shun-Shin MJ, Jones S, Howard JP, Cole GD, Francis DP and group Dw. Discrepancies in autologous bone marrow stem cell trials and enhancement of ejection fraction (DAMASCENE): weighted regression and meta-analysis. *BMJ*. 2014;348:g2688.

78. Perin EC, Dohmann HF, Borojevic R, Silva SA, Sousa AL, Mesquita CT, Rossi MI, Carvalho AC, Dutra HS, Dohmann HJ, Silva GV, Belem L, Vivacqua R, Rangel FO, Esporcatte R, Geng YJ, Vaughn WK, Assad JA, Mesquita ET and Willerson JT. Transendocardial, autologous bone marrow cell transplantation for severe, chronic ischemic heart failure. *Circulation*. 2003;107:2294-302.

79. Bolli R, Tang XL, Sanganalmath SK, Rimoldi O, Mosna F, Abdel-Latif A, Jneid H, Rota M, Leri A and Kajstura J. Intracoronary delivery of autologous cardiac stem cells improves cardiac function in a porcine model of chronic ischemic cardiomyopathy. *Circulation*. 2013;128:122-31.

80. Lee ST, White AJ, Matsushita S, Malliaras K, Steenbergen C, Zhang Y, Li TS, Terrovitis J, Yee K, Simsir S, Makkar R and Marban E. Intramyocardial injection of autologous cardiospheres or cardiosphere-derived cells preserves function and minimizes adverse ventricular remodeling in pigs with heart failure post-myocardial infarction. *Journal of the American College of Cardiology*. 2011;57:455-65.

81. Higuchi A, Ku NJ, Tseng YC, Pan CH, Li HF, Kumar SS, Ling QD, Chang Y, Alarfaj AA, Munusamy MA, Benelli G and Murugan K. Stem cell therapies for myocardial infarction in clinical trials: bioengineering and biomaterial aspects. *Lab Invest*. 2017;97:1167-1179.

82. Karantalis V, Suncion-Loescher VY, Bagno L, Golpanian S, Wolf A, Sanina C, Premer C, Kanelidis AJ, McCall F, Wang B, Balkan W, Rodriguez J, Rosado M, Morales A, Hatzistergos K, Natsumeda M, Margitich I, Schulman IH, Gomes SA, Mushtaq M, DiFede DL, Fishman JE, Pattany P, Zambrano JP, Heldman AW and Hare JM. Synergistic Effects of Combined Cell Therapy for Chronic Ischemic Cardiomyopathy. *J Am Coll Cardiol*. 2015;66:1990-1999.

83. Latham N, Ye B, Jackson R, Lam BK, Kuraitis D, Ruel M, Suuronen EJ, Stewart DJ and Davis DR. Human blood and cardiac stem cells synergize to enhance cardiac repair when cotransplanted into ischemic myocardium. *Circulation*. 2013;128:S105-12.

84. Avolio E, Meloni M, Spencer HL, Riu F, Katare R, Mangialardi G, Oikawa A, Rodriguez-Arabaolaza I, Dang Z, Mitchell K, Reni C, Alvino VV, Rowlinson J, Livi U,

Cesselli D, Angelini G, Emanueli C, Beltrami AP and Madeddu P. Combined intramyocardial delivery of human pericytes and cardiac stem cells additively improves the healing of mouse infarcted hearts through stimulation of vascular and muscular repair. *Circulation research*. 2015;116:e81-94.

85. Tibbitt MW and Anseth KS. Hydrogels as extracellular matrix mimics for 3D cell culture. *Biotechnol Bioeng*. 2009;103:655-63.

86. Gupta N, Liu JR, Patel B, Solomon DE, Vaidya B and Gupta V. Microfluidics-based 3D cell culture models: Utility in novel drug discovery and delivery research. *Bioeng Transl Med*. 2016;1:63-81.

87. Kim T, Echeagaray OH, Wang BJ, Casillas A, Broughton KM, Kim BH and Sussman MA. In situ transcriptome characteristics are lost following culture adaptation of adult cardiac stem cells. *Sci Rep*. 2018;8:12060.

88. Zimmermann WH, Melnychenko I, Wasmeier G, Didie M, Naito H, Nixdorff U, Hess A, Budinsky L, Brune K, Michaelis B, Dhein S, Schwoerer A, Ehmke H and Eschenhagen T. Engineered heart tissue grafts improve systolic and diastolic function in infarcted rat hearts. *Nature medicine*. 2006;12:452-8.

89. Voges HK, Mills RJ, Elliott DA, Parton RG, Porrello ER and Hudson JE. Development of a human cardiac organoid injury model reveals innate regenerative potential. *Development*. 2017;144:1118-1127.

90. Nugraha B, Buono MF, von Boehmer L, Hoerstrup SP and Emmert MY. Human Cardiac Organoids for Disease Modeling. *Clin Pharmacol Ther*. 2019;105:79-85.

91. Ong CS, Nam L, Ong K, Krishnan A, Huang CY, Fukunishi T and Hibino N. 3D and 4D Bioprinting of the Myocardium: Current Approaches, Challenges, and Future Prospects. *Biomed Res Int*. 2018;2018:6497242.

92. Noor N, Shapira A, Edri R, Gal I, Wertheim L and Dvir T. 3D Printing of Personalized Thick and Perfusable Cardiac Patches and Hearts. *Adv Sci (Weinh)*. 2019;6:1900344.

93. Huh D, Hamilton GA and Ingber DE. From 3D cell culture to organs-on-chips. *Trends Cell Biol*. 2011;21:745-54.

94. Saleh FA, Whyte M, Ashton P and Genever PG. Regulation of mesenchymal stem cell activity by endothelial cells. *Stem Cells Dev*. 2011;20:391-403.

95. Macosko EZ, Basu A, Satija R, Nemesh J, Shekhar K, Goldman M, Tirosh I, Bialas AR, Kamitaki N, Martersteck EM, Trombetta JJ, Weitz DA, Sanes JR, Shalek AK, Regev A and McCarroll SA. Highly Parallel Genome-wide Expression Profiling of Individual Cells Using Nanoliter Droplets. *Cell*. 2015;161:1202-1214.

96. Yu G, Wang LG, Han Y and He QY. clusterProfiler: an R package for comparing biological themes among gene clusters. *Omics : a journal of integrative biology*. 2012;16:284-7.

97. Gao E, Lei YH, Shang X, Huang ZM, Zuo L, Boucher M, Fan Q, Chuprun JK, Ma XL and Koch WJ. A novel and efficient model of coronary artery ligation and myocardial infarction in the mouse. *Circulation research*. 2010;107:1445-53.

98. Trac D, Maxwell JT, Brown ME, Xu C and Davis ME. Aggregation of Child Cardiac Progenitor Cells Into Spheres Activates Notch Signaling and Improves Treatment of Right Ventricular Heart Failure. *Circulation research*. 2019;124:526-538.

99. Nichols MG and Foster TH. Oxygen diffusion and reaction kinetics in the photodynamic therapy of multicell tumour spheroids. *Physics in medicine and biology*. 1994;39:2161-81.

100. Wu J, Rostami MR, Cadavid Olaya DP and Tzanakakis ES. Oxygen transport and stem cell aggregation in stirred-suspension bioreactor cultures. *PLoS One*. 2014;9:e102486.

101. Nichol D and Stuhlmann H. EGFL7: a unique angiogenic signaling factor in vascular development and disease. *Blood*. 2012;119:1345-52.

102. Quijada P, Salunga HT, Hariharan N, Cubillo JD, El-Sayed FG, Moshref M, Bala KM, Emathinger JM, De La Torre A, Ormachea L, Alvarez R, Jr., Gude NA and Sussman MA. Cardiac Stem Cell Hybrids Enhance Myocardial Repair. *Circulation research*. 2015;117:695-706.

103. Zheng H, Fu G, Dai T and Huang H. Migration of endothelial progenitor cells mediated by stromal cell-derived factor-1alpha/CXCR4 via PI3K/Akt/eNOS signal transduction pathway. *J Cardiovasc Pharmacol*. 2007;50:274-80.

104. Kanzler I, Tuchscheerer N, Steffens G, Simsekyilmaz S, Konschalla S, Kroh A, Simons D, Asare Y, Schober A, Bucala R, Weber C, Bernhagen J and Liehn EA. Differential roles of angiogenic chemokines in endothelial progenitor cell-induced angiogenesis. *Basic Res Cardiol*. 2013;108:310.

105. Hodgkinson CP, Bareja A, Gomez JA and Dzau VJ. Emerging Concepts in Paracrine Mechanisms in Regenerative Cardiovascular Medicine and Biology. *Circulation research*. 2016;118:95-107.

106. Wang M, Tsai B, Brown JW and Meldrum DR. Insulin-like growth factor-1 in myocardial tissue: interaction with tumor necrosis factor. *Crit Care*. 2003;7:417-9.

107. Kawaguchi N, Smith AJ, Waring CD, Hasan MK, Miyamoto S, Matsuoka R and Ellison GM. c-kitpos GATA-4 high rat cardiac stem cells foster adult cardiomyocyte survival through IGF-1 paracrine signalling. *PLoS One*. 2010;5:e14297.

108. Ellison GM, Torella D, Dellegrottaglie S, Perez-Martinez C, Perez de Prado A, Vicinanza C, Purushothaman S, Galuppo V, Iaconetti C, Waring CD, Smith A, Torella M, Cuellas Ramon C, Gonzalo-Orden JM, Agosti V, Indolfi C, Galinanes M, Fernandez-Vazquez F and Nadal-Ginard B. Endogenous cardiac stem cell activation by insulin-like growth factor-1/hepatocyte growth factor intracoronary injection fosters survival and regeneration of the infarcted pig heart. *J Am Coll Cardiol*. 2011;58:977-86.

109. Fontes JA, Rose NR and Cihakova D. The varying faces of IL-6: From cardiac protection to cardiac failure. *Cytokine*. 2015;74:62-8.

110. Nakamura T and Mizuno S. The discovery of hepatocyte growth factor (HGF) and its significance for cell biology, life sciences and clinical medicine. *Proc Jpn Acad Ser B Phys Biol Sci*. 2010;86:588-610.

111. Bauer M, Cheng S, Jain M, Ngoy S, Theodoropoulos C, Trujillo A, Lin FC and Liao R. Echocardiographic speckle-tracking based strain imaging for rapid cardiovascular phenotyping in mice. *Circulation research*. 2011;108:908-16.

112. de Lucia C, Wallner M, Eaton DM, Zhao H, Houser SR and Koch WJ. Echocardiographic Strain Analysis for the Early Detection of Left Ventricular Systolic/Diastolic Dysfunction and Dyssynchrony in a Mouse Model of Physiological Aging. *J Gerontol A Biol Sci Med Sci*. 2019;74:455-461.

113. Sussman MA. Cardiac nonmyocyte subpopulations: a secular congregation. *Regenerative medicine*. 2019.

114. Gude NA and Sussman MA. Chasing c-Kit through the heart: Taking a broader view. *Pharmacol Res*. 2018;127:110-115.

115. Khan M and Koch WJ. c-kit+ Cardiac Stem Cells: Spontaneous Creation or a Perplexing Reality. *Circulation research*. 2016;118:783-5.

116. Sultana N, Zhang L, Yan J, Chen J, Cai W, Razzaque S, Jeong D, Sheng W, Bu L, Xu M, Huang GY, Hajjar RJ, Zhou B, Moon A and Cai CL. Resident c-kit(+) cells in the heart are not cardiac stem cells. *Nat Commun*. 2015;6:8701.

117. van Berlo JH, Kanisicak O, Maillet M, Vagnozzi RJ, Karch J, Lin SC, Middleton RC, Marban E and Molkentin JD. c-kit+ cells minimally contribute cardiomyocytes to the heart. *Nature*. 2014;509:337-41.

118. Le LV, Mkrtschjan MA, Russell B and Desai TA. Hang on tight: reprogramming the cell with microstructural cues. *Biomed Microdevices*. 2019;21:43.

119. Kobel S and Lutolf M. High-throughput methods to define complex stem cell niches. *Biotechniques*. 48:ix-xxii.

120. Zuppinger C. 3D culture for cardiac cells. *Biochim Biophys Acta*. 2016;1863:1873-81.

121. Bolli R, Hare JM, March KL, Pepine CJ, Willerson JT, Perin EC, Yang PC, Henry TD, Traverse JH, Mitrani RD, Khan A, Hernandez-Schulman I, Taylor DA, DiFede DL, Lima JAC, Chugh A, Loughran J, Vojvodic RW, Sayre SL, Bettencourt J, Cohen M, Moye L, Ebert RF, Simari RD and Cardiovascular Cell Therapy Research N. Rationale and Design of the CONCERT-HF Trial (Combination of Mesenchymal and c-kit(+) Cardiac Stem Cells As Regenerative Therapy for Heart Failure). *Circulation research*. 2018;122:1703-1715.

122. Masumoto H, Ikuno T, Takeda M, Fukushima H, Marui A, Katayama S, Shimizu T, Ikeda T, Okano T, Sakata R and Yamashita JK. Human iPS cell-engineered cardiac tissue sheets with cardiomyocytes and vascular cells for cardiac regeneration. *Sci Rep*. 2014;4:6716.

123. Yoshida S, Miyagawa S, Fukushima S, Kawamura T, Kashiyama N, Ohashi F, Toyofuku T, Toda K and Sawa Y. Maturation of Human Induced Pluripotent Stem Cell-Derived Cardiomyocytes by Soluble Factors from Human Mesenchymal Stem Cells. *Mol Ther*. 2018;26:2681-2695.

124. van Marion MH, Bax NA, van Turnhout MC, Mauretti A, van der Schaft DW, Goumans MJ and Bouten CV. Behavior of CMPCs in unidirectional constrained and stress-free 3D hydrogels. *Journal of molecular and cellular cardiology*. 2015;87:79-91.

125. Gude N, Joyo E, Toko H, Quijada P, Villanueva M, Hariharan N, Sacchi V, Truffa S, Joyo A, Voelkers M, Alvarez R and Sussman MA. Notch activation enhances lineage commitment and protective signaling in cardiac progenitor cells. *Basic Res Cardiol*. 2015;110:29.

126. Hariharan N, Quijada P, Mohsin S, Joyo A, Samse K, Monsanto M, De La Torre A, Avitabile D, Ormachea L, McGregor MJ, Tsai EJ and Sussman MA. Nucleostemin rejuvenates cardiac progenitor cells and antagonizes myocardial aging. *Journal of the American College of Cardiology*. 2015;65:133-47.

127. Li SH, Sun L, Yang L, Li J, Shao Z, Du GQ, Wu J, Weisel RD and Li RK. Young Bone-Marrow Sca-1(+) Stem Cells Rejuvenate the Aged Heart and Improve Function after Injury through PDGFRbeta-Akt pathway. *Sci Rep*. 2017;7:41756.

128. Li SH, Sun Z, Brunt KR, Shi X, Chen MS, Weisel RD and Li RK. Reconstitution of aged bone marrow with young cells repopulates cardiac-resident bone marrow-derived progenitor cells and prevents cardiac dysfunction after a myocardial infarction. *European heart journal*. 2013;34:1157-67.

129. Arisi MF, Chirico EN, Sebeny R, Muthukumaran G, Mu A, De Jonghe BC, Margulies KB and Libonati JR. Myocardial apoptosis and mesenchymal stem cells with acute exercise. *Physiol Rep*. 2017;5.

130. Ferrini A, Stevens MM, Sattler S and Rosenthal N. Toward Regeneration of the Heart: Bioengineering Strategies for Immunomodulation. *Front Cardiovasc Med*. 2019;6:26.

131. Gomez I, Duval V and Silvestre JS. Cardiomyocytes and Macrophages Discourse on the Method to Govern Cardiac Repair. *Front Cardiovasc Med*. 2018;5:134.

132. Jansen Of Lorkeers SJ, Eding JE, Vesterinen HM, van der Spoel TI, Sena ES, Duckers HJ, Doevendans PA, Macleod MR and Chamuleau SA. Similar effect of autologous and allogeneic cell therapy for ischemic heart disease: systematic review and meta-analysis of large animal studies. *Circulation research*. 2015;116:80-6.

133. Zwetsloot PP, Vegh AM, Jansen of Lorkeers SJ, van Hout GP, Currie GL, Sena ES, Gremmels H, Buikema JW, Goumans MJ, Macleod MR, Doevendans PA, Chamuleau SA and Sluijter JP. Cardiac Stem Cell Treatment in Myocardial Infarction: A Systematic Review and Meta-Analysis of Preclinical Studies. *Circulation research*. 2016;118:1223-32.

134. Quijada P, Toko H, Fischer KM, Bailey B, Reilly P, Hunt KD, Gude NA, Avitabile D and Sussman MA. Preservation of myocardial structure is enhanced by pim-1 engineering of bone marrow cells. *Circulation research*. 2012;111:77-86.

135. Huang J, Zhang Z, Guo J, Ni A, Deb A, Zhang L, Mirotsou M, Pratt RE and Dzau VJ. Genetic modification of mesenchymal stem cells overexpressing CCR1 increases cell viability, migration, engraftment, and capillary density in the injured myocardium. *Circ Res*. 2010;106:1753-62.

136. Korski KI, Kubli DA, Wang BJ, Khalafalla FG, Monsanto MM, Firouzi F, Echeagaray OH, Kim T, Adamson RM, Dembitsky WP, Gustafsson AB and Sussman MA. Hypoxia Prevents Mitochondrial Dysfunction and Senescence in Human c-Kit(+) Cardiac Progenitor Cells. *Stem Cells*. 2019;37:555-567.

137. Durdu S, Iskar M, Revenu C, Schieber N, Kunze A, Bork P, Schwab Y and Gilmour D. Luminal signalling links cell communication to tissue architecture during organogenesis. *Nature*. 2014;515:120-4.

138. Bedzhov I and Zernicka-Goetz M. Self-organizing properties of mouse pluripotent cells initiate morphogenesis upon implantation. *Cell*. 2014;156:1032-44.

139. Chen WC, Baily JE, Corselli M, Diaz ME, Sun B, Xiang G, Gray GA, Huard J and Peault B. Human myocardial pericytes: multipotent mesodermal precursors exhibiting cardiac specificity. *Stem Cells*. 2015;33:557-73.

140. Lemcke H, Voronina N, Steinhoff G and David R. Recent Progress in Stem Cell Modification for Cardiac Regeneration. *Stem Cells Int*. 2018;2018:1909346.

141. Quijada P and Sussman MA. Making it stick: chasing the optimal stem cells for cardiac regeneration. *Expert Rev Cardiovasc Ther*. 2014;12:1275-88.

142. Hatzistergos KE and Vedenko A. Cardiac Cell Therapy 3.0: The Beginning of the End or the End of the Beginning? *Circulation research*. 2017;121:95-97.

143. Hawksworth J, Satchwell TJ, Meinders M, Daniels DE, Regan F, Thornton NM, Wilson MC, Dobbe JG, Streekstra GJ, Trakarnsanga K, Heesom KJ, Anstee DJ, Frayne J and Toye AM. Enhancement of red blood cell transfusion compatibility using CRISPR-mediated erythroblast gene editing. *EMBO Mol Med*. 2018;10.

144. Hayashi M, Li TS, Ito H, Mikamo A and Hamano K. Comparison of intramyocardial and intravenous routes of delivering bone marrow cells for the treatment of ischemic heart disease: an experimental study. *Cell Transplant*. 2004;13:639-47.

145. Dib N, Khawaja H, Varner S, McCarthy M and Campbell A. Cell therapy for cardiovascular disease: a comparison of methods of delivery. *J Cardiovasc Transl Res*. 2011;4:177-81.

146. Lee WY, Tsai HW, Chiang JH, Hwang SM, Chen DY, Hsu LW, Hung YW, Chang Y and Sung HW. Core-shell cell bodies composed of human cbMSCs and HUVECs for functional vasculogenesis. *Biomaterials*. 2011;32:8446-55.

147. Scuderi GJ and Butcher J. Naturally Engineered Maturation of Cardiomyocytes. *Front Cell Dev Biol*. 2017;5:50.

148. Zhang S, Fei T, Zhang L, Zhang R, Chen F, Ning Y, Han Y, Feng XH, Meng A and Chen YG. Smad7 antagonizes transforming growth factor beta signaling in the nucleus by interfering with functional Smad-DNA complex formation. *Mol Cell Biol*. 2007;27:4488-99.

149. Bujak M and Frangogiannis NG. The role of TGF-beta signaling in myocardial infarction and cardiac remodeling. *Cardiovascular research*. 2007;74:184-95.

150. Okada H, Takemura G, Kosai K, Li Y, Takahashi T, Esaki M, Yuge K, Miyata S, Maruyama R, Mikami A, Minatoguchi S, Fujiwara T and Fujiwara H. Postinfarction gene therapy against transforming growth factor-beta signal modulates infarct tissue dynamics and attenuates left ventricular remodeling and heart failure. *Circulation*. 2005;111:2430-7.

151. Ghiroldi A, Piccoli M, Cirillo F, Monasky MM, Ciconte G, Pappone C and Anastasia L. Cell-Based Therapies for Cardiac Regeneration: A Comprehensive Review of Past and Ongoing Strategies. *Int J Mol Sci*. 2018;19.

152. Lin RZ and Chang HY. Recent advances in three-dimensional multicellular spheroid culture for biomedical research. *Biotechnol J*. 2008;3:1172-84.